Quantification of gamma-secretase activity in an endogenous context reveals biphasic GSI-mediated Notch/APP selectivity switch and the novel detection of potential proteolytic cleavage fragments of the Notch Intracellular Domain

Matthew Craig Mueller, B.Sc. (Honours)

A thesis submitted in partial fulfillment of the requirements for the degree of

Master of Science

Biological Sciences (Cell & Molecular Biology)

Department of Biological Sciences

Brock University
St. Catharines, Ontario, Canada

I – Abstract:

Specific proteases can serve a multitude of cell-specific functions. For example, gamma-secretase (γ-secretase) is a promiscuous intra-membrane protease implicated in the proteolytic processing of over 100 substrates in the cell, some of which depend on this proteolytic event for key functions in cellular development, homeostasis, and cell-fate lineage. For example, two notable substrates of γ-secretase are amyloid-precursor-protein (APP), in which γ-secretase will irreversibly cleave to produce amyloid-β (Aβ) in Alzheimer's disease (AD); and the Notch receptor, where γ-secretase is essential for liberating the Notch intracellular domain (NICD) to activate Notch-mediated transcriptional regulation in the nucleus.

γ-secretase inhibitors such as DAPT and Avagacestat have been tested as therapies to prevent the formation of Aβ plaques, however, off-target interference with the Notch signalling pathway leading to Notch-related malignant side effects in clinical trials makes these pharmaceuticals unsuitable. The high-throughput search for selective drugs that block the production of Aβ but don't interfere with the Notch signalling pathway has been hindered by a lack of consistency and sensitivity in detecting Notch signal inhibition in pre-clinical, cell-based assays with ectopic substrate expression. Therefore, the development of a highly-sensitive, high-throughput cell-based assay to quantify the level of proteolytic processing of APP and Notch by γ-secretase is a promising addition to the γ-secretase inhibitor drug discovery pipeline.

This thesis presents the combination of immunofluorescence staining, western blotting, and the bromo-deoxyuridine (BrdU) cell proliferation assay as three orthogonal methods to sensitively quantify the γ-secretase cleavage of Notch and APP in SH-SY5Y human neuroblastoma cells, which rely on active Notch signalling to maintain proliferation. With the

exception of the BrdU assay, the tripartite assay was also validated using HEK 293 and HeLa cells. Using our assay, we found that the selectivity for γ-secretase to cleave APP versus Notch was dependent on the time the GSI was replenished before harvesting, which may directly reflect a GSI concentration-dependent selective potency. In addition, a number of novel Notch1 bands (25-75 kDa) were discovered on western blot that may be novel biologically relevant γ-secretase-independent proteolytic products that could play a role in differentially activating or competitively inhibiting the expression of Notch target genes. The Notch proteolytic profile detected on Western blot was cell-type specific and unique between HEK 293 human stem cells, and human cancer lines HeLa and SH-SY5Y cells. In summary, using our high-throughput cell-based assay, cleavage of APP and Notch activation by γ-secretase was sensitively quantified; while a novel profile of cell-type specific proteolytic fragments of the Notch ICD have been identified that may have biological implications in normal development and the pathological proliferation and metastasis of some cancers.

II - Keywords:

Cell-cell signalling, gamma-secretase, notch signalling, cell fate, transcriptional regulation, neuronal differentiation, neuroblastoma, Alzheimer's disease, Amyloid-precursor protein, amyloidogenesis, intramembrane proteolysis, vesicular trafficking, proteolytic processing, tumorigenesis, cellular proliferation

III - Acknowledgements:

Firstly, I would like to thank my supervisor, Sasha (Dr. Aleksandar Necakov) for support, encouragement, and discussions that shaped our relationship and our research over the last three years. It has been a pleasure and an honour to work under your supervision and you have helped me grow both as a person and a scientist.

Next, thank you to the faculty and staff at Brock for their support throughout this process. A special thank you to my committee, Drs. Rebecca MacPherson, Jens Coorssen, and Aleksandar Necakov for their dedication, support, and technical guidance with projects. Also, special thanks to Drs. Jeff Stuart, Rebecca MacPherson, Val Fajardo, and Jens Coorssen for guidance and allowing me to use their lab spaces and resources. A special thanks to Drs. Nicholas Vesprini and Amanda Lepp for making the teaching labs an enjoyable and enriching experience. Thanks to custodial staff Heather and Elaine for their friendliness and encouragement day and night at the lab.

Next, I would like to thank my lab mates, past and present, for support and friendship over the last 3 years. To Sonia Aksamit, Olivia Bagshaw, Hagar Deyab, Sofya Ermolina, Dr. Joao Fonesca, Gregory Foran, Ryan Hallam, Taylor Lidster, Lucas Maddalena, Marvel Megaly, Christopher Moffatt, Fereshte Moradi, Nour Noaman, Ciara Pember, Matthew Sudiyuno, Samantha Toole, Andrew Valente, and Devin Ward; thanks for the great times, the support, and the long hours you all invested. It was a pleasure working with you all and I'll cherish our times together. I could not have done it without each of you.

A special thanks for financial support from the National Sciences and Engineering Research Counsel (NSERC) for summer research support, the Ontario Student Assistance Plan (OSAP), the Ontario Government for the Ontario Graduate Scholarship (OGS) and the Queen

Elizabeth II Graduate Scholarship in Science and Technologies, and the family and friends of Dr. M. S. Manocha for the Dr. M. S. Manocha Memorial Prize.

Lastly, I would like to thank family and friends for their faithful support throughout this process. To Jennifer and Craig (Mom and Dad), Sarah and Tanay Chowdhury (sister and brother-in-law), and Nicole Mueller (sister). A very special thanks to my lovely and supportive girlfriend Alannah Quinn and family. I could not have done it without each one of you. Thanks for the laughs, encouragement, support, and belief in me.

Table of Contents:

IV – Contributions:

I performed all experiments, data presentation, statistical analyses, and chapter writing.

Samantha Toole, an undergraduate thesis student (2018-2019), assisted in performing immunocytochemistry and western blotting experiments under my direction and supervision.

Andrew Valente, a Master's student, assisted in creating a python script for high-throughput nuclear Notch quantification of immunofluorescent images, which I used as a guide for the design of a modified script used for final image analysis of the nuclear notch ratio.

V – Dissemination of Results:

Experimental findings of this thesis were presented in some capacity at the following scientific conference:

Matthew C. Mueller, Andrew J. Valente, Aleksandar S. Necakov. (Apr. 13, 2018). A highly-sensitive, cell-based screening assay to quantify the proteolytic activity of γ-secretase. Canadian Society for Molecular Biology (CSMB): Membrane Proteins in Health and Disease 2018. Poster Presentation.

VI – List of Abbreviations:

AICD – Amyloid Precursor Protein Intracellular Domain
APLP1 – Amyloid Precursor-Like Protein 1
APP – Amyloid Precursor Protein
APH1 – Anterior Pharynx Defective Protein 1
BACE – Beta-secretase Cleaving Enzyme
"BMS-708163" – Avagacestat
BrdU – Bromo-deoxyuridine
BSA - bovine serum albumin
CTF – C-terminal Fragment
DAPT - t-butyl (2S)-2-[[(2S)-2-[[2-(3,5-difluorophenyl)acetyl]amino]propanoyl]amino]-2-phenylacetate
DCC – *Deleted in Colorectal Carcinoma* protein
DMEM - Dulbecco's modified eagle medium
DMSO - dimethylsulfoxide
DTT – dithiothreitol
ECD – Extracellular Domain
EDTA - ethylenediaminetetraacetic acid
EGFR – Epidermal-like growth factor receptor protein
FBS - fetal bovine serum
FIJI - FIJI is just ImageJ
GSI – γ-secretase Inhibitor
GSM – γ-secretase Modulator
HDAC – Histone Deacetylase
HEPES - ((4-(2-hydroxyethyl)-1-piperazineethanesulfonic acid)
HSP – Heat shock protein
$I.C._{50}$ - half maximal inhibitory concentration
ICD – Intracellular Domain
LRP – Lipoprotein receptor-related protein
Nct – Nicastrin
NEAA – Non-essential Amino Acids
NICD – Notch Intracellular Domain
PBS - phosphate-buffered saline
PBST - phosphate-buffered saline with Tween-20
PEN2 – Presenilin Enhancer Protein 2
P/S – Penicillin and Streptomycin
PSEN – Presenilin
"sAPPα" – soluble Amyloid precursor protein alpha
SD – Standard Deviation
SEM - standard error of the mean
TD – transmembrane domain
TBS – Tris-buffered saline
TBST -Tris-buffered Saline with Tween-20

VII – List of Figures and Tables:

Chapter 1.0

Chapter 2.0

Chapter 3.0

Chapter 4.0

Appendix I – Data

Appendix II - Methodology

Chapter 1.0 - Introduction

1.1 General Overview

Alzheimer's disease (AD) is the leading cause of dementia effecting millions of people each year, however its etiology remains poorly understood. The production and accumulation of Aβ plaques through the proteolytic processing of amyloid precursor protein (APP) by a series of enzymes ending with γ-secretase is a major hallmark of the disease. Pharmacologically blocking γ-secretase has been proposed and tested as a treatment for AD using a number of promising drugs that have reached late-stage clinical trials. However, off-target effects of inhibiting γ-secretase include inhibiting Notch signalling, which is important for healthy development and cell/tissue homeostasis, remains problematic. A major roadblock on the path to the development of effective and viable γ-secretase inhibitors is a preclinical screening assay that can reliably quantify γ-secretase cleavage of both Notch and APP.

The first part of this thesis will describe the development, validation, and novel biological findings of a cell-based γ-secretase activity assay that combines Western blotting, immunocytochemistry, and a cellular proliferation assay in SH-SY5Y human neuroblastoma cells. We describe the observation of a dose-dependent biphasic response to γ-secretase inhibitors that might explain the paradoxical rise in Aβ when inhibitor concentrations are low. We then use our current findings to extend the proposed mechanism underlying this phenomenon.

The second part of this thesis describes the use of our tripartite assay in the novel detection of potential truncated Notch fragments that may have cell-type-specific biological relevance. This finding has the potential to transform our current understanding of the canonical

Notch signaling pathway in health and disease and may provide new promising therapeutic targets for specific cancers.

1.2 γ-secretase

The central focus of this thesis is the function of γ-secretase: a promiscuous intramembrane di-aspartyl protease (Wolfe *et al*., 1999). The molecular structure of γ-secretase was recently elucidated via single-particle cryo-electron microscopy (Figure 1.1; Bai *et al*., 2015).

1.2.1 The structure and function of γ-secretase

γ-secretase includes four main components: presenilin (PSEN), nicastrin (NCT), anterior-pharynx defective 1 (APH1), and presenilin enhancer-2 (PEN2), each of which are required to form the functional complex (Figure 1.1; De Strooper, 2003). PSEN is the catalytic component of γ-secretase, containing the pair of aspartyl residues that behave as molecular scissors which cleave substrates bound within the substrate binding pocket (Wolfe *et al.,* 1999). γ-secretase is expressed heterogeneously in the context of two main PSEN homologues (PSEN1/2) which have functional and locational distinctions (Wolfe & Yankner, 2016; Sannerud *et al*., 2016).

PSEN1 and PSEN2 have distinct subcellular locational specificities. For example, γ-secretase containing PSEN1 is predominantly trafficked to the plasma membrane via recycling endosomes. However, PSEN2-containing γ-secretase is trafficked from the trans-golgi network to late endosomes and lysosomes (Wolfe & Yankner, 2016). In addition to locational variation caused by PSEN1/2 isoforms, several APH1 homologues expressed in different tissues account for tissue-specific functional variation. In humans, the two possible PSEN isoforms, combined with three possible APH1 homologues make a total of six unique γ-secretase isotypes.

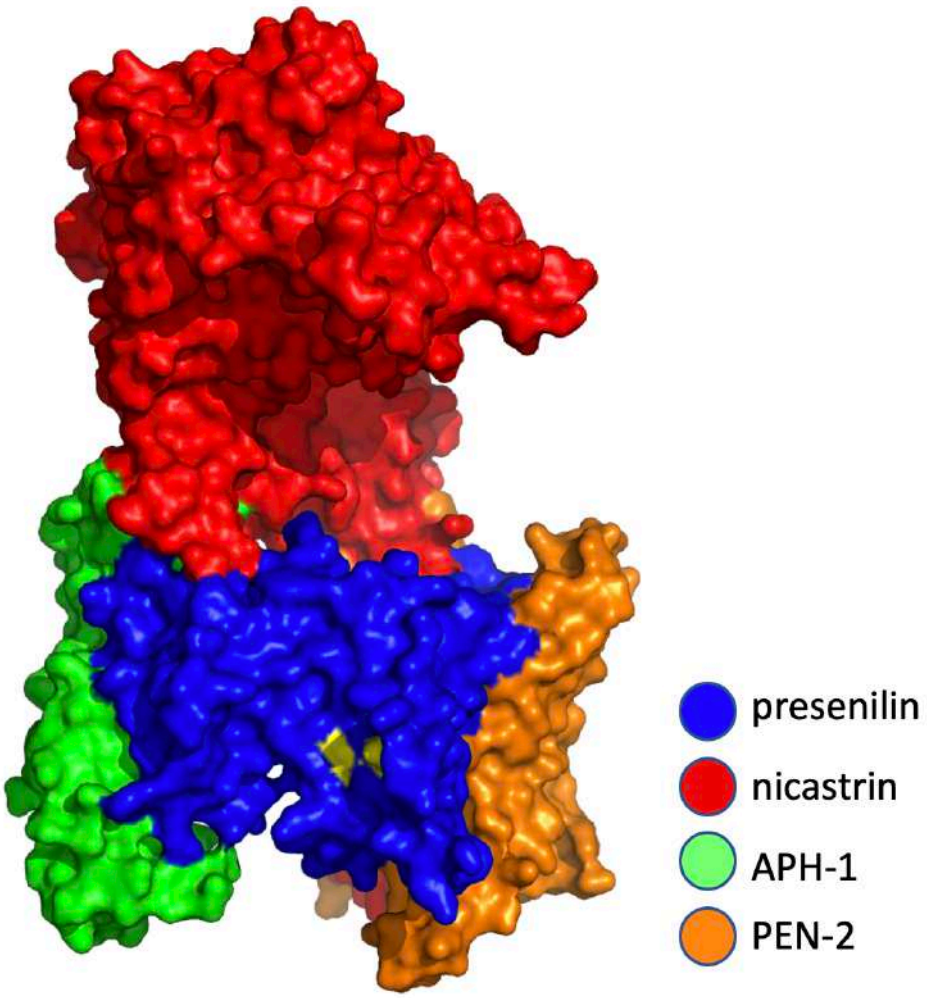

Figure 1.1: Cryo-EM structure of the γ-secretase complex (Bai *et al.*, 2015). Presenilin (blue), presenilin Enhancer Protein 2 (orange), and Anterior Pharynx Defective Protein 1 (green) are tethered to the plasma membrane. Nicastrin (red) has a single-pass transmembrane region, but largely lies in the extracellular matrix. Two aspartate residues (yellow) are thought to make up the catalytic site of the protein complex.

The four subunits of γ-secretase are necessary for assembly, trafficking, and functionality of the γ-secretase complex, as evidenced by the functional loss that results when even just one of the components of the complex is genetically altered or removed (De Strooper, 2003). The formation of functional γ-secretase is regulated by the stoichiometric expression of its components and the step-wise assembly of the complex. First, Nct and APH1 complex with each

other to form an initial scaffold in the which PEN2 and PSEN1/2 will later associate to form the full complex (LaVoie *et al*., 2003). The formation of the APH1-Nct subcomplex is dependent upon mediation with the golgi-ER transition cargo receptor RER1p (Spasic *et al*., 2007). PSEN and PEN2 can then bind to the APH1-Nct scaffold in the Golgi apparatus to form the complete complex. Once the protein complex has assembled, PEN2 binds to the transmembrane domain of PS1 and causes endoproteolysis of PSEN1 to activate the catalytic action of γ-secretase (Thinakaran *et al*., 1996). APH-1 and Nct function in the assembly and stability of γ-secretase, but APH-1 also contains a conserved α-helix binding motif that is critical to γ-secretase's catalytic function (Niimura *et al*., 2005). Nct has a relatively large extracellular domain that sterically prevents substrates from being cleaved until they have been pre-processed by α-secretase (Bolduc *et al*., 2016).

1.2.2 The substrates of γ-secretase

Discovered by geneticists looking into a mutation that lead to familial AD (Sherrington *et al*., 1995), presenilin was originally discovered for its function in catalyzing the terminal cleavage of APP resulting in the release of Aβ. However, the biological understanding of γ-secretase in health and disease is rapidly growing.

In total there is a growing list of over 100 substrates of γ-secretase (Figure 1.2; Haapasalo & Kovacs, 2011). Many of these substrates have several features in common. For example, nearly all of the γ-secretase substrates are Type-1 transmembrane proteins containing a large N-terminal ectodomain, single-pass membrane spanning domain, and a C-terminal domain facing the cytoplasm. The γ-cleavage efficiency of substrates depends largely on the length of the remaining extracellular domain following cleavage by α- or β-secretase. The shorter the length

of the ECD, the more efficiently γ-secretase is able to cleave the substrate (Struhl & Adachi, 2000).

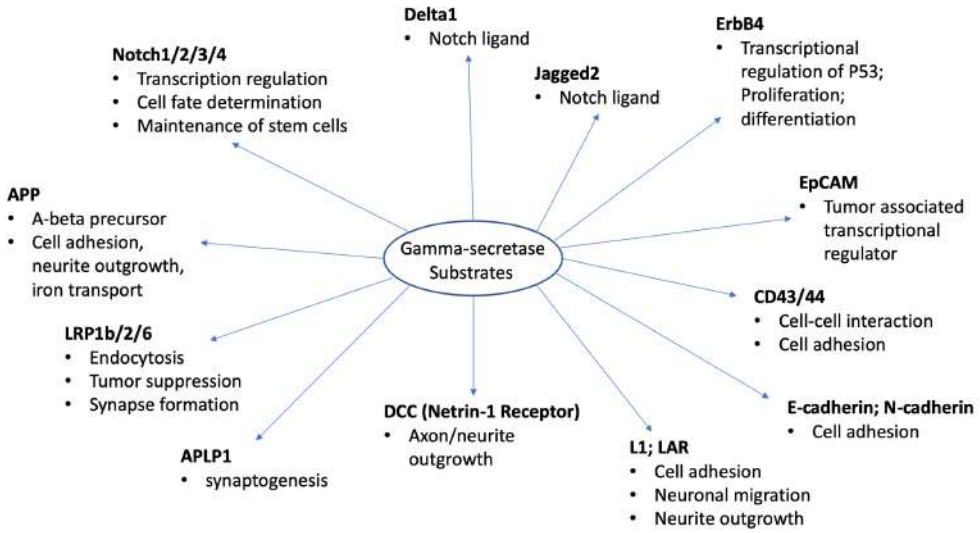

Figure 1.2: γ-secretase is a promiscuous enzyme. Commonly studied substrates are involved in proliferation, differentiation, cell adhesion, tumour suppression, and regulation of neuronal outgrowths.

Secondly, many of the substrates of γ-secretase appear to function as signalling molecules that regulate cell fate determination, development, and regulation of a variety of cell and tissue fates. In the context of neural cell fates, many γ-secretase substrates are jointly involved in proliferation, differentiation (Notch1/2/3/4, Delta, Jagged, ErbB4), cell adhesion (E-cadherin, N-cadherin, CD43/44), neurite and axonal outgrowths (APP, Neuregulin, L1, LAR, DCC), endocytic trafficking (LRP1b/2/6), tumor suppression (EpCam), and synapse formations (APLP1) (Haapasalo & Kovacs, 2011). Many of these same substrates are involved/disrupted in the pathogenic mechanisms of neurodegeneration and cancer. As discussed earlier, γ-secretase is responsible for the proteolytic cleavage of APP that leads to the generation of Aβ plaques: a hallmark of AD (Kopan & Ilagan, 2009). Overall, γ-secretase has a number of functions for

living cells, and it is thought to play a central role in the pathology of AD through APP processing and the onset/progression of certain cancers through Notch signal regulation.

1.2.3 Localization of γ-secretase

γ-secretase is ubiquitously expressed throughout development in both neural and non-neural cell types (Kovaks *et al*., 1996; Lee *et al*., 1996; Ye & Fortini, 1998), however it has a higher expression level particularly in hippocampal neurons (Lee *et al*., 1996). It is localized mainly within membranes of the endoplasmic reticulum and the Golgi, and is transported between membranes via vesicles (Kovaks *et al*., 1996). The process of vesicular membrane recycling to and from the plasma membrane is important for the transport of γ-secretase to the plasma membranes of cells (Selkoe *et al*., 1998), which is vital for its cellular functions. Once at the plasma membrane, γ-secretase participates in its various cellular processes, including its necessary function in Notch receptor activation at the plasma membrane and APP processing on the plasma membrane or intracellular vesicles.

1.3 Notch Signaling

The development and maintenance of multicellular organisms requires tightly regulated cellular responses. Organisms must coordinate numerous complex processes with a high degree of spatial and temporal precision for successful development and regulation of homeostasis. On the cellular level, relatively few pathways regulate the developmental fate of a differentiating cell. One of these central and highly conserved pathways is the Notch signalling pathway. Notch receptors are repeatedly used to regulate a multiplicity of outcomes. The Notch receptor, along with its ligands delta and jagged have multiple roles during development, including lateral inhibition signalling in the developing nervous system, differential cell lineage decisions, and tissue boundary formation.

Even minor disturbances in the Notch pathway can have drastic effects. For example, Notch activity is implicated in several cancers, including T-cell lymphoblastic leukemia. One study found that more than half of all T-cell acute lymphoblastic leukemia (T-ALL) patients carried a mutation in Notch-1 (Weng *et al*., 2004). Furthermore, mutations leading to a truncated Notch ICD lacking the C-terminal PEST domain and a mutation effecting the function of FBXW7 E3 ubiquitin ligase are both associated with T-ALL and T-cell non-Hodgkin lymphoma (O'neil *et al*., 2007; Park *et al*., 2010). Both the lack of a PEST domain on the ICD and the reduced ability of the PEST domain to be ubiquitinylated would hinder the proteasomal turnover of Notch activation, illustrating the importance of the time-sensitive transience of the Notch signal in the nucleus.

Cell-to-cell signaling through Notch is conserved in multicellular organisms and serves a vast range of cellular functions. How a seemingly uniform mechanism can drive such a vast range of cellular outcomes in time, space, and cell-type is a fascinating question that remains incompletely understood.

1.3.1 The canonical Notch signaling mechanism

The Notch signaling cascade is a cell-to-cell signaling mechanism used to regulate various processes in development and homeostasis (*Figure 1.3*). In mammals, there are four Notch isoforms (Notch 1-4). Like APP, the Notch receptor is a Type-I transmembrane protein that consists of an extracellular domain (ECD), transmembrane domain (TD), and intracellular domain (ICD). The Notch ECD contains a conserved set of repeated motifs that resemble Epidermal Growth Factor (EGF). These EGF repeats comprise the binding site for neighboring cell ligands such as Delta and Jagged in mammals; or Delta and Serrate in drosophila. The molecular mechanism of Notch signaling begins before the Notch receptor even reaches the

plasma membrane. The ECD of the Notch receptor is proteolytically pre-processed by a Furin protease in the trans-golgi apparatus (S1 cleavage; Blaumueller *et al*., 1997). The resulting two fragments are held together via a non-covalent interaction, which allows the receptor to be trafficked to the plasma membrane. The Notch receptor is tethered to the plasma membrane of the signal-receiving cell, which when in contact with a neighbouring ligand-expressing cell will cause the binding of the extracellular domain (ECD) to the ligand. This allows the receptor to undergo a conformational change that permits proteolytic cleavage by an ADAM10 metalloprotease (α-secretase). This process is denoted as S2 cleavage and allows the removal of the steric extracellular domain which enables the sequential cleavage of Notch by γ-secretase (S3 cleavage). γ-secretase liberates the Notch intracellular domain from the membrane via a tripeptide mechanism similar to that of APP (Okochi *et al*. 2002). The intracellular Notch domain will then translocate to the nucleus to combine with other transcriptional regulators to remove suppression of transcription of specific target genes. Therefore, the function of γ-secretase is essential for Notch activation (Kopan & Ilagan, 2009). As previously mentioned, the PEST domain plays a major role in temporally regulating its presence in the nucleus, and even minor disruptions to this tightly-controlled turnover can lead to disease.

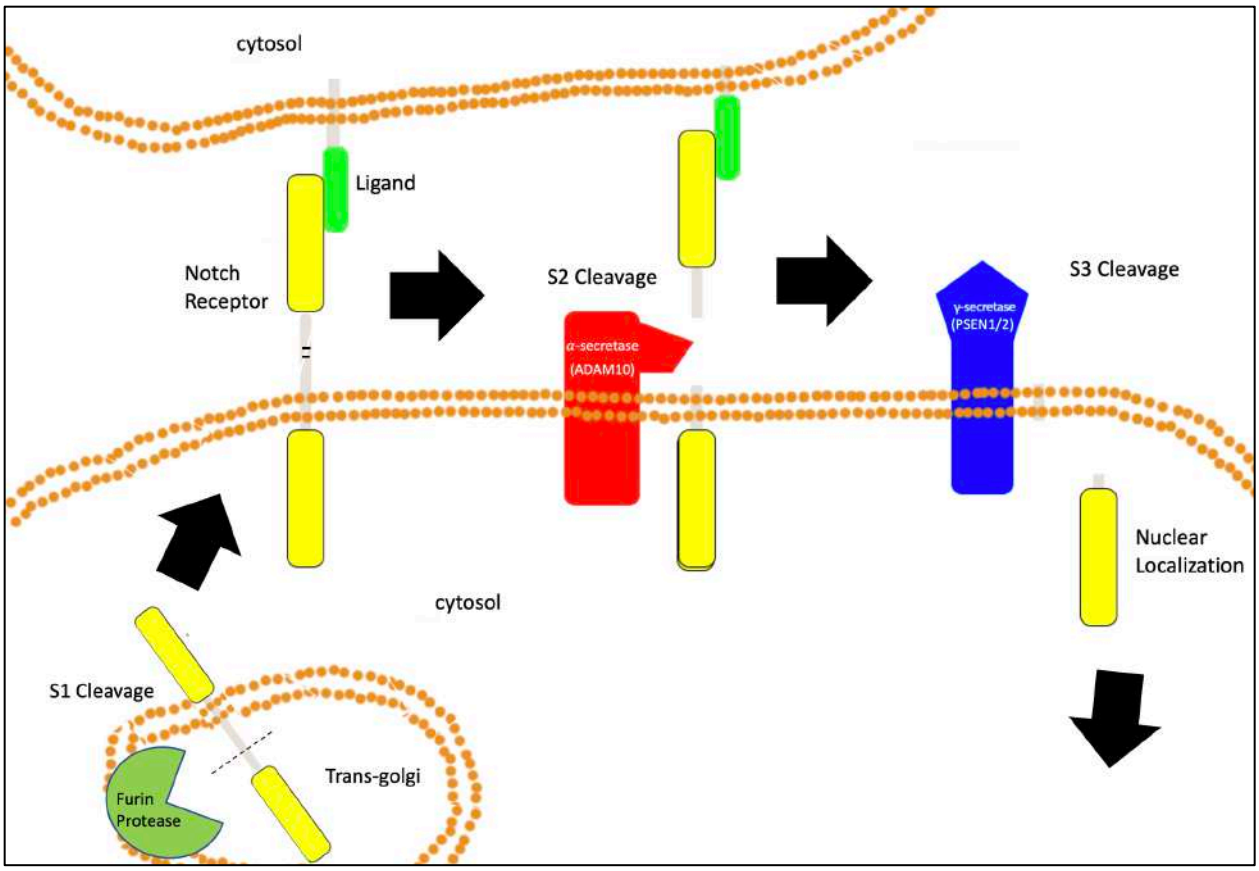

Figure 1.3: Notch proteolytic activation mechanism. The Notch receptor is initially cleaved by a furin protease in the trans-golgi (S1 cleavage). The covalent breakage is held together via non-covalent salt-bridge attachment. Notch is trafficked via vesicles to the PM where it can interact with a ligand on an adjacent cell. This ligand-receptor binding changes the conformation of the protein to expose the α-secretase binding site. This cleavage by ADAM10 metalloprotease (S2 cleavage) displaces the sterically hindering extracellular domain, allowing γ-secretase to bind and process the receptor (S3 cleavage). γ-secretase frees the intracellular domain from the membrane so that is can be translocated to the nucleus and regulate transcription.

1.3.2 The functional architecture of the Notch Intracellular Domain

The NICD contains several highly conserved functional motifs that regulate its transcriptional activity and turnover. These include (in order from N- to C-terminus) the RPB-J Associated Molecule (RAM) domain, the ankyrin repeats, a transcriptional activator domain (TAD) sequence, and the PEST (proline, glutamate, serine, threonine) sequence(s).

Upon translocation to the nucleus, the RAM motif and Ankyrin repeats of the Notch ICD associate with the co-transcriptional machinery to form a functional transcriptional complex (Tani *et al*., 2001). The NICD binds with the Epstein-Barr virus (EBV) latency C promoter binding factor (CBF1)/recombination signal binding protein of the Jκ immunoglobulin gene (CBF1/RBP-Jκ), suppressor of Hairless, Lag-1 (CSL) family of transcription factors (Deregowski *et al*., 2006). The CBF1 protein mediates repression of transcription through recruitment of co-repressors *Silencing Mediator of Retinoic Acid and Thyroid Hormone Receptor (SMRT)* and Histone Deacetylase (HDAC) (Kao *et al*., 1998). Binding of the Notch ICD to CBF1 initiates the displacement of the co-repressors and mitigates transcriptional repression of the target gene (Tani *et al*., 2001).

Although the ankyrin repeats are involved in stabilizing the CSL complex, this motif also has a high binding affinity for a protein called Deltex-1. Deltex-1 is a transcriptional mediator of the Notch signaling pathway that will bind to the ankyrin repeats of the Notch ICD and regulates transcription to ultimately drive the suppression of development of neural-specific cell fates (Yamamoto *et al*., 2001). Furthermore, the ankyrin repeats and TAD domain also function to recruit/bind histone acetyltransferase proteins that will catalyze the unraveling of chromatin and activate transcription (Kurooka & Honjo, 2000). The turnover of the Notch ICD once liberated to the nucleus is tightly controlled by the rate-limiting FBXW7 ubiquitin ligase that signals the nuclear-localized protein for degradation at the PEST domain by the proteasome (Matsumoto *et al*., 2011). In addition to these four highly-conserved functional motifs, two Nuclear Localization Sequences (NLS) are present on the ICD of Notch: one before and one after the ankyrin repeats. These domains target the Notch ICD to the nucleus and may be involved in subnuclear

localization and differential gene expression is one, the other, or both NLS domains are present (Hooper *et al.,* 2007).

1.3.3 The importance of γ-secretase in Notch signaling

The role of γ-secretase in Notch signaling has also been demonstrated in adulthood by various cell and animal knockout experiments. Aberrant T-cell differentiation (Doerfler *et al.,* 2001), dysfunctional intestinal goblet cell differentiation causing bloody diarrhea (van Es *et al.*, 2005), and hair and skin defects such as tumorigenesis (Xia *et al.*, 2001; Tournoy *et al.*, 2004) have all been observed in *in vivo* models lacking PSEN1/2. Interestingly but not surprisingly, some of the adverse symptoms observed in clinical trials of DAPT and Avagacestat recapitulate the defects caused by Notch interference experiments in cells and animal models. Because of this, the development of a truly selective inhibitor of γ-secretase that blocks APP processing but not Notch activation could be a ground-break in the field of Alzheimer's therapy.

1.3.4 Regulation of the Notch Signaling Pathway

The activated NICD forms complexes that ultimately control chromatin organization via histone deacetylation and acetylation that facilitate the transcription of target genes. There are multiple levels of mechanisms that have evolved to regulate levels of Notch activation. These mechanisms regulate the level, duration, and spatial distribution of the active NICD, which has been found to be crucial to normal development and homeostasis. These systems of control manifest in the form of epigenetic regulation of ligands and receptors, nuances in interactions between Notch and its ligands, and post-translational modifications of the Notch receptor including ubiquitination, phosphorylation, glycosylation, hydroxylation, and acetylation. In addition to these aforementioned mechanisms, several proteolytically-processed truncated

variants of the NICD have been noted in the literature that may provide an additional level of regulation (Wesley & Saez, 2000; Fassa *et al*., 2007).

Coordinated Notch activation relies on the ample expression of a number of proteases and cofactors. Firstly, the production of the signal-competent Notch receptor is dependent on the expression of a Furin protease in the Golgi (S1 cleavage). Next, the rate-limiting S2 cleavage is cell-to-cell contact-dependent and relies on the sufficient expression of the ligands delta/jagged on an adjacent plasma membrane. Additionally, these Notch receptor ligands are both targets of the γ-secretase/presenilin complex, in which cleavage by γ-secretase will terminate the ligands' signaling competence, thus antagonizing the abundance of Notch activation. The process of S2 Notch activation depends on the availability of the functionally-active ADAM10 metalloprotease on the plasma membrane. The ADAM10 metalloprotease and subsequent γ-secretase/presenilin complex have been found to cleave delta to liberate the delta ECD to the extra-cellular environment (which is subsequently cleaved by γ-secretase). The functionality of this liberated cell contact-independent delta ECD has been called into controversy (Klueg *et al*., 1998; Qi *et al*., 1999; Mishra-Gorur *et al*., 2002), with evidence indicating that immobilization of the ligand is probably necessary for Notch activation and a soluble ligand ECD can bind to but does not activate the Notch receptor (Sun & Artavanis-Tsakonis, 1997; Varnum-Finny *et al*., 2000; Small *et al*., 2001). Therefore, it seems to be the case that cleavage of Notch ligands Delta and Serrate/Jagged may act as dominant negative molecules to irreversibly inactivate these ligands and serve as another form of regulation of signal activation (Small *et al*., 2001; LaVoie & Selkoe, 2003). The ICD of Delta that is released from the membrane upon γ-secretase cleavage may also be biologically relevant as a transcriptional regulator in the nucleus (Bland *et al*., 2003; Kolev *et al*., 2005; Dyczynska *et al*., 2007).

Additionally, functional specializations in specific regions of the extracellular domain is likely involved in regulation of Notch signaling (Baron *et al*., 2002). For example, within the three EGF repeat domains that show high sequence conservation (11-13; 23-27; 31-34), it has been found that EGF repeats 11-13 are vital for binding of both Delta and Serrate/Jagged (de Celis *et al*., 1993); while the EGF repeats 23-27 are necessary for Serrate/Jagged-dependent Notch activation (Lawrence *et al*., 2000). Specific point mutations in the EGF repeats have also been discovered that show selective effects in certain tissue types as a result of a change in Notch signal activation, the culprit behind several tissue-specific developmental defects and cancers (Kelley *et al*., 1987; de Celis & Garcia-Bellido, 1994; Joutel *et al*., 1996; Garg *et al*., 2005). Therefore, nuances in the extracellular ligand/receptor interaction may provide an additional level of regulation of Notch signal output.

In addition to the trans-interaction between the Notch receptor of one cell and a ligand from an adjacent cell membrane, cis-interactions between the Notch receptor and ligands on the same cellular membrane have been identified (Fehon *et al*., 1990). These cis-interactions have been shown to mutually inhibit the Notch receptor and its ligand Delta by formation of a stable, irreversible cis-complex (Sprinzak *et al*., 2010), thus reducing the ability of a signal to be received by the Notch receptor from ligands on adjacent cells, which has been seen to drive the cell to a neurogenic phenotype (Jacobson *et al*., 1998). Therefore, over-expression of the Notch receptor may reduce a cell's ability to transmit Delta signals to neighboring cells and over-expression of the Delta ligand may limit a cell's ability to receive signals from neighboring Delta ligands.

The Notch ligands and Notch receptors are both proteolytically processed by specific proteases at the ECD and membrane-spanning domain. Likewise, other relatively undefined

proteolytic processes may occur to regulate Notch activity at the ICD of the Notch receptor. For example, Wesley & Saez were the first to characterize an ICD-truncated form of the Notch receptor in drosophila embryos that was prevalent at specific points in time and space in the developing fly (Wesley & Saez, 2000). They first noted differences in the spatial distribution of Notch when using an antibody specific for the C-terminus versus an antibody specific for the N-terminus, which disproportionally predominated in neural precursor cells of the developing nervous system. They observed a spike in the level of truncated-Notch protein (missing the last ~50 kDa of the C-terminus) in 3-6 hour-old embryos that was seen to associate with delta. Based on their findings, Wesley & Saez theorized that an uncharacterized proteolytic event was leading to the generation of this truncated form of Notch missing the portion of the ICD downstream of the ankyrin repeats. This truncated form of Notch, observed to associate with delta1, regulated levels of suppressor of hairless and other transcriptional regulators. This was observed to ultimately drive cells to a neurogenic cell fate. Therefore, they concluded that this newly characterized truncated Notch may have major implications in the process of lateral inhibition and neuronal differentiation.

Additionally, Fassa *et al*. characterized a novel proteolytic cleavage event of the Notch ICD in HEK293 cells that generated a prominent ~79 kDa band on immunoblot (Fassa *et al*., 2007). They found through selective pharmacological inhibition that a cysteine protease was responsible for cleaving the Notch ICD once it was trafficked to the plasma membrane from the Golgi, leading to the generation of a truncated form of the Notch ICD that could potentially exert novel functions or compete with the normal pathway of the Notch ICD.

In addition to these novel proteolytic events that may play important roles in regulating and diversifying Notch signal output, some cell assays have detected appreciable levels of a

fragment of the Notch ICD containing only the ankyrin repeats, implying that there are likely proteolytic sites before and after this domain (Baron *et al*., 2002). The discovery of new potential proteases that play a role in Notch signalling would lead to a deeper understanding of how Notch activation is regulated. This information may even be useful in the development of therapies for novel Notch-related diseases, such as certain cancer types.

1.3.5 Post-translational Modifications of the Notch Receptor

A high level of spatial and temporal control of the Notch signaling pathway is vital for normal signal function. A post-translational modification (*Table 1.4*) strongly implicated in the regulation of Notch signaling is ubiquitination. Ubiquitin is a small regulatory protein (7.8 kDa). Ubiquitination of proteins functions to target them to specific organelles. Most notably, ubiquitination tags proteins for degradation by the proteasome. Additionally, ubiquitination of membrane-tethered proteins can target them to the lysosome via endocytic trafficking. Both of these mechanisms are implicated in the turnover of the Notch receptor and associated proteins.

Table 1.4: Number of specific post-translational modifications found on human Notch1-4

Modification	NICD1	NICD2	NICD3	NICD4
Acetylation	**18**	**0**	**2**	**0**
Hydroxylation	**2**	**2**	**2**	**0**
Methylation	**5**	**0**	**1**	**1**
Phosphorylation	**26**	**26**	**2**	**0**
Ubiquitination	**2**	**1**	**1**	**0**

The PEST domain of the Notch receptor, located on the C-terminal end of the ICD, is the site of ubiquitination. Once released from the membrane by γ-secretase, the Notch ICD's presence in the nucleus is regulated by its relatively rapid proteasomal turnover. The rate-limiting step of ubiquitination of the PEST domain of Notch in the nucleus is mediated by an E3 ubiquitin ligase called FBXW7. Interestingly, mutations in the functional domain of FBXW7 and the PEST domain of Notch causing dysregulation in the turnover of time-sensitive activation of Notch in the nucleus have been linked to T-cell Acute Lymphoblastic Leukemia (Park *et al*., 2009; Demarest *et al*., 2008).

The ability to turn off Notch is arguably just as important to normal development and cellular homeostasis as the ability to activate it. With some rare exceptions, the C-terminal PEST domain is ubiquitously found across bilaterian species (Gazave *et al*., 2009). In most multi-cellular bilaterian species, at least one isoform of Notch exists that contains a second PEST domain found closer to the γ-secretase cleavage site, either before or after the ankyrin repeats (Gazave *et al*., 2009). Interestingly, it was found in *C. elegans* that the worm homologue of FBXW7 called Sel-12, forms a physical association with the worm homologue of the presenilin/γ-secretase complex, Sel-10 (Wu *et al*., 1998). This pioneering work introduced the idea of a physical, but also functional, association between PSEN and the E3 ubiquitin ligase responsible for negatively regulating PSEN, and the Notch ICD PEST domain, likely at the additional PEST domain found closer to the membrane as oppose to the C-terminal PEST domain (Oberg *et al*., 2001; Wu *et al*., 2001; Gupta-Rossi *et al*., 2001). For example, in human Notch1, a second PEST domain is found just after the ankyrin repeats domain flanking a second NLS, a ubiquitin ligase binding site, a USP7 deubiquitination binding site, and a Nardilysin cleavage site. This combination of motifs suggests that a second cleavage independent of γ-

secretase cleavage may occur that could be involved in sending a differential Notch signal to the nucleus. Another E3 ubiquitin ligase, Suppressor of deltex (Su(dx)) has also been shown to associate with Notch at the PEST domain, independent of the presence of the TAD and C-terminal PEST domain. Interestingly, this nardilysin cleavage would separate two distinctly-typed sumoylation sites (www.elm.eu.org) that may play a role in determination of subnuclear localization (Terui *et al*., 2004; Anderson *et al*., 2012), to produce a fragment that is 45 kDa and a fragment that is 55 kDa respectively. The differential sumoylation of the two fragments is an idea that would be supported by the findings of Hooper *et al*., 2007, who found that when fluorescently-tagged versions of either halves of the Notch ICD were ectopically expressed in SH-SY5Y cells, they localized to distinct subnuclear foci.

Other post-translational modifications have been characterized to play a role within the Notch receptor. These include acetylation, hydroxylation, and phosphorylation sites throughout the RAM domain, ankyrin repeats, and TAD domain, which modify the receptor's binding affinity with various interacting cofactors.

1.4 Alzheimer's Disease

Along with its role in Notch signaling, γ-secretase has also been implicated as a major factor in the pathogenesis of AD. AD is the most common neurodegenerative disorder and the most prevalent form of dementia. Approximately 47 million people world-wide live with the disease (Prince *et al*., 2015). Consequently, the widespread prevalence of AD poses immense medical, social, and economic adversities across the globe. The AD brain has characteristic atrophy due to cell loss, with the first regions to experience atrophy being the hippocampus and prefrontal cortex (Coyle *et al*., 1983). At the onset and in the progression of AD, two specific proteins accumulate in the brain: Aβ, which accumulates extracellularly to form Aβ plaques, and

hyperphosphorylated tau, which accumulates intracellularly to form neurofibrillary tangles. Both proteins are prone to misfolding, resulting in the formation of toxic homo-oligomers (Benilova *et al*., 2012). The continued build-up of these proteins eventually leads to the formation of insoluble aggregates, which are characteristic of AD (Selkoe *et al*., 1996).

1.4.1 Proteolytic processing of Amyloid Precursor Protein and the Amyloidogenesis Hypothesis

Normally, in a non-pathological scenario, APP is initially processed by α-secretase, which allows for the sequential intramembranous cleavage by γ-secretase. In AD, β-secretase initially binds and cleaves APP at one of its unique binding sites (Asp672 or Glu682), followed by γ-secretase cleavage that releases a 42-residue long polypeptide called amyloid-beta 42 (Aβ42; Aβ), which self-aggregates to form plaques that eventually lead to synaptic interference, neurotoxicity, and ultimately neurodegeneration (*Figure 1.5*). Other forms of Aβ can be produced including Aβ40 and Aβ38, both of which are much less pathological due to a decreased homo-affinity.

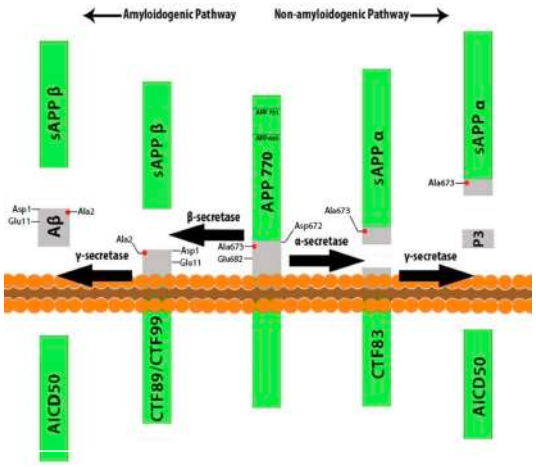

Figure 1.5: Proteolytic processing of APP in normal and pathological conditions (Mueller *et al.*, 2018). In a non-pathological scenario, APP is initially processed by α-secretase, which allows for the sequential intramembranous cleavage by γ-secretase (Figure 1.5, middle to right). In AD, β-secretase initially binds and cleaves APP at its unique binding site, followed by γ-secretase cleavage that releases a 42-residue long polypeptide called Amyloid-β 42 (AB42; Figure 1.5, middle to left), which self-aggregates to form plaques.

About one fifth of AD cases are familial, leading to early-onset AD (<65 y/o), and can be attributed to mutations on any one of three genes involved in Aβ42 production: APP, and PSEN1 or PSEN2 of γ-secretase (Karch *et al*., 2014). These mutations cause an increase in production of Aβ42 by γ-secretase by altering the substrate/enzyme interaction to favor cleavage by β-secretase. Hardy & Higgins (1992) previously hypothesized that this Aβ42 accumulation is the primary trigger of AD; the amyloidogenesis hypothesis has been consistently supported by scientific consensus (Selkoe & Hardy, 2016). Aβ42 aggregates are also characteristic in late-onset/sporadic forms of AD, however, the etiology in these forms of the disease is less clear. Currently, no therapies exist which prevent the onset or progression of AD. Therefore, to provide insight which will guide and inform the rational design of novel therapies, it is important to incorporate a clear picture of APP processing on the molecular level into drug discovery pipelines to understand how these systems are influenced in response to potential therapeutic interventions.

1.4.2 γ-secretase activity determines the pathogenicity and prevalence of Aβ

Several forms of Aβ have been discovered, the most common two are Aβ42, being 42 residues in length; and Aβ40, being 40 residues in length. Aβ42 has a much higher homo-affinity and therefore is associated with a higher pathogenicity. Aβ40, as well as the less common Aβ38 are less prone to self-aggregation and are associated with a lower pathogenicity. Therefore, the ratio of Aβ42/Aβ40 is commonly measured in laboratories as an indication of the severity of the disease. Recently, a tripeptide sequential γ-secretase cleavage mechanism was elucidated to explain the proteolytic processing of APP to generate Aβ peptides (Bolduc *et al*., 2016). To produce Aβ42, γ-secretase will initially bind and cleave at residue 48, then subsequently cleave at residue 45, and finally at residue 42. To produce Aβ40, γ-secretase will initially bind and

cleave at residue 49 of β, then cleave at residue 46, 43, and finally 40. Therefore, not only have γ-secretase inhibitors (GSIs) been explored as therapies to prevent the overproduction of Aβ plaques in AD, but γ-secretase modulators (GSMs) have also been sought after as a pharmacological means of shifting the production of Aβ42 to Aβ40, instead of completely inhibiting the function of this protease. Tripeptide homologues of the γ-secretase binding site of APP have shown high efficacy in decreasing the Aβ42/Aβ40 ratio by competitively binding to the active site of PSEN *in vitro* (Bolduc *et al*., 2016). However, these compounds have shown extremely low bioavailability and are not tenable clinical remedies.

1.5 γ-secretase inhibitors

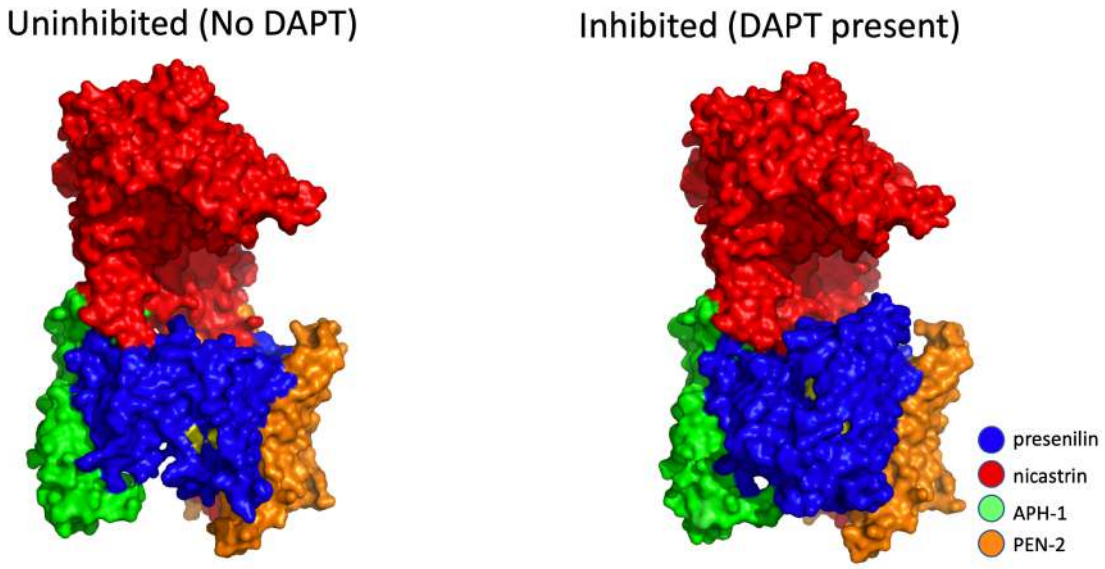

Figure 1.6: DAPT is well-known non-selective γ-secretase inhibitor. (Bai *et al.*, 2015). Cryo-EM structure of uninhibited γ-secretase, with the two aspartate residues shown in yellow (left). Cryo-EM structure of γ-secretase with DAPT bound to unique binding site, the active site that holds the aspartate residues is now sterically blocked due to conformational change in protein structure (right).

N-[N-(3,5-difluorophenacetyl)-L-alanyl]-S-phenylglycine t-butyl ester (DAPT; GSI IX; *Figure 1.6*) is one of the most well-studied γ-secretase inhibitors (GSIs; *Figure 1.7*). DAPT is a

dipeptide analog that arose from a high-throughput screening campaign (Dovey *et al*., 2001). Relative to other GSIs it is very potent, showing an IC-50 of 20 nM in HEK-293 human embryonic kidney cells ectopically expressing APP_{swe} (Burton *et al*., 2008) and 115 nm in SK-MES-1 human lung squamous carcinoma cells (Cao *et al*., 2012) for its ability to block Aβ production. It was also the first GSI shown to be effective when administered orally in mice, which lowered Aβ levels in the brain with an ED-50 of 100 mg/kg. DAPT binds to a unique binding site on the C-terminal fragment of PSEN, leading to a conformational change in the tertiary structure of γ-secretase that blocks access to the active site (*Figure 1*.6; Morohashi *et al*., 2006; Bai *et al*., 2015). DAPT is considered by many to be a non-selective GSI because it blocks γ-secretase activity for all substrates indiscriminately. It has been shown via *in vitro* assays that DAPT partially blocks Notch activation at the same concentrations needed to block Aβ production (Yang *et al*., 2008). Therefore, it is likely not a viable clinical treatment to lower Aβ levels. Nonetheless, because of its potency and *in vivo* bioavailability, it has become a central research tool in the study of γ-secretase in both *in vitro* and *in vivo* models.

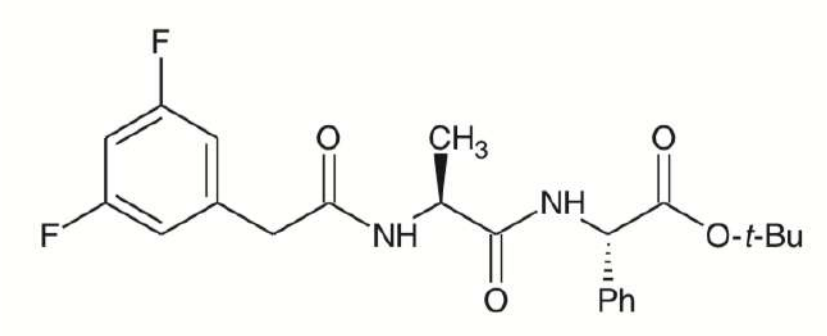

Figure 1.7: DAPT (N-[N-(3,5-difluorophenacetyl)-L-alanyl]-S-phenylglycine t-butyl ester). DAPT is a well-studied dipeptide analogue non-selective γ-secretase inhibitor.

Another GSI that has recently undergone clinical trials (Coric *et al*., 2015) to test its use as an AD therapy is a compound called Avagacestat (BMS-708163; *Figure 1.8*). Avagacestat showed a 193-fold selectivity in blocking γ-secretase's ability to cleave APP but not Notch (Gillman *et al*., 2010). Avagacestat faired as initial Phase 1 clinical trials showed initial doses were well tolerated with mild GI and dermatologic side effects. However, cases of non-melanoma skin cancer and worsening cognitive function were observed in further clinical trials (Coric *et al*., 2012; Mikulca *et al*., 2014). Ultimately, Avagacestat was a letdown as it was terminated from a long-term Phase II clinical trial due to adverse side effects including the development of skin lesions and gastrointestinal complications, which further studies attributed to off-target effects of the drug involving the Notch pathway (Coric *et al*., 2015; Godyn *et* al., 2016). The validity of the initial *in vitro* finding showing selectivity (Gillman *et al*., 2010) has since been put in to question by these clinical trials and by work investigating the molecular mechanism of the drug-enzyme interaction (Crump *et al*., 2012), highlighting the importance of reliable *in vitro* assays.

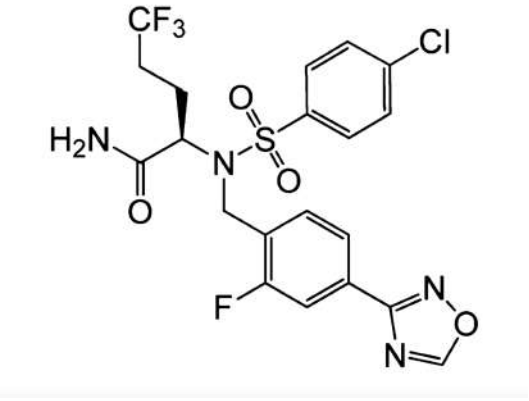

Figure 1.8: Avagacestat (BMS-708163) is a selective γ-secretase inhibitor. This compound recently showed a 193-fold selectively to block APP processing but not Notch. However, due to unforeseen Notch-related adverse side effects, clinical trials were prematurely halted.

γ-secretase has been targeted by pharmaceutical companies for its relevance in the formation and accumulation of Aβ plaques. However, even extremely minor perturbations in the spatially-sensitive and time-sensitive mechanisms of the Notch signalling system can have tissue-specific consequences on the health status of biological systems. Deregulation of the Notch signalling pathway, including both overactivation and inhibition, is pathogenic by way of cell fate lineage determination that governs tissue homeostasis. For example, in the gut, Notch inhibition prevents intestinal stem cell differentiation which can manifest as intestinal lesions and gastrointestinal bleeding when the intestinal stem cells are no longer able to asymmetrically divide to replenish damaged enterocytes (van Es *et al*., 2005). Overactivation of the Notch pathway can also be problematic as stem cell differentiation into secretory lineages is prevented, and the pool of progenitor cells accumulates (Fre *et al*., 2005). A hallmark of several gut neoplasms is the overactivation of the Notch signalling pathway, further displaying its importance in homeostasis (van Es *et al*., 2005). Therefore, to develop pharmaceuticals that prevent or reduce the formation of Aβ plaques without causing off-target harm, it is widely understood that therapeutic inhibitors must be developed that selectively inhibit γ-secretase to prevent the cleavage of APP, but to not disturb the γ-cleavage of the Notch receptor.

1.6 Current Quantification Methods

Preclinical assays have been developed to characterize the selective activities of γ-secretase inhibitors such as Avagacestat, however, many of them are labour intensive and limited in the level of insight they provide. Retrospectively reflecting on the preclinical assays developed for Avagacestat, these preclinical assays lacked the ability to predict the actual selectivity of γ-secretase in its ability to cleave APP and Notch substrates at a clinical level. This was evidenced

by the incidences of skin and gut complications despite an early indication of altered Notch target gene expression.

Some of the *in vitro* cell-free assays to test GSIs use variable levels of synthetic substrate and/or purified enzymes (Yang *et al*., 2008; Gillman *et al*., 2010), approaches that may not represent physiological contexts. Next, some of the cell-based approaches used different detection methods (McKee *et al*., 2013) depending on whether they were assessing APP processing or Notch processing. This is a questionable practice because there will be inherent variability in data collected from one type of assay versus another type. Next, different cell lines are often chosen depending on whether APP or Notch is being quantified. Typically, a cell line with robust expression of APP is chosen for testing the GSI's AB-inhibiting potency, whereas a cell line that abundantly expresses Notch is chosen to measure Notch inhibition capacity of the GSI (Mayer *et al*., 2008; Kreft *et al*., 2008). This is problematic because cell types have unique expression profiles of proteins that may affect the potency of the inhibitor. For example, it has been shown that the potency of γ-secretase inhibitors is dependent on substrate concentration or relative ratio of substrate to inhibitor (Burton *et al*., 2008), creating further problems when using a different cell type for APP quantifications than that which was used for Notch quantifications. For this reason, cell-based assays that use transfected cell lines that ectopically express substrates may be providing quantifications that are completely different than that of their non-transfected counterparts.

As trials move *in vivo*, standard quantifications of γ-secretase activity involve measuring CSF or plasma levels of Aβ and Notch target gene expression levels (Albright *et al*., 2012; Tong *et al*., 2012; Coric *et al*., 2012; Coric *et al*., 2015). For the case of Notch quantification *in vivo*, the downstream expression of Notch target genes such as HES1 in the plasma may not be a

sensitive-enough method of assessing interference with the Notch pathway. Furthermore, the development of a high-throughput, highly-sensitive cell-based screening assay to directly quantify the relative levels of endogenous APP and Notch proteolytic processing by γ-secretase in a non-transfected context would provide more accurate insight in the development of selective γ-secretase inhibitors in the combat of AD.

In summary, cell-free and cell-based assays for γ-secretase activity have been developed but are labour-intensive and/or limited by the effectiveness in detecting differential activity of APP and Notch cleavage. Therefore, the further development of *in vitro* assays to test γ-secretase modulators could be useful to quickly and easily perform large-scale screens for potential modulators and their relative Notch cleavage and APP cleavage activities.

1.7 Notch inhibition stimulates differentiation in SH-SY5Y human neuroblastoma cells

The functions of Notch were first understood in the context of Drosophila neurogenesis, where it was discovered that Notch regulates the differentiation of neuronal precursor cells (Simpson, 1990). The term lateral inhibition was used to describe the pattern in which differentiating pluripotent cells will develop either neural or glial cell fates (Heitzler & Simpson, 1991; Goriely et al., 1991). Notch activation was seen to inhibit neural differentiation and drove differentiation into glial cell fates. Delta-expressing pluripotent cells that were not in contact with other delta-expressing cells did not undergo ligand-dependent Notch activation and were therefore driven into a neuronal cell-type.

In several cancer cell lines relying on Notch to maintain proliferation, disease recapitulates development. For example, in the human neuroblastoma cell line, SH-SY5Y, it has been shown that Notch activity may be necessary to maintain the tumor cells' proliferative state; when Notch activation is inhibited, the cells differentiate and decrease proliferation rates, while

adopting a neuronal-like morphology and expression profile (Ferrari-Toninelli *et al*., 2010; Chang *et al*., 2010). Treatment of SH-SY5Y cells with all trans retinoic acid (at-RA) also induces differentiation of the SH-SY5Y cells (Pahlman *et al*., 1984; Encinas *et al*., 2000) which can be used as a positive control for cell differentiation and Notch inhibition. Using this cell line as a model to quantify γ-secretase activity provides a non-transfected, orthogonal means of measuring Notch inhibition.

1.8 Summary and Purpose

The fight against neurodegenerative diseases is limited by the present knowledge of the molecular mechanisms that govern these diseases and how these mechanisms respond to potential therapeutic interventions. The lack of molecular tools available to study diseases is often a limiting factor in the advancement of research leading to effective therapies. For example, advancements in cryo-electron microscopy have recently led to the elucidation of the structure of γ-secretase. However, AD is still not completely understood, and current research is limited by poor sensitivity in quantifying some of the molecular players in disease pathology. Recent failures in clinical trials of selective γ-secretase inhibitors such as Avagacestat have indicated that a key missing piece in the pipeline to effective discovery of selective γ-secretase inhibitors is a reliable means of which to quantify γ-secretase activity, specifically in relation to substrates APP and Notch. The goal of this series of experiments is to develop a standard means to directly quantify the proteolytic processing of Notch and APP by γ-secretase that would contribute to a highly-sensitive, high-throughput cell-based assay that could be added to a drug discovery pipeline to discover compounds that inhibit APP cleavage, but not Notch. The assay involves three components: western blotting to quantify the levels of substrate and products as a result of γ-secretase-mediated cleavage; immunocytochemistry to quantify APP and Notch

cellular localization; and the use of a BrdU cell proliferation assay to quantify relative levels of cell proliferation as a measure of Notch inhibition-induced differentiation of SH-SY5Y human neuroblastoma cells (*Figure 1.9*). This represents the first example to our knowledge in which a non-transfected cell line has been quantify the potency of γ-secretase inhibitors towards substrates APP and Notch, and will provide a novel cellular method to be added to the GSI preclinical pipeline.

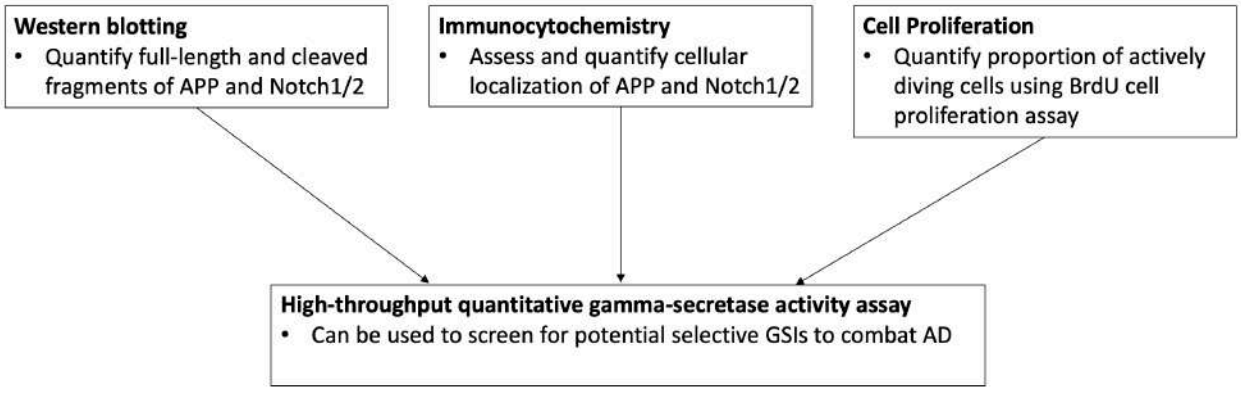

Figure 1.9: Three-part method to quantify γ-secretase activity in non-transfected SH-SY5Y human neuroblastoma cells. The highly-sensitive, high-throughput γ-secretase activity assay is based on 3 orthogonal methods used in tandem to directly measure the cleavage of both APP and Notch. These methods include: Western blotting to quantify substrates and products of the γ-cleavage of both Notch and APP; Immunocytochemistry to assess the quantity and cellular localization of Notch within or outside of the nucleus, and APP tethered or liberated from the plasma membrane; and a BrdU cell proliferation assay to quantify the level of notch-inhibition-dependent cellular differentiation occurring using different γ-secretase inhibitors.

Chapter 2.0 – Experimental Methodology

2.1 Materials

G3G4 (anti-BrdU) was deposited to the DSHB by Kaufman, S.J. (DSHB Hybridoma Product G3G4 (anti-BrdU), Iowa City, USA). Mouse polyclonal anti-APP antibody raised against the last 20 residues of the C-terminal fragment of APP was purchased from BioLegend (cat#SIG039152; San Diego, USA). sAPPα BioLegend cat#SIG39139), and sAPPβ (BioLegend cat# SIG-39138) were obtained and used during this study. Polyclonal antibodies raised against portions of the intracellular domain of Notch1 (bTAN 20) was deposited to the DSHB by Artavanis-Tsakonas, S. (DSHB Hybridoma Products bTAN 20; Iowa City, USA). Goat polyclonal secondary antibody to Rat IgG (Alexa Flour 488; ab150157) and goat anti-mouse IgG secondary antibody (Alexa Flour 568; ab175473) were purchased from AbCam (Cambridge, UK).

2.2 Collagen-coating of culture plates

In some immunofluorescence experiments, cells were plated on multi-well glass-bottom plates. In order for the cells to adhere, the glass had to be pre-coated with collagen. To do this, purified Type I collagen from bovine skin (Sigma #C4243) was used. All collagen coating procedures were done under sterile conditions in the biological safety cabinet to minimize risk of contamination. First, the collagen solution was diluted in sterile-filtered 0.1 M acetic acid to obtain a 0.1% (w/v) collagen solution. The falcon tube containing this solution was rocked for 3 hours at room temperature. Once thoroughly mixed, the solution was transferred to a glass bottle with a plastic screw cap. A layer of chloroform was carefully added to the bottom of the bottle at a volume of ~10% of the total volume of the solution. The solution was not shaken or stirred after this point and was allowed to stand overnight at 4°C. Glass-bottom wells were incubated

for 3 hours at 37°C with the collagen solution at an amount of 10 ug/cm^2. The excess fluid was then removed and the plate(s) were allowed to dry with the lids removed in the BSC for about an hour. Once dry, the lid was replaced and the plate was kept in the BSC and irradiated under UV light for 6 hours. The wells were rinsed twice with sterile-filtered PBS immediately before introducing cells.

2.3 Cell culture and drug treatments

SH-SY5Y human neuroblastoma cells (passage #12; a gift from Dr. Jeffrey A. Stuart), HEK 293 cells (passage #15; a gift from Dr. Adam J. Macneil), or HeLa cells (passage #7; a gift from Dr. Jeffrey A. Stuart) were thawed from liquid nitrogen and rapidly warmed to 37°C while gently agitating. Cells were diluted with 5 mL of warmed (37°C) Dulbecco's Modified Eagle Medium (DMEM) and spun at 240 x g for 3 minutes. The supernatant was removed and the cell pellet was resuspended in DMEM with high glucose (25 mM; 4500 mg/L), 10% fetal bovine serum, 2% nonessential amino acids, 1% penicillin/streptomycin solution (Sigma-Aldrich; St. Louis, USA). Cells were seeded at a concentration of ~2 x 10^5 cells/cm^2 on 10 cm plastic culture plates (Sarstedt; Nümbrecht, Germany). All cells were maintained at 37°C in a humidified incubator containing 5% CO_2. The media was replaced every 3-4 days.

When cellular confluency of the plate reached ~90% (3-4 days), cells were split and seeded (~2 x 10^5 cells/cm^2) on new plates. To do this, the media was removed, and the 10-cm plate was briefly rinsed with 3 mL pre-warmed sterile PBS. 3 mL of pre-warmed 0.25% trypsin/EDTA solution (Sigma-Aldrich; St. Louis, USA) was added to the plate and the cells were incubated at 37°C for 3 min. Next, adherence of the cells to the plate was assessed using a light microscope. If cells were still adherent after trypsinization, they were gently agitated by

tapping the side of the plate with a screwdriver handle. Once all cells were unadhered, the trypsin was quenched with 5 mL of pre-warmed DMEM. The cells were transferred to a falcon tube and pelleted at 240 x g for 3 min. The supernatant was decanted, and the cells were resuspended in 5 mL high-glucose DMEM containing 10% FBS, 2% NEAA, and 1% P/S by gently pipetting up and down for 1 minute. Care was taken as to minimize the formation of foam/bubbles. At this point, the cell density could be counted with a hemocytometer, and ~2 x 10^5 cells/cm^2 cells can be added to each plate containing 10 mL (10 cm plate) or 3 mL (35 mm plate) of pre-warmed media. The plates were gently swirled and placed back into the incubator.

Cells were allowed to form unhindered focal adhesions for 8 hours, after which cells were treated with either DMSO vehicle control, 10 uM DAPT, 2 uM Avagacestat, 2 uM LY-2886721 (BACE1 inhibitor), or 10 uM at-RA (positive control for Notch inhibition in BrdU assay). To do this, drugs were first dissolved in sterile-filtered DMSO at 1000x stock concentrations and frozen at -20°C. at-RA was purchased from Sigma-Aldrich (St. Louis, USA) and dissolved in sterile-filtered DMSO to a stock concentration of 10 mM (1000X). The γ-secretase inhibitor, DAPT (LY-374973), was purchased from Selleckchem (Houston, USA) and dissolved in sterile-filtered DMSO to a stock concentration of 10 mM (1000X). Selective γ-secretase inhibitor, Avagacestat (BMS-708163) was also purchased from Selleckchem (Houston, USA) and dissolved in sterile-filtered DMSO to a stock concentration of 2 mM (1000X). The potent BACE1 inhibitor LY2886721 was purchased from Caymen Chemical (Ann Arbor, Michigan). Aliquots of the dissolved drugs were stored at -20°C and thawed immediately before use. Aluminum foil was used to protect stock solutions from light exposure and prevent photo-oxidation of inhibitors or DMSO. The treatments were added by first removing the pre-existing

media from the culture plate, and briefly rinsing the plate with ~1mL of pre-warmed sterile PBS. Next, the 10 uL of the 1000X stock of each drug was added to every 10 mL of pre-warmed culture media in a falcon tube. The media (supplemented with 10% FBS, 2% NEAA, and 1% P/S) containing the drugs were gently mixed before being added to the dish. The media was replaced with supplemented media containing fresh drug every 48 hours, with the last treatment occurring either 24 or 72 hours prior to experiment termination. Cells were treated with GSIs for 120 hours (with media changes every 48 hours) before being prepped for immunocytochemical imaging or harvested for western blot. For the at-RA control treatment, the FBS concentration. In some experiments, western blot data was collected at 24 hrs, 72 hrs, and 120 hrs after initial drug treatment.

2.4 Immunocytochemistry to assess APP and Notch in the nucleus vs. the cytoplasm

Upon removal from the incubator, cells were rinsed 3 times for 5 seconds each in PBS containing protease inhibitor cocktail. Next, cells were stained in Membrite Pre-stain Solution for 5 min at 37°C. The Pre-stain solution was removed and 2X Membrite 660/680 was added to the plate and the plate was incubated for 5 min at 37°C. The stain was removed and the plates were rinsed 3 times for 5 minutes each in PBS containing protease inhibitor. Next, the cells were fixed using 200 uL 10% Neutral Formalin rocking for 10 min at room temperature. Special care was taken prior to fixation to minimize vibrational agitation and ensure cells remained adhered to the glass. Also, buffers were not pipetted directly to the glass to minimize the flow forces that may disturb cells prefixation. After 10 min, the fixative was removed, and the cells were rinsed 3 times for 5 minutes each in ice-cold PBS containing protease inhibitor. Next, to allow for antibodies to penetrate the nucleus and access nuclear antigens, cells were permeabilized for 10 minutes gently rocking at room temperature using 0.25% Triton X-100 detergent in PBS

containing protease inhibitor. Next, the cells were rinsed 3 times with PBS for 5 minutes each time. Once permeabilization buffer was rinsed away, the cells were rocked in blocking buffer: 2% skim milk powder in PBST (PBS + Tween 20) for 1 hour. Next, the cells were washed 3 times for 5 minutes each time in PBS. The primary antibodies (specific for Notch1-ICD and APP-CTF) were added to the plate at a concentration of 2 ug/mL (Notch1) and 4 ug/mL (APP-CTF) in PBST containing 2% skim milk powder. The primary antibodies were left to incubate on the plate overnight at 4°C. The following day, the primary antibody solution was removed and cells were washed 3 x 5 minutes in PBS. The secondary antibody was then added to the plate at a concentration of 0.1 ug/mL in 2% skim milk powder and gently rocked for 1 hour, under tinfoil to minimize light exposure. The plates were then washed 3 times for 5 minutes each in PBS. 1X DAPI was added to each plate and rocked for 10 min at room temperature (under tinfoil), and then the plate was washed 3 times for 5 minutes in PBS and imaged using the Zeiss Airyscan confocal fluorescence microscope.

2.5 Preparation of human cell lysates for Western blot

To harvest 10 cm plates of cells for immunoblot analysis, cells were first removed from the incubator and placed on ice. Ice-cold PBS containing protease inhibitor cocktail was used to rinse the plates 3 times for 2 minutes each time. Next, 1 mL of 1X Laemlli buffer containing protease inhibitor was placed on each dish and gently rocked on ice for 10 min. The plates were then sonicated on high 3 times for 10 seconds each time. If cells were still visibly adherent (under light microscope) then a scraper was used to scrape the cells off the bottom of the dish. The 1 mL of Laemlli buffer containing the cells was then transferred to a Pyrex glass pestle tissue grinder (Fisher Scientific) and 10 up/down strokes were employed to lyse the cells on ice, while minimizing the formation of bubbles/foam. Once homogenized, the cells were placed back

into a 1.5 mL tube and spun at 240 x g for 5 min at 4°C to pellet excess cell debris. The supernatant was collected and flash frozen in liquid nitrogen before being stored at -80°C.

2.6 Nuclear and Cytoplasmic Cell Fractionation

Alternative to the above protocol in which the protein contents are extracted from the cells indiscriminately, cell fractions containing mostly the nucleus or mostly the cytoplasm were harvested to quantify APP and Notch in specific subcellular locations. To isolate the cytoplasmic fraction, a hypotonic lysis buffer was initially used. The buffer was prepared fresh before use, only thawing and adding the PMSF and DTT immediately before use. The hypotonic lysis buffer contains 10 mM Tris-HCl (pH 7.6), 1.5 mM $MgCl_2$, 10 mM KCl, 0.5 mM Dithiothreitol (DTT), 0.2 mM Phenylmethanesulfonyl fluoride (PMSF), and 1X Protease Inhibitor cocktail (1 mM Benzamidine, 0.2 mM DTT, 0.4 ug/mL Aprotinin, 0.4 ug/mL pepstatin, 0.4 ug/mL leupeptin, and 2 ug/mL 4-benzenesulfonyl fluoride hydrochloride [AEBSF]). Cells were removed from the incubator and immediately placed on ice. They were rinsed 3X with ice-cold PBS containing protease inhibitor. Next, the PBS was decanted and 1 mL of hypotonic lysis buffer was added to each 10-cm plate. The plates containing the hypotonic lysis buffer were rocked on ice for 5-min, ensuring the entire surface of the plate was covered by buffer. Plates were then sonicated twice for 5 seconds each time, scraped, and collected into a 1.5 mL microcentrifuge tube. To increase protein concentration to appropriate ranges for SDS-PAGE, this same protein-containing buffer was then used as the hypotonic solution on an identical replicate plate. This was repeated a total of 3X so that each 1 mL of hypotonic lysis buffer contained three 10-cm plates worth of cellular material from the same treatment group. Next, the cell-containing buffer was added to a Pyrex glass pestle tissue grinder (Fisher Scientific). 5 up/down/twist strokes were used to homogenize the cells over ice, carefully as to not produce foam. The homogenate was transferred back to the

1.5 mL tube and places on ice. In between samples, the glass homogenizer was cleaned thoroughly by rinsing with dH_2O and ethanol and drying. The samples were spun at 10,000 x g for 20 min at 4°C. After spinning, the samples were placed back on ice and the supernatant, which is the isolated cytoplasmic fraction was transferred to a new pre-chilled tube and labelled. The cytoplasmic fraction was kept on ice until it was flash frozen in liquid N_2 and stored at -80°C.

To isolate the nuclear fraction from the remaining pellet, the pellet was first resuspended in ice-cold High-Salt Nuclear Extraction Buffer at a volume of ~2X the estimated volume of the pellet. In our case, the pellet was roughly 50 uL in volume, and so 100 uL of High-Salt Nuclear Extraction Buffer was used. The High-Salt Nuclear Extraction Buffer consisted of 20 mM Tris-HCl (pH 7.6), 1.5 mM $MgCl_2$, 1.4 M KCl, 0.2 mM EDTA, 25% (V/V) glycerol, 0.5 mM PMSF, 0.2 mM DTT, and 1X protease inhibitor cocktail (1 mM Benzamidine, 0.2 mM DTT, 0.4 ug/mL Aprotinin, 0.4 ug/mL pepstatin, 0.4 ug/mL leupeptin, and 2 ug/mL 4-benzenesulfonyl fluoride hydrochloride [AEBSF]). The High-Salt Nuclear Extraction Buffer was prepared fresh each time before use and the DTT and PMSF were added directly before use. The Pyrex glass tissue homogenizer was used to carefully homogenize the sample via 10 up/down/twisting strokes, being careful not to produce bubbles or foam. Next, the sample was agitated at 4°C for 30 min. The sample was then centrifuged at 21,000 x g for 40 min at 4°C. The viscous pellet was removed with a pipette and the remaining liquid in the tube is the final nuclear protein fraction. The samples were kept on ice until flash frozen and stored at -80°C. To assess the success of the nuclear/cytoplasmic fractionation, immunoblotting was performed on nuclear, cytoplasmic, or whole-cell samples using antibodies specific for proteins localized to the nucleus (Histone

Deacetylase-2; HDAC2), cytoplasm (Heat Shock Protein-90; HSP90), or cellular membranes (Epidermal Growth Factor Receptor; EGFR).

2.7 Total Protein Quantification

To ensure minimal variability in total protein loaded between wells on SDS-PAGE, the Coomassie-based total protein quantification assay (Noaman & Coorssen, 2018) was compared with the standard Bicinchoninic acid (BCA) protein quantification assay (Smith *et al*., 1985), while also comparing Bovine Serum Albumin (BSA) (Sigma-Aldrich; St. Louis, USA) and Tubulin (Cytoskeleton Inc; Denver, USA) protein standards. Ultimately, the BSA protein standard with the Coomassie-based protein quantification method yielded the lowest variability in total protein loaded between samples on SDS-PAGE and was used to quantify protein samples to normalize total protein quantity between wells for Immunoblotting.

2.7.1 Calibration of Protein Standard

To make the BSA (1 mg/mL) and Tubulin (1 mg/mL) protein standard stock solutions, the the purified proteins were first weighed and added to distilled water to a concentration of 2 mg/mL. The concentrations of these solutions were then calibrated and adjusted to 1 mg/mL using the Beer-Lambert Equation:

$$A_{280} = ELc$$

where A_{280} is the absorbance of 280 nm light by the sample; E is the extinction coefficient of the protein ($E_{a\text{-}tubulin} = 1.020$; $E_{b\text{-}tubulin} = 1.018$; $E_{BSA} = 0.646$); L is the pathlength of light in the spectrophotometer; and c is the concentration of the protein sample. The BSA and Tubulin samples were diluted to 0.6 mg/mL and loaded into the spectrophotometer. Each absorbance value was collected in duplicate and averages were used in the Beer-Lambert calculations. The

concentrations attained from this method were used to calculate the stock concentrations of the protein samples before proceeding with the protein quantification assays.

2.7.2 Copper-chelation-based Bicinchoninic acid (BCA) Assay

A BSA or Tubulin standard curve consisted of serial dilutions of 2 ug/uL, 1 ug/uL, 0.5 ug/uL, 0.25 ug/uL, 0.125 ug/uL, 0.06 ug/uL, 0.03 ug/uL, and 0 ug/uL (dH_2O). Once the standard protein dilutions were made, the samples being assessed were all diluted 1/20 with distilled water to make 60 uL of each diluted sample. Next, 10 uL of each standard dilution and sample dilution was added in triplicate to the 96-well plate. Next, 200 uL of 50:1 BCA:$CuSO_4$ was added to each well that contained a sample. The plate was wrapped with plastic wrap to avoid evaporation and incubated at 37°C for 30 min. After incubating, the plastic wrap was removed and the absorbance at 562 nm was read using a 96-well plate reader. The standard curve trendline equation was used to calculate the concentrations of each of the samples. Once calculated, the samples were all normalized to the same concentration (~1mg/mL).

2.7.3 Coomassie-based solid-phase protein assay

A BSA or Tubulin protein standard was also used in this quantification assay to make a standard curve. 0.5 mg/mL, 0.4 mg/mL, 0.3 mg/mL, 0.2 mg/mL, 0.1 mg/mL, and 0.05 mg/mL samples were all made to a volume of 100 uL each. 1/5, 1/10, and 1/20 dilutions to a volume of at least 10uL in 1X Laemlli buffer were made for each sample. Next, filter paper was cut to size and sandwiched between a steel 96-hole plate and the bottom of a 96-well plastic plate. This created a template apparatus to blot the samples onto the filter paper with uniform size and spaces between samples. 1 uL of each standard and sample was blotted in triplicate onto the filter paper, without stabbing the pipette tip into the filter paper. Once finished blotting and all of the blots had dried, the filter paper was placed in 100% Methanol and rocked in a clean glass

container for 5 minutes. After fixation, the filter paper was allowed to dry. Drying was sometimes catalyzed by gently using an air hose to create airflow above the filter paper. In the meantime, fresh Coomassie stain was made by combining reagents to create a final stain consisting of 10% NH_4SO_4, 2% H_2PO_4, 0.1% G250 Coomassie; and 20% Methanol. This stain was made immediately before use and the filter paper was added to the stain once completely dried of methanol. The filter paper rocked in the Coomassie stain for 10 minutes at room temperature. The filter paper was then de-stained with ddH_2O for 5 washes, 5 minutes each wash. The filter paper was flipped at least twice in the washing process to ensure de-staining completion. The filter paper was allowed to dry and Coomassie signal was imaged on the BioRad calibrated densitometer. The concentrations of each sample could be calculated by using the standard curve trendline equation. Background was calculated for each blot separately by choosing two unblotted regions adjacent to each sample and subtracting the average background signal/mm^2 from each sample value. Once the total protein concentrations of the samples had been determined, the concentrations were normalized to produce 1X laemlli reducing buffered 1 mg/mL samples. The samples were boiled for 5 minutes at 100°C and loaded into the gel for SDS-PAGE.

2.8 Western blotting

2.8.1 Gel Composition

10% acrylamide tris-glycine 1 mm or 1.5 mm gels were casted and used for SDS-PAGE. On occasion, 7.5/15% acrylamide tris-glycine gradient gels were produced to get better resolution of both high- and low-molecular weight proteins in the same gel.

2.8.2 SDS-PAGE

10X Tris/glycine gel running buffer stock was prepared to contain 250 mM Tris base, 1.92 M glycine, and 1% SDS. Transfer buffer was prepared to contain 25 mM Tris Base, 192 mM Glycine, and 20% Methanol.

1X tris/tricine (optimized for improving resolution of low molecular weight APP fragments) or tris/glycine running buffer was prepared fresh before each use. Gels ran at 120V for 3 min, and then 90V until completion (~1.5 hours) at room temperature. The protein was transferred onto nitrocellulose with a pore-size of 0.2 um in 1X transfer buffer containing 20% Methanol at 100 V for 1 hr at room temperature. The membranes were placed face-up in separate containers and blocked with 10% skim milk in TBST, gently agitated for 1 hour. The membranes were then rinsed 3 X 5 minutes with TBST. The primary antibodies were added according to the manufacturer's recommended concentration (0.2 – 2 ug/mL) and blocked in either 5% BSA in TBST or 5% skim milk in TBST overnight at 4°C. The membranes were rinsed 3 X 5 min in TBST and the secondary antibodies were diluted according to the manufacturer's recommendations (1:2000 – 1:10,000) in 2% skim milk in TBST. The membranes were rocked in their respective secondary antibody solution for 1 hour at room temperature. The membranes were once again rinsed 3 X 5 minutes. Perkin-Elmer's HRP substrate Western Lightning Plus reagents were mixed 1:1 and rocked on the membranes for 1 minute, according to the manufacturer's instructions. The "auto-expose optimal" setting was used to determine optimal exposure on the BioRad detector.

Post-transferred gels were immediately placed in fixative solution (10% Methanol, 7% Acetic Acid) for at least 2 hours before rocking in freshly made Coomassie G250 stain for at

least 20 hours. The gels were then destained by rinsing 5 times with ddH_2O for 20 minutes each rinse, and imaged on the BioRad Calibrated Densitometer.

Post-blotted membranes were rocked overnight in Ponceau S stain at room temperature before destaining by rinsing 3 times with dH_2O and imaged on the BioRad Calibrated Densitometer.

2.8.3 Analysis of Western blot

Western blots were analysed using Image Lab software from BioRad. If the variability between lanes on ponceau was greater than 10%, western blot bands were normalized to the relative total protein loaded according to the Ponceau S staining. In some cases, the treatment groups were normalized to the intensity of the DMSO control group and values are presented as ratios relative to the control.

2.9 Immunofluorescence and Bromo-deoxyuridine (BrdU) staining

The protocol for treatment of cells with GSI's started with the initial supplementation of media with either DMSO, 10 uM DAPT, 2 uM Avagacestat, or 10 uM at-RA. The media was replaced with fresh media containing drug every 48-hours, with the last media replacement occurring 24 hours prior to cell harvesting (western blot) or fixation (immunofluorescent imaging; *Figure 3.21*).

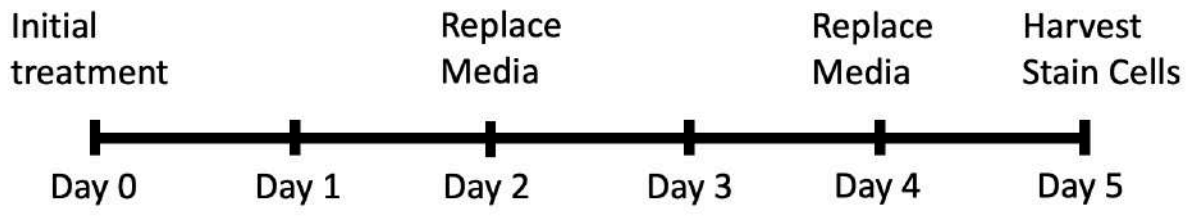

Figure 2.1: Treatment protocol timeline. Cells were initially treated with GSIs on Day 0 and drug-containing media was replaced every 48 hours. After 120 hours, cells were fixed or harvested. In this experiment, the media was last replaced 24 hours prior to fixation/harvesting.

In some experiments in which cells were co-immunostained for APP and Notch1, the replacement of the media with fresh media containing fresh GSIs on Day 4 was missed (*Figure 3.31*). The rest of the experiment was carried on as normal. The only difference being that the last drug replacement occurred 72 hours prior to fixation instead of 24 hours prior.

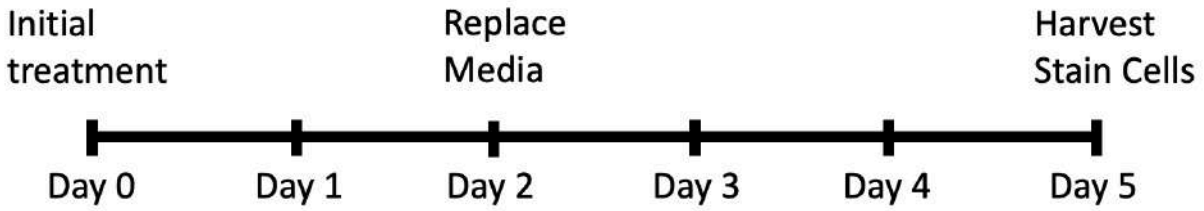

Figure 2.2: Alternate treatment protocol timeline. Cells were initially treated with GSIs on Day 0 and drug-containing media was replaced after 48 hours. After 120 hours, cells were fixed or harvested. In this experiment, the media was last replaced 72 hours prior to fixation/harvesting.

After 120 hours of treatment with the various GSIs, cells plated on 1.0 mm thick glass-bottom Mattek imaging plates were fixed and stained according to the following protocol. First, the cell culture media was decanted and cells were rinsed three times with PBS. After removing the final PBS wash, cells were incubated in 10% neutral formalin for 10 minutes. After 10 minutes, the neutral formalin was decanted and cells were rinsed while rocking three times with PBS for 5 minutes each rinse. Once fixed, cells were permeabilized by adding PBS with 0.25% Triton X-100 to the plate and rocking for 10 minutes. The solution was removed after 10 minutes and once again the cells were rinsed with PBS three times for 5 minutes each time. Next, a blocking solution was added to the plate consisting of 2% skim milk powder and 0.1% Tween-20 in PBS. Cells were rocked at room temperature for 1 hour with the blocking solution. Next, the blocking solution was removed and cells were rinsed with PBS three times for 5 minutes each time. Primary antibodies were diluted to 5 ug/mL in 2% skim milk, 0.1% Tween-20 PBS

and exposed to cells overnight at 4°C. In the case of the immunofluorescent staining for Notch and APP, the rat Notch1 (bTan-20) or rat Notch2 (C651.6DbHN) primary monoclonal antibodies combined with the mouse APP-CTF C-terminal fragment monoclonal antibody (C1/6.1) from BioLegend were used. The next morning, the primary antibody solution was removed from the plate and the plate was rinsed three times with PBS for 5 minutes each time while rocking. Anti-rat AlexaFlour 488 and anti-mouse Alexaflour 568 secondary antibodies were diluted 1:2000 in PBS containing 2% skim milk and 0.1% Tween-20, and rocked on the plate for 1 hour. Cells were then rinsed three times for 5 minutes each with PBS, and counter stained using 1X DAPI combined with 1X Cell Mask Deep Red stain for 10 minutes. Lastly, cells were rinsed again three times for 5 minutes each time. Cells were then ready for imaging on the Zeiss fluorescent microscope.

The BrdU assay was identical to the above immunostaining protocol, except for a 24-hour pretreatment with sterile-filtered 10 uM BrdU treatment to the media (from a 10 mM BrdU stock dissolved in water) before proceeding with cell fixation. For this assay, the mouse G3G4 anti-BrdU monoclonal antibody from the DSHB was used at a concentration of 5 ug/mL.

2.10 Quantifying immunofluorescent images by design of a series of ImageJ Macros

ImageJ macros were made to allow for the high-throughput quantification of a mass number of images. These macros are available in the appendix at the end of this thesis document. To quantify Notch activation, the pixel intensity of Notch signal in the nucleus was expressed as a ratio of nuclear Notch signal to the total cellular Notch signal of each image. In a similar fashion to Notch, for APP quantification, non-membrane-associated APP signal (subtraction of pixels positive for Cell Mask) was compared to total cellular APP signal and expressed as a ratio.

For the BrdU cell proliferation assay analysis, nuclei containing above-threshold BrdU signal were counted and expressed as a fraction of total nuclei.

For each treatment condition, three individual glass-bottom plates were prepared, representing biological triplicates. A minimum of 4 positions in the XY plane were captured per plate, each captured as a Z-stack spanning the depth of the cells within the field of view. The integrated density values from the images across the Z-axis were summated and graphically presented as a single data point. Therefore, $n \geq 12$ for each treatment condition.

Chapter 3: Results

3.0 SH-SY5Y human neuroblastoma cells treated with 10 uM at-RA for 120 hours experience morphological changes

As a positive control to assess neuronal differentiation, we wanted to validate similar conditions as those proposed by Encinas *et al*. (2000) as sufficient to induce neuronal differentiation of SH-SY5Y human neuroblastoma cells. SH-SY5Y cells were treated with 10 uM at-RA for 120 hours, changing the media every 48 hours. After 120 hours, cells were fixed and stained. Clear morphological differences can be observed between the at-RA-treated cells and the DMSO control-treated cells (*Figure 3.1*). SH-SY5Y cells treated with at-RA elongate and extend neurites. However, not all cells appear to undergo this transformation.

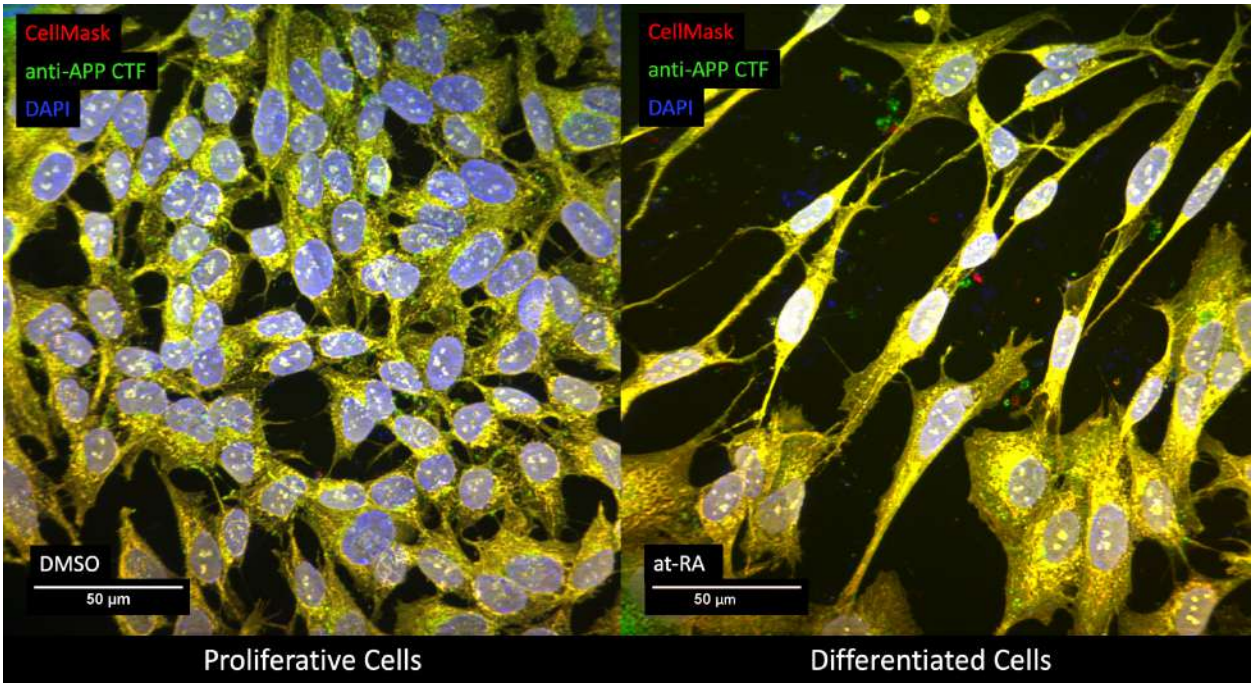

Figure 3.1: Morphological change observed between 5-day vehicle-control treated cells and 5-day 10 uM at-RA-treated SH-SY5Y cells. By treating with 10 uM all-trans retinoic acid for 120 hours, the results of Encinas *et al.*, 2000 were verified. Even though subsequent treatment with neurotrophic factors was not performed, changes in cell morphology suggest that these SH-SY5Y neuroblastoma cells may have at least partially differentiated into a neuronal-like cell type.

3.1 SH-SY5Y Human Neuroblastoma Cells last treated with GSIs 24 hours before harvesting experience inhibition of γ-secretase cleavage of APP but not Notch

The protocol for treatment of cells with GSI's started with the initial supplementation of media with either DMSO, 10 uM DAPT, 2 uM Avagacestat, or 10 uM at-RA. The media was replaced with fresh media containing drug every 48 hours, with the last media replacement occurring 24 hours prior to cell harvesting (western blot) or fixation (immunofluorescent imaging; *Figure 3.21*).

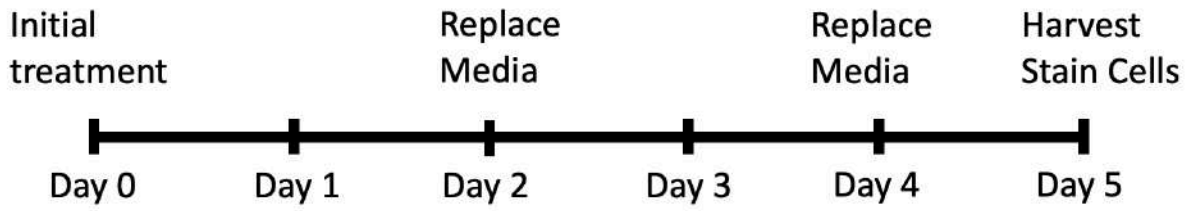

Figure 2.1: Treatment protocol timeline. Cells were initially treated with GSIs on Day 0 and drug-containing media was replaced every 48 hours. After 120 hours, cells were fixed or harvested. In this experiment, the media was last replaced 24 hours prior to fixation/harvesting.

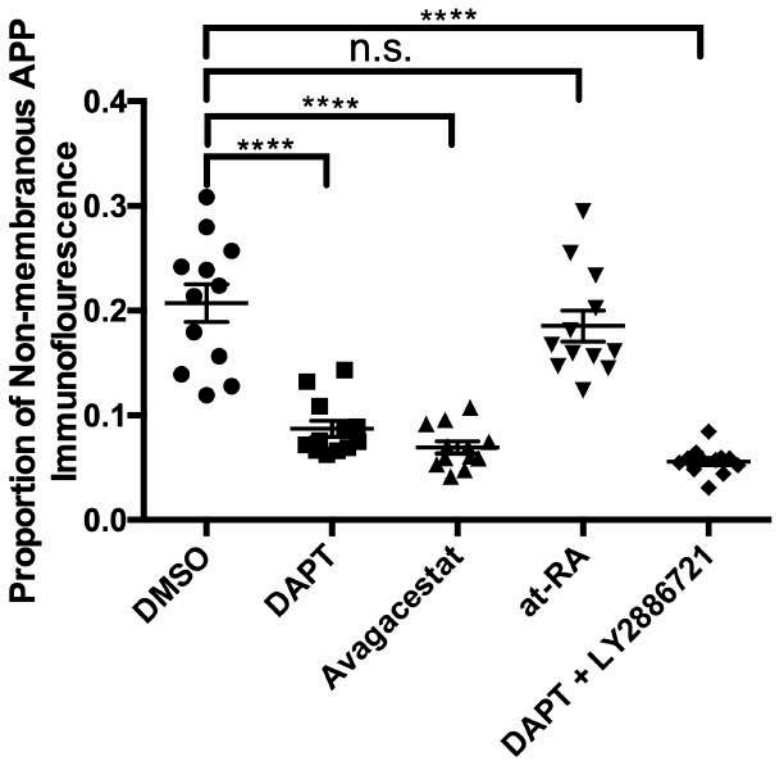

Figure 3.22: Immunocytochemistry analysis for non-membanous APP-CTF signal in SH-SY5Y cells treated with DMSO, 10 uM DAPT, 2 uM Avagacestat, 10 uM at-RA, or 2 uM DAPT + 10 uM LY2886721 (BACE1 Inhibitor) for 120 hours, with the last treated media change occurring 24 hours prior to fixation. Ordinary one-way ANOVA and Dunnett's Multiple Comparison's Test was used for statistical analysis. Three biological replicates were analyzed per treatment group.

When analysing the images to calculate the ratio of APP signal not spatially associated with membrane signal from Cell Mask (*Figure 3.22*), the non-membranous (largely cytosolic) APP signal ratio decreased between DMSO-treated SH-SY5Y cells (0.207 ± 0.018; n = 12) and DAPT-treated cells (0.087 ± 0.008; n = 12; $p < 0.0001$) as well as with Avagacestat-treated cells (0.069 ± 0.006; n = 12; $p < 0.0001$). No significant differences were observed between DMSO-treated cells and at-RA-treated cells (0.185 ± 0.015; n = 12; $p = 0.47$). The most potent GSI treatment group in terms of APP processing inhibition was the combination of DAPT and the BACE1 inhibitor LY2886721 (0.056 ± 0.004; n = 12; $p < 0.0001$).

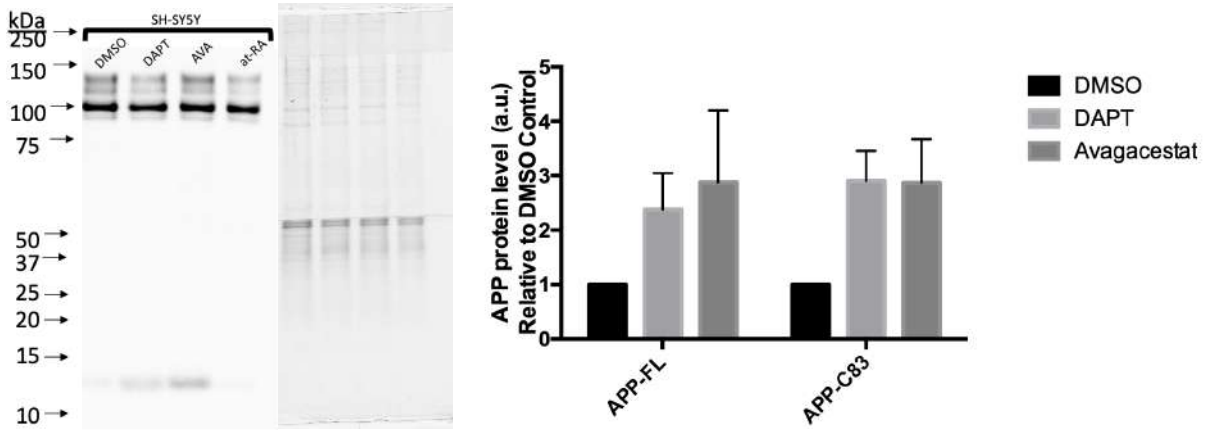

Ponceau

Figure 3.23: Western blot for APP-CTF in SH-SY5Y cells treated with DMSO, 10 uM DAPT, 2 uM Avagacestat, or 10 uM at-RA for 120 hours, with the last treated media change occurring 24 hours prior to cell harvesting. Five biological replicates were analyzed per treatment group.

To validate our results from the immunostains, we western blotted SH-SY5Y cell lysates for APP-CTF using the same drug treatments. We observed an increase in intensity of a ~13-kDa band in response to γ-secretase inhibition using both DAPT and Avagacestat (*Figure 3.23*). The accumulation of a 13-kDa band on Western blot in response to γ-secretase inhibition is well characterized in the literature (for example, Hemming *et al*., 2008). This research group also used Mass Spectrometry to validate the identity of this fragment as C83 (cleaved by α-secretase), the immediate APP substrate of γ-secretase. Although the γ-secretase APP product, AICD50 should theoretically be about 10 kDa on Western blot, and diminish in response to γ-secretase inhibition, it was not detected, a result that is consistent with widespread Western blot data across the literature (Chang *et al*., 2003; Hemming *et al*., 2008; Zhang *et al*., 2017). This may be because of its relatively rapid degradation and turnover once released from the membrane. Although no significant changes were observed in full-length APP between the control or treatment groups, the accumulation of ~13 kDa APP-CTF in response to DAPT and Avagacestat

treatments was observed. This result is widely observed in the literature (Chang *et al*., 2003; Hemming *et al*., 2008; Zhang *et al*., 2017) and is the ADAM-cleaved APP cleavage fragment APP-C83. Despite efforts to optimize low-molecular weight separation (tris-tricine; longer run time, 5% acrylamide) and transfer conditions (20% methanol buffer; 0.2 uM pore-size nitrocellulose), western blot bands corresponding to BACE cleavage fragments APP-C89/C99 were not detected in the SH-SY5Y lysates, nor were appreciable levels of sAPP-β (data not shown), possibly because the proportion of β-secretase cleaved APP is much lower than the α-secretase cleaved form.

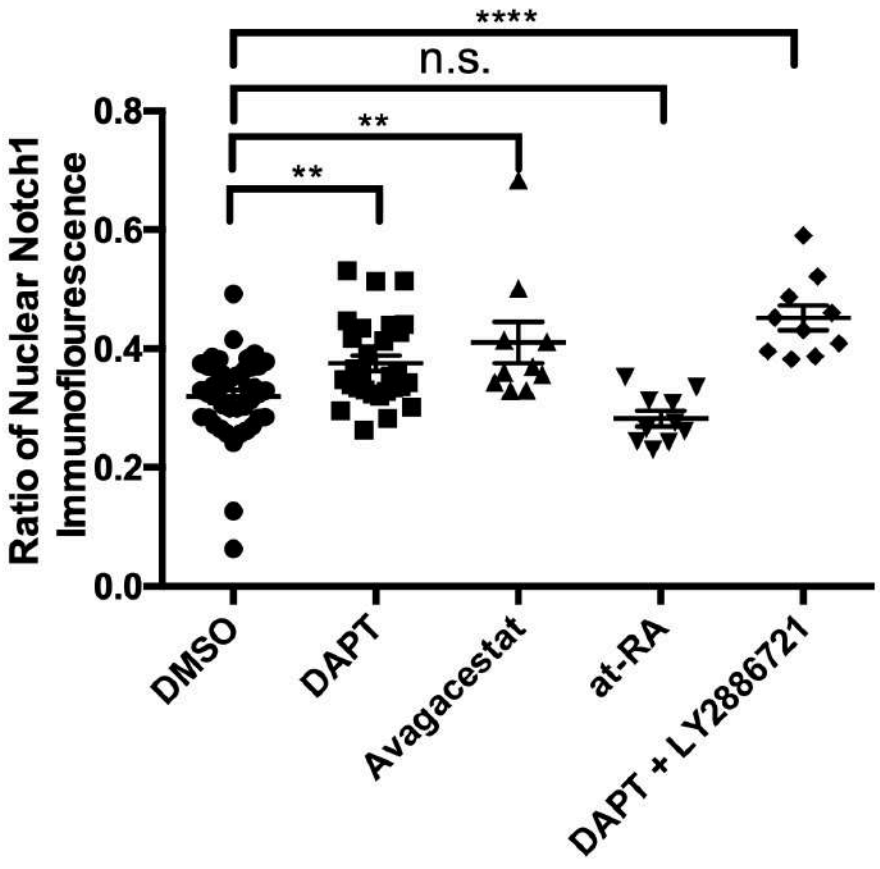

Figure 3.24: Immunocytochemistry analysis for nuclear Notch1 ratio in SH-SY5Y cells treated with DMSO, 10 uM DAPT, 2 uM Avagacestat, 10 uM at-RA, or 2 uM DAPT + 10 uM LY2886721 (BACE1 Inhibitor) for 120 hours, with the last treated media change occurring 24 hours prior to fixation. A minimum of 10 z-stacks were captured across three biological replicates. Ordinary one-way ANOVA and Dunnett's Multiple Comparison's Test was used for statistical analysis. Adjusted p-values: 0.0068 (DMSO:DAPT), 0.0023 (DMSO:Avagacestat), 0.4014 (DMSO:at-RA), <0.0001 (DMSO: DAPT + LY2886721).

To assess the level of γ-secretase activity on Notch1 processing, we used immunocytochemistry to quantify the proportion of Notch1 in the nucleus vs. whole-cell Notch1 using the monoclonal DSHB antibody with an epitope on the C-terminus of the ICD of Notch1 (*Figure 3.24*). These cells were co-stained with both anti-APP and anti-Notch antibodies. We hypothesized that cells treated with DAPT and Avagacestat would show significant decreases in nuclear Notch1 due to the inhibition of γ-secretase to cleave Notch from the membrane prior to its localization to the nucleus. In SH-SY5Y cells, we found significant increases of nuclear Notch1 signal between DMSO-treated cells (control) and cells treated with DAPT, Avagacestat, and DAPT + LY2886721 for 120 hours. Treatment with γ-secretase inhibitors DAPT (0.376 ± 0.014), Avagacestat (0.410 ± 0.036), and the combination of DAPT and LY2886721 (0.452 ± 0.021) all significantly increased the proportion of nuclear Notch1 signal when compared with the DMSO vehicle control (0.320 ± 0.011). Treatment with at-RA showed no change in proportion of Notch1 fluorescence signal in the nuclei (0.282 ± 0.011; *Figure 3.24*).

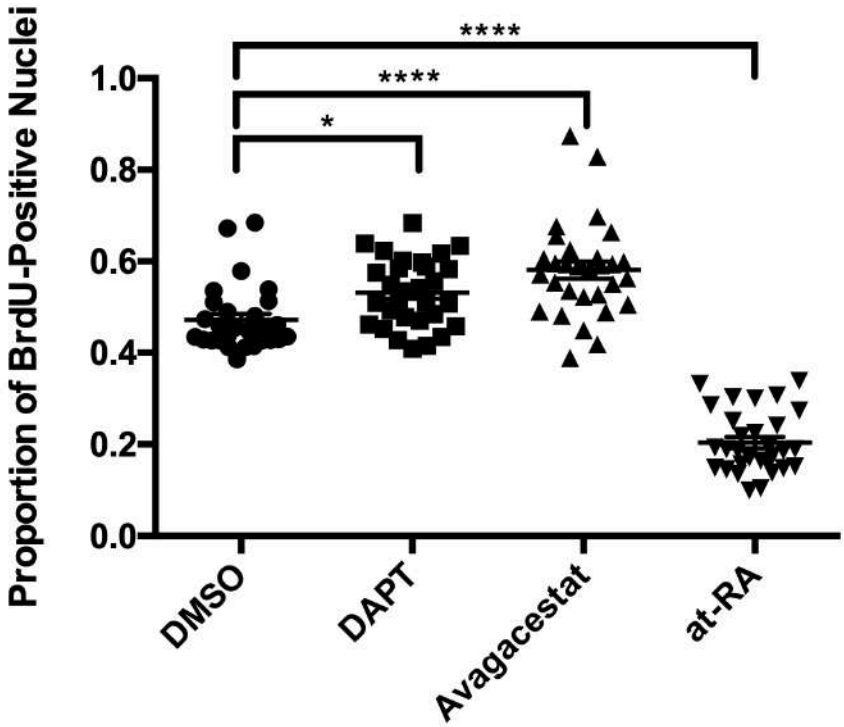

Figure 3.25: Immunocytochemistry stainings for BrdU in SH-SY5Y cells treated with DMSO, 10 uM DAPT, 2 uM Avagacestat, or 10 uM at-RA for 120 hours, with the last treated media change occurring 24 hours prior to fixation. BrdU was added 24 hours prior to cell fixation. Ordinary one-way ANOVA and Dunnett's Multiple Comparison's Test was used for statistical analysis. A minimum of 10 images were captured across 3 biological replicates per treatment group.

Complimenting the unexpected results of the effect of GSI treatment on proportion of nuclear Notch1 signal, the BrdU nuclear incorporation rate (*Figure 3*.25) significantly increases with DAPT (0.510 ± 0.017) and Avagacestat (0.614 ± 0.031), in comparison to DMSO-treated cells (0.464 ± 0.013). The at-RA-treated cells represent the positive control for successful Notch inhibition, showing a robust decrease in proportion of BrdU-positive nuclei (0.176 ± 0.015).

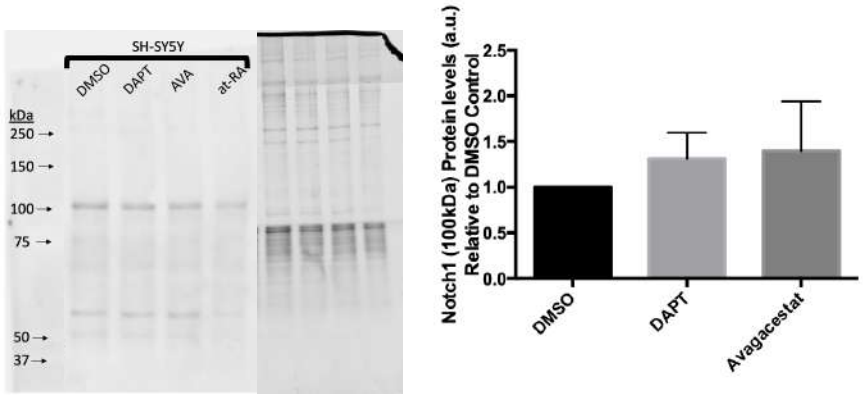

Figure 3.26: Western blot for Notch1 in SH-SY5Y cells treated with DMSO, 10 uM DAPT, 2 uM Avagacestat, or 10 uM at-RA for 120 hours, with the last drug-treated media replacement occurring 24 hours prior to cell harvesting. Blot is shown on the left and Coomassie-stained post-transfer gel is shown on the right. Three biological replicates were analysed per treatment group.

In tandem with the immunostaining and BrdU cell proliferation assay, Western blotting of total cell lysate showed no significant differences for Notch1 content between treatment and control groups when SH-SY5Y cells were treated with DAPT or Avagacestat for 120 hours and the drug was last replaced 24 hours prior to harvesting the cells (*Figure 3.26*).

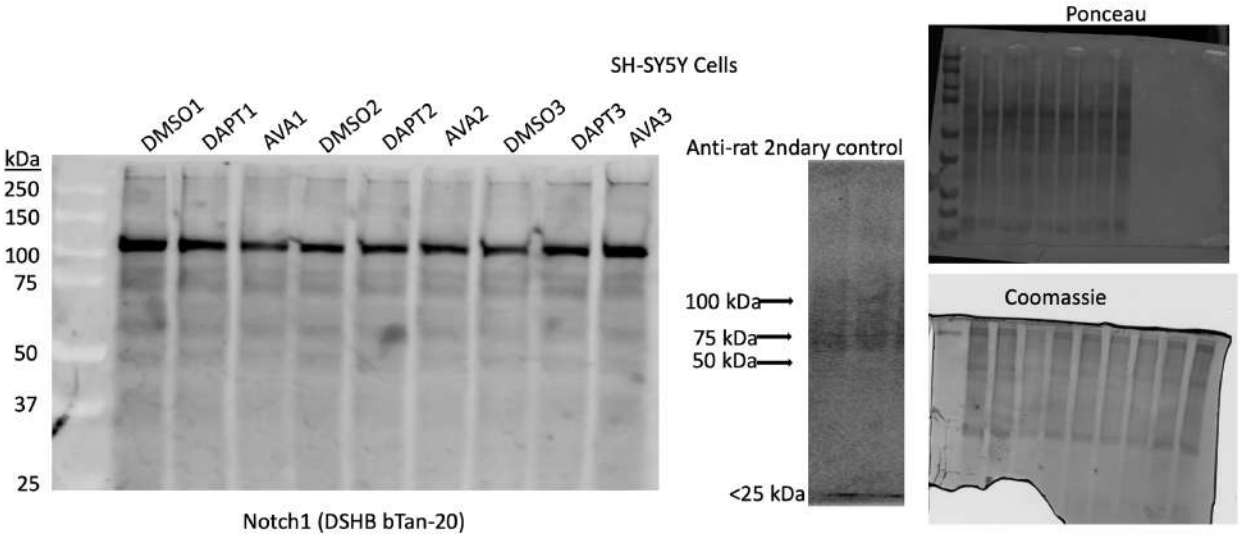

Figure 3.27: Western blot for Notch1 in SH-SY5Y cells treated with DMSO, 10 uM DAPT, 2 uM Avagacestat, or 10 uM at-RA for 120 hours, with the last drug-treated media replacement occurring 24 hours prior to cell harvesting. Transfer conditions were slightly modified to favour the transfer of larger proteins: Methanol in transfer buffer was reduced from 20% to 15%, and transfer time was extended by 10% (66 minutes instead of 60 minutes). n = 3 per treatment group.

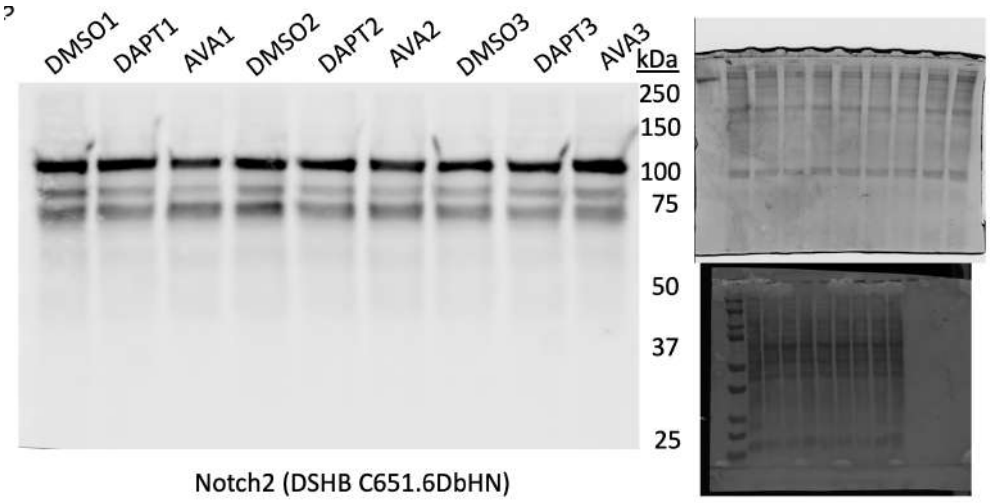

Figure 3.28: Western blot for Notch2 in SH-SY5Y cells treated with DMSO, 10 uM DAPT, 2 uM Avagacestat, or 10 uM at-RA for 120 hours, with the last drug-treated media replacement occurring 24 hours prior to cell harvesting. Transfer conditions were slightly modified to favour the transfer of larger proteins: Methanol in transfer buffer was reduced from 20% to 15%, and transfer time was extended by 10% (66 minutes instead of 60 minutes). n = 3 per treatment group.

To verify the above results, the western blot was repeated in biological triplicate for separate pools of SH-SY5Y cells with antibodies specific for both Notch1 and Notch2 (*Figure 3.27*; *Figure 3.28*). We verified that there were no significant differences in total Notch1/2 levels in the absence of presence of DAPT or Avagacestat. Furthermore, a secondary control experiment in which the primary antibody was omitted, was used to verify that the bands appearing on the blot at ~100 kDa were not a result of off-target binding of the secondary antibody. The secondary control revealed a single faint band around ~25 kDa that is likely a result of the secondary antibody binding to protein other than the primary antibody (*Figure 3.27*).

3.2 SH-SY5Y Human Neuroblastoma cells last treated 72 hours before harvesting experience inhibition of γ-secretase cleavage of Notch but not APP

To test whether the time between the last media change and cell harvesting/fixation effects the gamma-secretase activity on APP and Notch, cells were co-immunostained for APP and Notch1, except the replacement of the media with fresh media containing fresh GSIs on Day 4 was omitted (*Figure 3.31*). The rest of the experiment was carried on as normal. The only difference being that the last drug replacement occurred 72 hours prior to fixation instead of 24 hours prior.

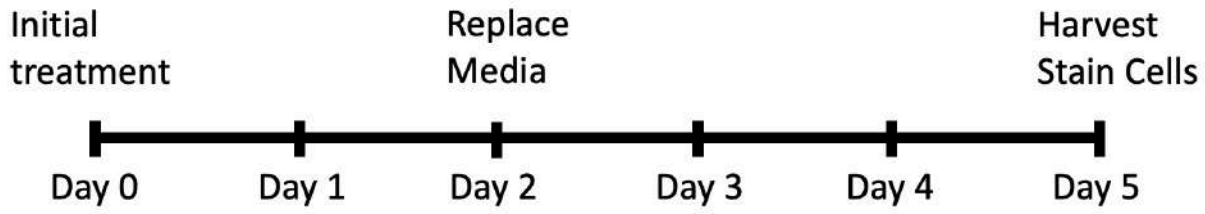

Figure 2.2: Alternate treatment protocol timeline. Cells were initially treated with GSIs on Day 0 and drug-containing media was replaced after 48 hours. After 120 hours, cells were fixed or harvested. In this experiment, the media was last replaced 72 hours prior to fixation/harvesting.

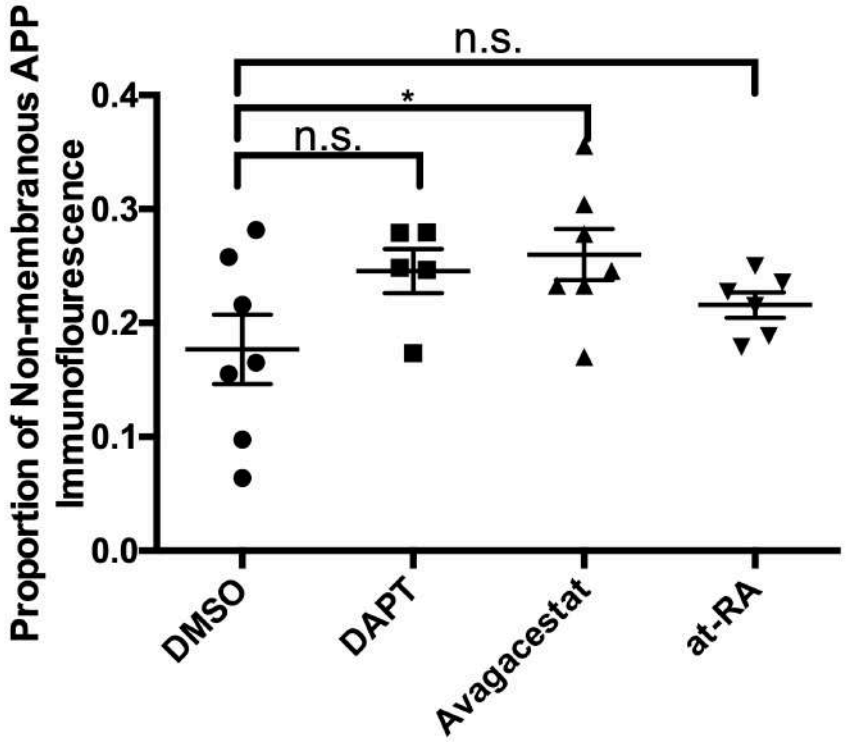

Figure 3.32: Immunocytochemistry analysis for non-membrane-associated APP-CTF in SH-SY5Y cells treated with DMSO, 10 uM DAPT, 2 uM Avagacestat, 10 uM at-RA, or 2 uM DAPT + 10 uM LY2886721 (BACE1 Inhibitor) for 120 hours, with the last treated media change occurring 72 hours prior to fixation. Ordinary one-way ANOVA and Dunnett's Multiple Comparison's Test was used for statistical analysis. A minimum of 5 images were captured across one imaging plate per treatment group.

Interestingly, treatment with Avagacestat increased the level of non-membranous APP signal (0.260 ± 0.022), while DAPT (0.245 ± 0.019) and at-RA (0.216 ± 0.011) did not, compared to the DMSO control (0.177 ± 0.030; *Figure 3.33*). The effect of replacing the drug-containing media 72 hours versus 24 hours before fixation changed the effect of the inhibitors on APP cleavage (*Figure 3.32*). Instead of the inhibitors decreasing the levels of non-membranous APP-CTF, the trend reverses. Although not statistically significant ($p = 0.137$), DAPT unexpectedly raises the level of APP-CTF not associated with membranes, while Avagacestat significantly increases ($p = 0.037$) cleaved APP-CTF levels. At-RA does not significantly affect the level of cleaved APP-CTF ($p = 0.497$).

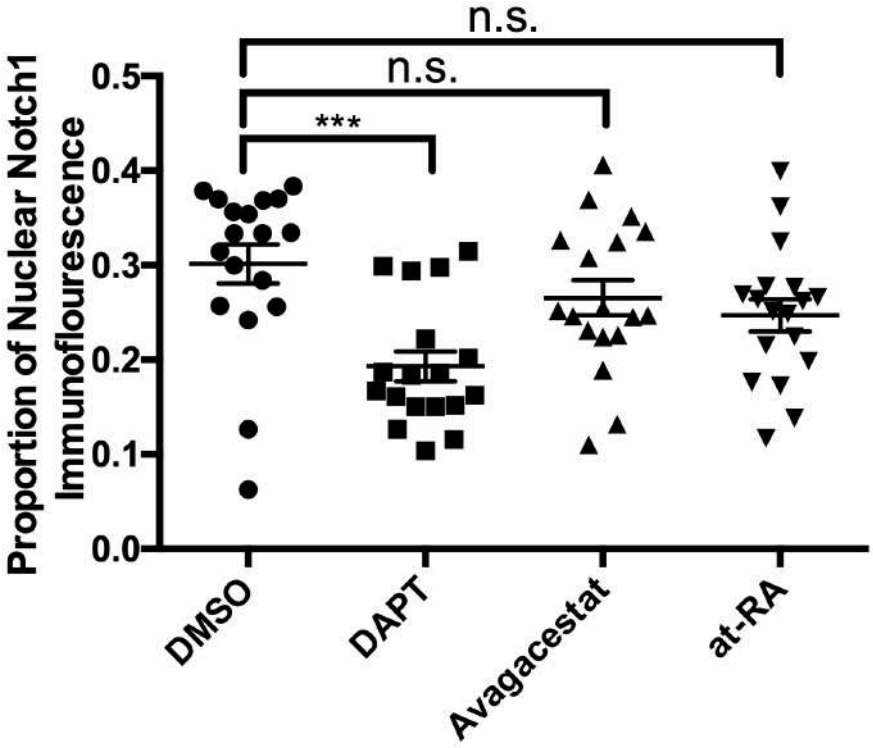

Figure 3.33: Immunocytochemistry analysis for nuclear Notch1 ratio in SH-SY5Y cells treated with DMSO, 10 uM DAPT, 2 uM Avagacestat, or 10 uM at-RA for 120 hours, with the last treated media change occurring 72 hours prior to fixation. Ordinary one-way ANOVA and Dunnett's Multiple Comparison's Test was used for statistical analysis. A minimum of 5 images was captured for each of the three biological replicates per treatment group,

In addition to the opposite effects of APP cleavage when the drug-containing media was replaced 72 hours prior to fixation, immunostaining analysis revealed that the ratio of Notch1 in the nucleus of SH-SY5Y cells decreases with DAPT (0.193 ± 0.016), but not with Avagacestat (0.265 ± 0.019) in comparison to the DMSO-control (0.301 ± 0.021). At-RA also did not affect the ratio of Notch1 signal in the nucleus.

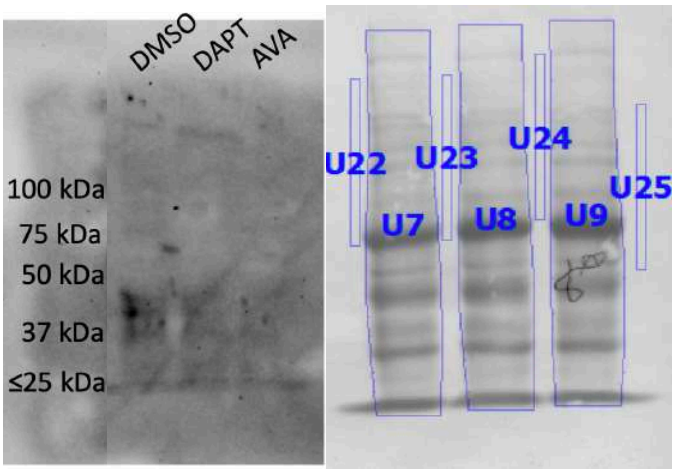

Figure 3.34: Western blot for activated-Notch1 (γ-cleaved) treated with DMSO, 10 uM DAPT, or 2 uM Avagacestat for 120 hours, last treated 72 hours before harvesting. Blue boxes U7, U8, and U9 indicate region used to quantify ponceau total protein stain signal. Blue boxes 22, 23, 24, and 25 indicate boxes used to calculate local background that was subtracted from signal calculations. n = 1 per treatment condition.

Western blots for APP under this condition would need to be done to validate this finding (*Figure 3.34*). However, Notch1 blots of SH-SY5Y cells using an antibody that only recognizes the γ-cleaved NICD confirmed that when the cells are last treated 72 hours before harvesting, the levels of Notch1 ~37 kDa, ~40 kDa, and ~45 kDa all decrease in abundance with DAPT and Avagacestat treatment. The ~100 kDa full-length NICD was not detected, presumably because of the low endogenous expression levels in SH-SY5Y cells paired with suboptimal transfer conditions for larger proteins. This observation is supported by the detection of a previously-observed dominant ~45 kDa Notch1 band in SH-SY5Y cells using similar transfer conditions with a Notch1 antibody with a unique epitope site.

Overall, a trend that approaches somewhat of a reciprocal potency shift was observed for SH-SY5Y cells treated with GSIs last administered 24-hours before fixation (APP processing inhibited; Notch processing promoted); versus 72-hours prior to fixation (APP processing promoted; Notch activation inhibited).

3.3 α-secretase Activity levels correspond to a γ-secretase inhibitor potency shift in SH-SY5Y cells treated with GSIs 24 hours, 72 hours, or 120 hours before harvesting

sAPP-α is the C83 complimentary N-terminal product that results from α-secretase cleavage. It has been found that cleavage by α-secretase is strongly regulated by γ-secretase activity, and that protein levels of the proteolytic fragment, sAPP-α increase in response to γ-secretase inhibition (Siegenthaler *et al*., 2016). As a statistically-independent means to test the apparent APP potency shift that occurs with the γ-secretase inhibitors with the last media change either 24-hours or 72-hours before cell harvesting, sAPP-α and full-length/processed APP protein levels were assessed when 10 uM of DAPT or 2 uM of Avagacestat were supplemented in media for SH-SY5Y cells either 24 hours, 72 hours, or 120 hours prior to cell harvesting (*Figure 3.41*).

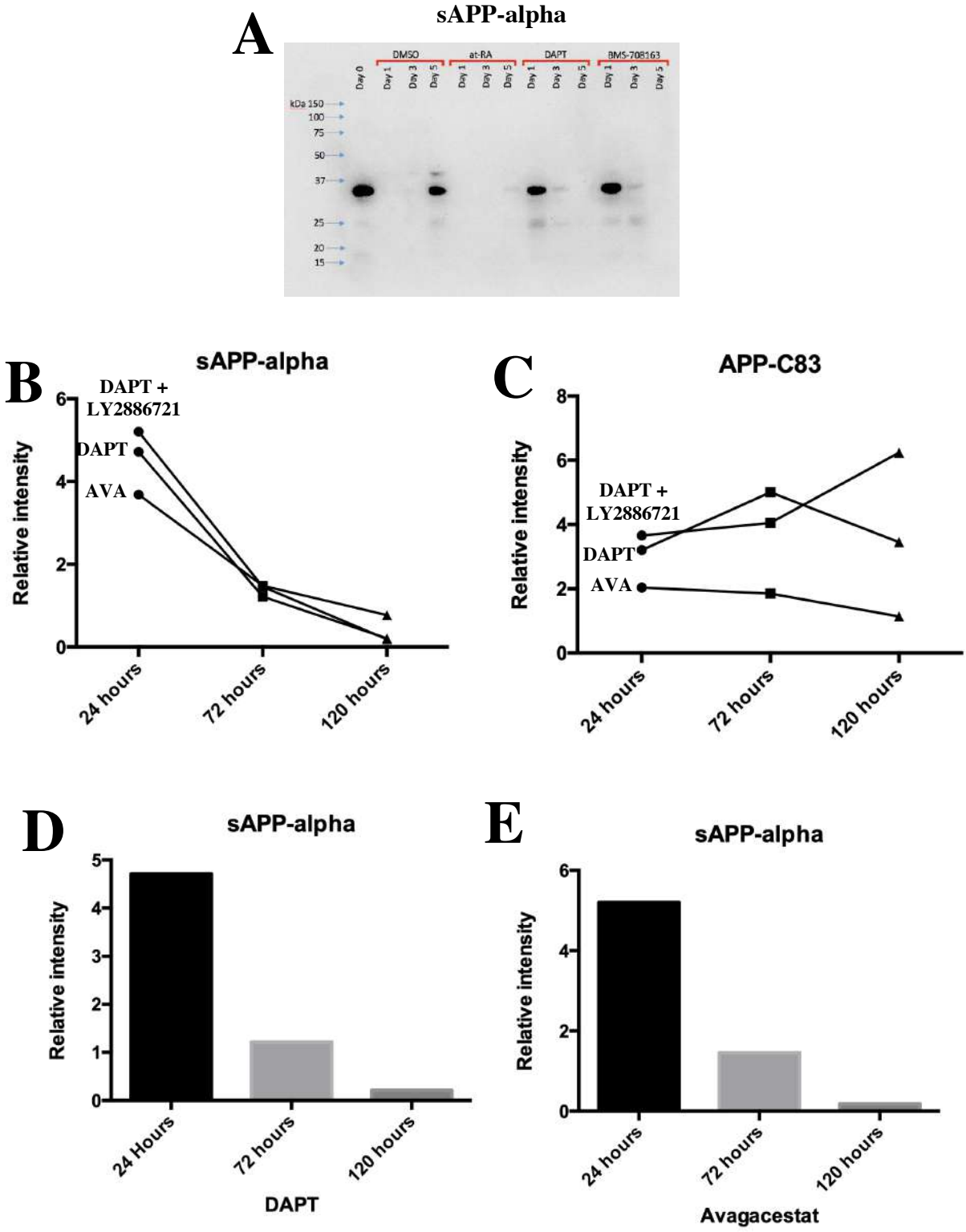

Figure 3.41: The detection of the APP proteolytic products of α-secretase. A) Western blot for sAPPα in SH-SY5Y cells treated with GSIs and harvested 24 hours, 72 hours, or 120 hours after initial treatment. B) Western blot analysis for sAPP-α and C) APP-CTF in SH-SY5Y cells treated with DMSO, 10 uM DAPT (D), or 2 uM Avagacestat (E), with the last drug-treated media replacement occurring either 24 hours (Day 1), 72 hours (Day 3), or 120 hours (Day 5) prior to cell harvesting. The values for each drug treatment group were normalized to the protein levels of the DMSO control group for each time point. n = 1 for each treatment group at each time point.

The expected size of sAPP-α is ~100 kDa, however, the observed band on Western blot appeared at 35 kDa. This could be due to additional proteolytic processing of APP by a caspase protease or MT3-MMP, which processes APP within the sAPP-α region and has enriched expression levels specifically in SH-SY5Y cells (*The Human Protein Atlas*). Future research using selective pharmacological inhibition would support or refute this hypothesis.

Interestingly, the level of sAPP-α changed dramatically depending on the time since last treatment. The harvesting of cells 24-hours after GSI treatment resulted in about a 4-fold increase in sAPP-α protein levels, indicative of γ-secretase inhibition (*Figure 3.41*). This sAPP-α rise disappears when cells are harvested 72 hours post-treatment, paralleling the results from the immunostaining non-membranous APP-CTF showing the loss of GSI potency when cells are harvested 72 hours post-treatment versus 24-hours post treatment. When cells were harvested 120 hours post-treatment, a 3-fold decrease in sAPP-α compared to the DMSO-control resulted (*Figure 3.41*), suggesting a complete potency shift from γ-secretase inhibition to γ-secretase activation.

To see if this result was consistent with the protein levels of APP-CTF, the complement proteolytic fragment of sAPP-α Western blotted for APP-CTF in the same samples. Overall, treatment with GSIs resulted in an overall increase in APP-CTF across the time points.

3.4 HEK293 and HeLa cells show a similar GSI potency response to SH-SY5Y cells and also have a biphasic GSI inhibitor Notch1 cleavage response when last treated either 24 hours or 72 hours before harvesting

Next, we wanted to test the efficacy of DAPT and Avagacestat in their ability to block APP cleavage by γ-secretase in multiple cell lines to assess whether our results were cell-type specific or uniform across multiple cell lines (*Figure 3.51*). An anti-APP-CTF monoclonal

antibody specific for the last 20 amino acids of the C-terminus of APP was used to assess the proteolytic processing of APP by γ-secretase in the presence and absence of GSI's DAPT and Avagacestat in HEK 293, HeLa, and SH-SY5Y cells. Although no significant changes were observed in the full-length APP molecules (~100 kDa), the effects of the GSI's DAPT and Avagacestat were observed via the accumulation of a ~13 kDa fragment consistently across cell types. These differences were most marked in HeLa cells, followed by HEK 293 cells, with the least prominent accumulation observed in SH-SY5Y cells.

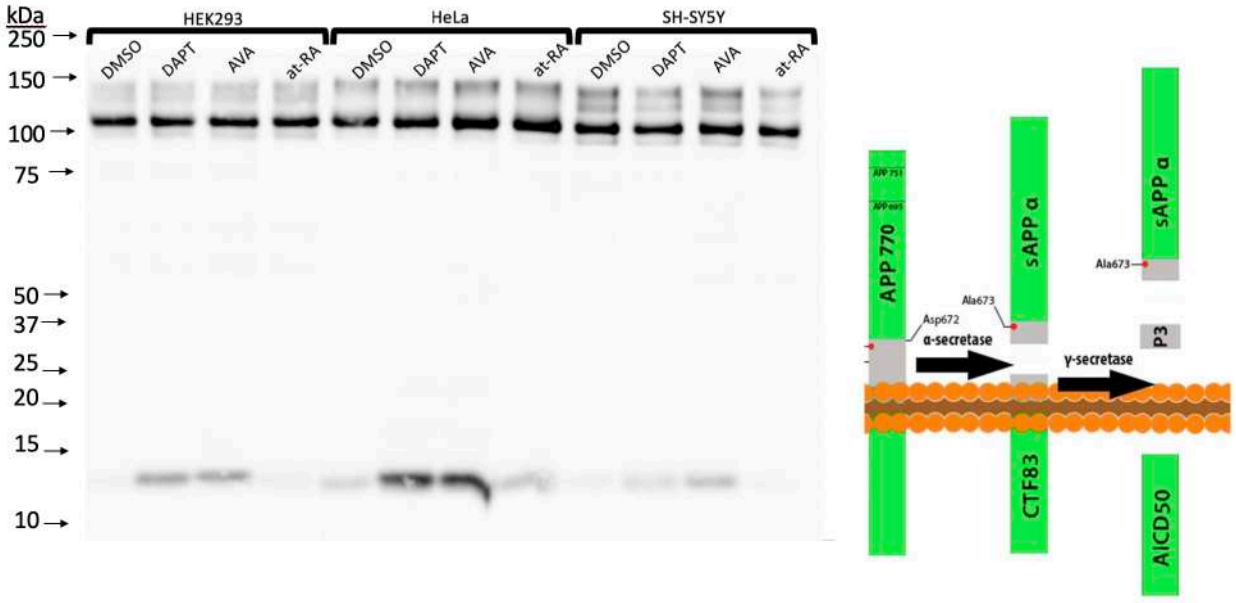

Figure 3.51: Western blot APP-CTF in HEK293, HeLa, and SH-SY5Y cells treated with DMSO, 10 uM DAPT, or 2 uM Avagacestat (BMS-708163) for 120 hours, with the last drug-treated media replacement occurring 24 hours prior to cell harvesting. One biological replicate was blotted per treatment group per cell type.

In this next experiment, in which cells were harvested 72 hours after the last drug-containing media replacement, the γ-secretase inhibitors DAPT and Avagacestat reduced the levels of activated Notch1 at ~100 kDa in HEK 293 and HeLa cells (*Figure 3.52*). In addition, bands were detected at ~63 kDa and ~40 kDa that were both diminished by treatment with

DAPT and Avagacestat in HEK 293 cells, suggesting that these fragments may be truncated Notch1 ICD fragments that have also been processed by γ-secretase. The 100 kDa gamma-cleaved NICD band was not detected in SH-SY5Y cells, possibly because of a comparatively higher turnover or lower Notch1 expression (when compared to HEK293 and HeLa cells) of this fragment in this cell type. A unique truncated banding pattern appeared, including 3 bands between 37 - 50 kDa that deplete with GSI treatment.

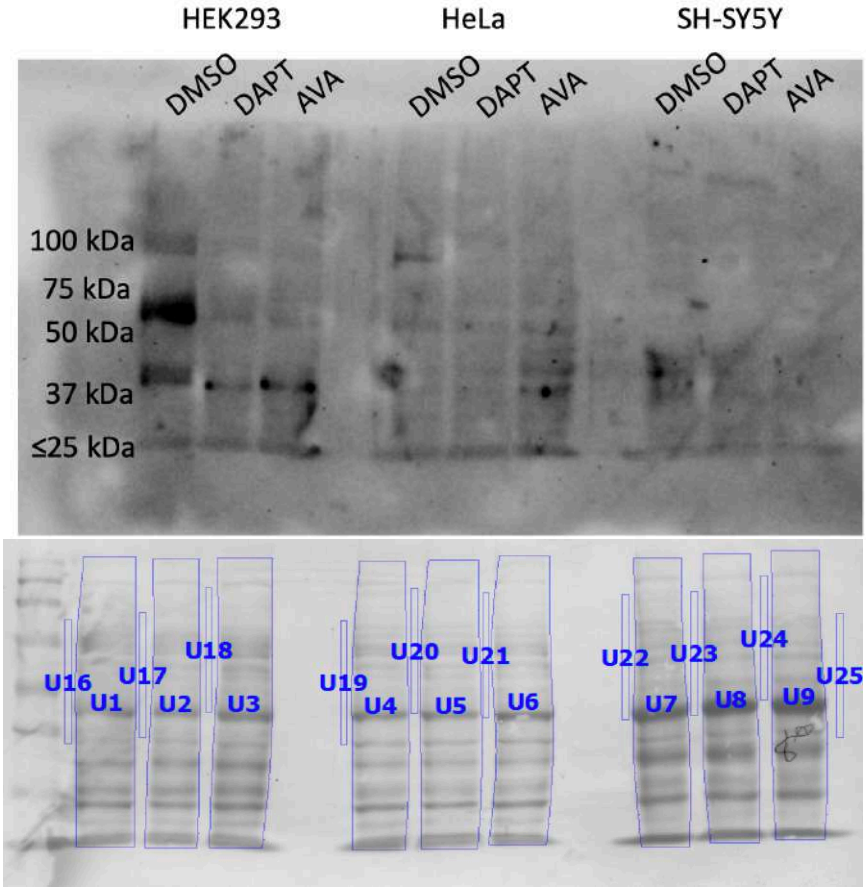

Figure 3.52: Western blot for activated-Notch1 (γ-cleaved) in HEK 293, HeLa, or SH-SY5Y cells treated with DMSO, 10 uM DAPT, or 2 uM Avagacestat for 120 hours, last treated 72 hours before harvesting. One biological replicate was blotted per treatment group per cell type.

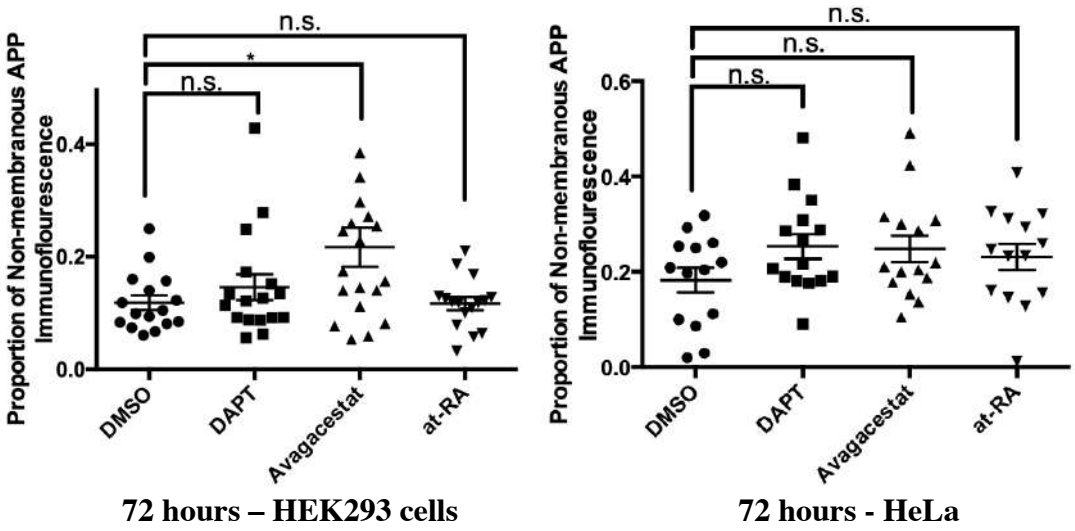

Figure 3.53: Immunofluorescence analysis of non-membrane-associated APP ratio in HEK 293 and HeLa cells treated with either DMSO, DAPT, Avagacestat, or at-RA, last replaced with drug-containing media 72 hours prior to fixation. A minimum of three Z-stack images were taken per biological replicate, with three biological replicates per treatment group.

To assess whether or not the loss of GSI potency occurs in cell types other than SH-SY5Y cells, the immunostaining experiment was repeated in HEK 293 and HeLa cells. APP-CTF was immunostained in cells treated after 120 hours of treatment with 10 uM DAPT, 2 uM Avagacestat, or 10 uM at-RA, with the drug/media replacement occurring 72 hours prior to fixation (*Figure 3.53*). In both HEK 293 cells and HeLa cells, a lack of GSI potency was observed, and in the case of the HEK 293 cells, Avagacestat increased APP cleavage by γ-secretase.

In terms of Notch1 processing, the potency shift, although not statistically significant in HEK 293 and HeLa cells, approaches the trend of SH-SY5Y cells (*Figure 3.54; Figure 3.55*). When the GSI concentration is high, APP processing is blocked and Notch1 processing is promoted, and when the GSI concentration is lower, APP processing rises, and Notch1 cleavage is inhibited. Interestingly in these cell types, at-RA treatment affects the proportion of nuclear

Notch1; in HEK 293 cells at-RA treatment significantly increases nuclear Notch1, and in HeLa cells, at-RA significantly decreases nuclear Notch1.

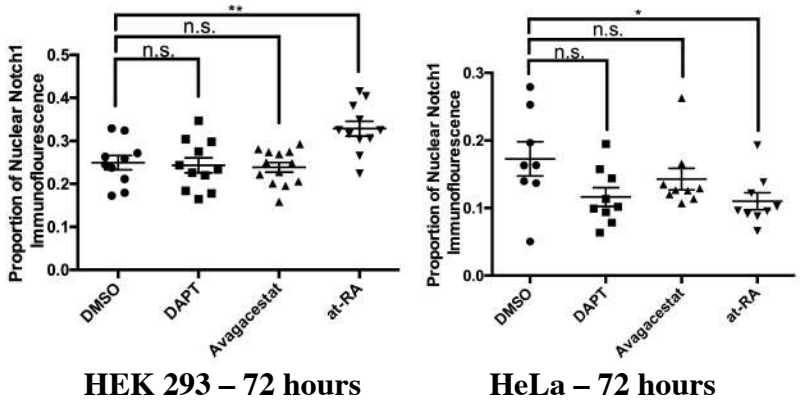

Figure 3.54: Immunofluorescence analysis of nuclear Notch1 ratio in HEK 293 and HeLa treated with DMSO, DAPT, Avagacestat or at-RA cells last treated either 72 hours prior to fixation. A minimum of three Z-stack images were taken per biological replicate, with three biological replicates per treatment group.

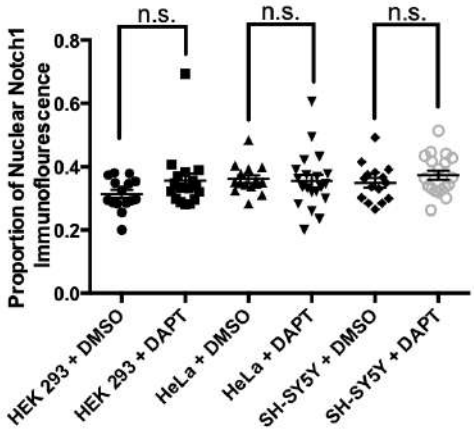

Figure 3.55: Immunofluorescence analysis of nuclear Notch1 ratio in HEK 293, HeLa, and SH-SY5Y cells treated with DMSO or DAPT, last treated either 24 hours prior to fixation. A minimum of three Z-stack images were taken per biological replicate, with three biological replicates per treatment group.

3.5 The Responses of Notch2 activation to DAPT, Avagacestat, and at-RA compliment those of Notch1

Although also not statistically significant, the overall responses of nuclear Notch2 ratios to 5-day treatment with DAPT, Avagacestat, and at-RA last treated 72 hours prior to fixation are very similar to those of Notch1 (*Figure 3.6*).

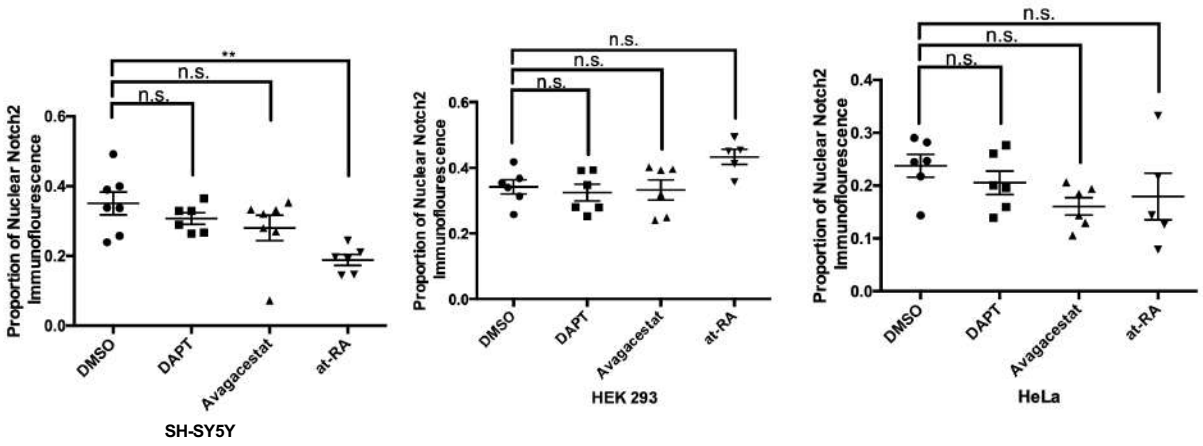

Figure 3.6: Immunofluorescence analysis of nuclear Notch2 ratio in SH-SY5Y, HEK 293, or HeLa cells treated with either DMSO, DAPT, Avagacestat, or at-RA, with the last drug-containing media replacement occurring 72 hours prior to fixation. A minimum of four Z-stack images were taken per biological replicate, with one biological replicate per treatment group.

3.6 Treatment with GSIs leads to a difference in intracellular vesicle accumulation in HEK293, HeLa, and SH-SY5Y cells last treated 24 and 72 hours before fixation

While analysing the immunostains of cells in the presence or absence of DAPT or Avagacestat, we noticed that GSI-treated cells seemed to have a higher proportion of APP-CTF-containing intracellular vesicles (*Figure 3.71*). To assess whether there were differences in APP-containing vesicle accumulation when cells were last treated either 24 hours or 72 hours before

fixation, we produced an image analysis macro on FIJI to quantify the numbers of APP-containing vesicles between treated and control cells in the two conditions.

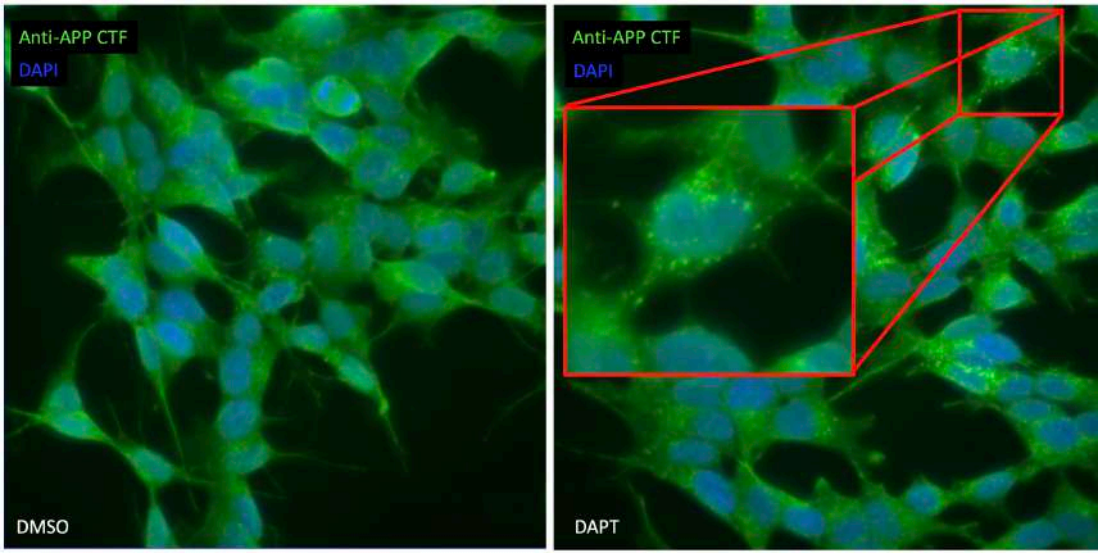

Figure 3.71: APP-CTFs accumulate in vesicles in the presence of the GSI DAPT, last replenished 72 hours prior to fixation.

There was a massive difference in APP vesicle count depending on whether the GSI was replenished 72 hours or 24 hours prior to fixation (*Figure 3.72*). In the former case, both DAPT and Avagacestat lead to about a 4-fold increase in vesicles containing APP-CTF. On the contrary, when the GSI was replenished 24 hours prior to fixation, the vesicles containing APP virtually dissappeared upon treatment with DAPT or Avagacestat, indicating a differential cellular response.

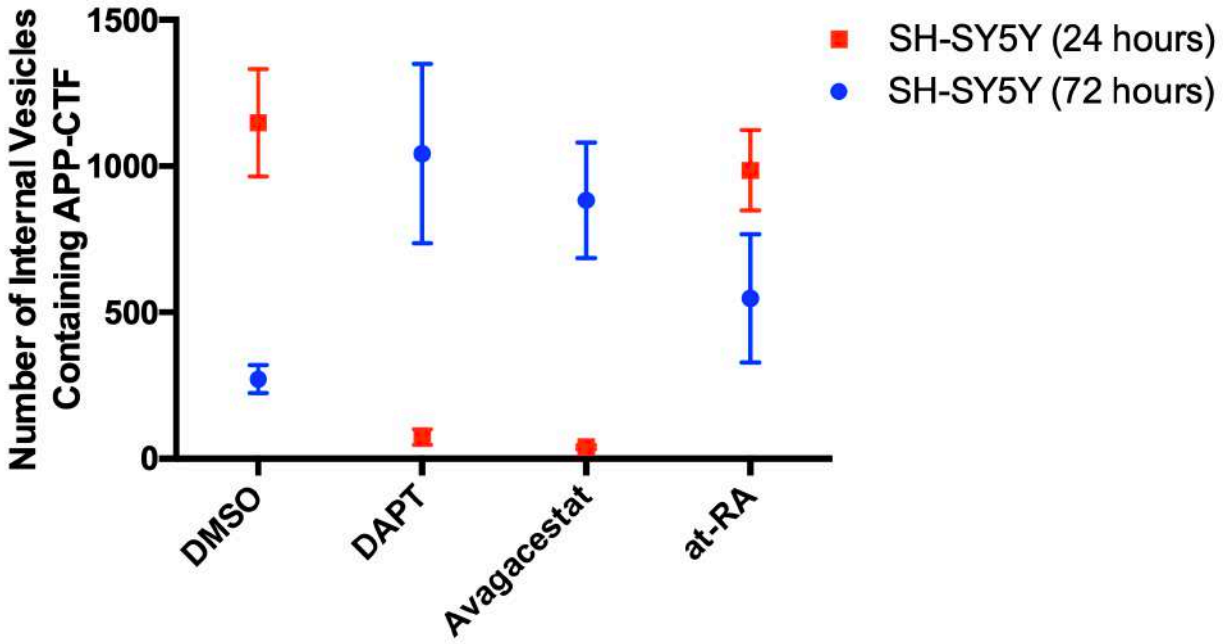

Figure 3.72: Average Number of APP-Containing Vesicles in SH-SY5Y human neuroblastoma cells upon treatment with DAPT, Avagacestat, or at-RA last replenished either 24 hours or 72 hours prior to fixation.

Next, the changes in APP-containing vesicles upon treatment with GSIs last replenished 72 hours prior to fixation were compared between cell types HEK 293, HeLa, and SH-SY5Y (*Figure 3.73*). Among the three cell types, HeLa cells contained the most vesicles on average. All three cell types generally displayed increases in APP-containing vesicles in response to GSI treatment.

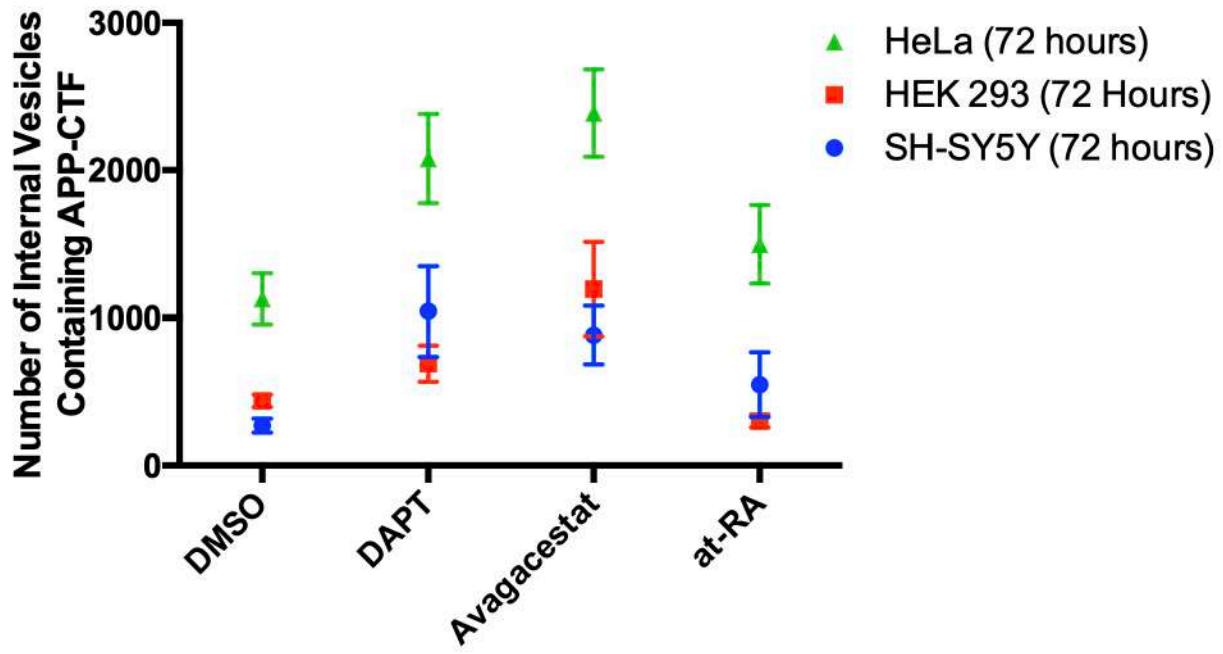

Figure 3.73: Average Number of APP-Containing Vesicles in SH-SY5Y, HEK 293, and HeLa cells upon treatment with DAPT, Avagacestat, or at-RA last replenished 72 hours prior to fixation.

3.7 Prominent bands resembling Notch intracellular truncated fragments detected on Western blot using a Notch-CTD antibody in SH-SY5Y cells

Western blotting for Notch1/2 not only revealed a time-dependent biphasic response to GSIs DAPT and Avagacestat, but it also revealed a prominent and unexpected band apparent at about 40 kDa, that for Notch1 was much more intense than the expected 100 kDa band, and for Notch2 had a roughly equal intensity to the 100 kDa band (*Figure 3.81*).

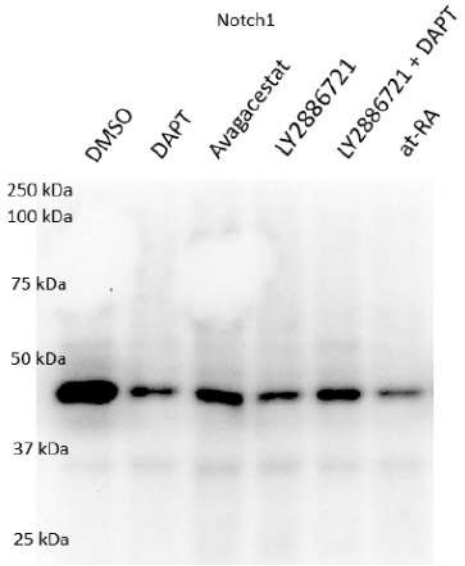

Figure 3.81: Western blot for Notch1 in SH-SY5Y cells treated for 120 hours with DMSO, DAPT, Avagacestat, BACE1 inhibitor LY2886721, DAPT + BACE1 Inhibtitor LY2886721, or at-RA, with the last treatment occurring 72 hours prior to cell harvesting.

3.7.1 HEK293, HeLa, and SH-SY5Y cells show unique Notch1 bands around ~50 kDa, suggesting cell-type specific Notch1-ICD proteolytic profile

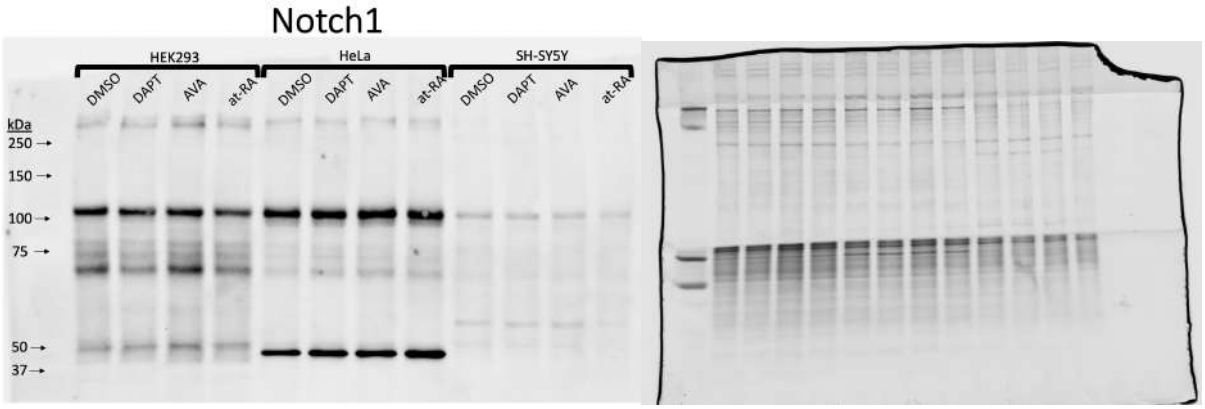

Figure 3.82: Western blot for Notch1 in HEK293, HeLa, and SH-SY5Y cells treated with DMSO, 10 uM DAPT, 2 uM Avagacestat, or 10 uM at-RA for 120 hours, with the last treatment-containing media replacement occurring 24 hours prior to cell harvesting.

To see whether this 45 kDa band was observed in other cell types, or if it was an SH-SY5Y-specific finding, we repeated the Western blot for HEK 293, HeLa, and SH-SY5Y cells (*Figure 3.82*). We found a unique band profile for each cell type between 37-60 kDa. In HEK 293 cells, a band at ~40 kDa and a band at ~50 kDa was detected. In HeLa cells, a strong single

~45 kDa band was observed. Lastly, for SH-SY5Y cells, two bands were observed, one at ~45 kDa and the second ~55 kDa. Additionally, the bands found between ~65-79 kDa were found consistently across cell types, as were the bands at 100 kDa (presumably a combination of S1-S2- and S3-cleaved Notch) and ~270 kDa (Full-length Notch receptor).

3.7.3 The appearance of the ~50 kDa bands on Western blot for Notch1/2-CTDs is sensitive to differences in transfer conditions

We noticed a degree of variability across the literature in that some groups reported the detection of truncated Notch-ICD bands on Western blot and immunostaining experiments (for example, Wesley & Saez, 2000; Fassa *et al*., 2007; Fortini 2009), whereas most others did not. We were interested to see the degree of variability attributed to nuances in transfer conditions. Because many lab groups would naturally use conditions to optimize the transfer of the full-length (270 kDa) and cleaved (100 kDa) forms of the Notch receptor, we were interested to see how using such transfer conditions would affect the final intensity of the cryptic ~50 kDa bands.

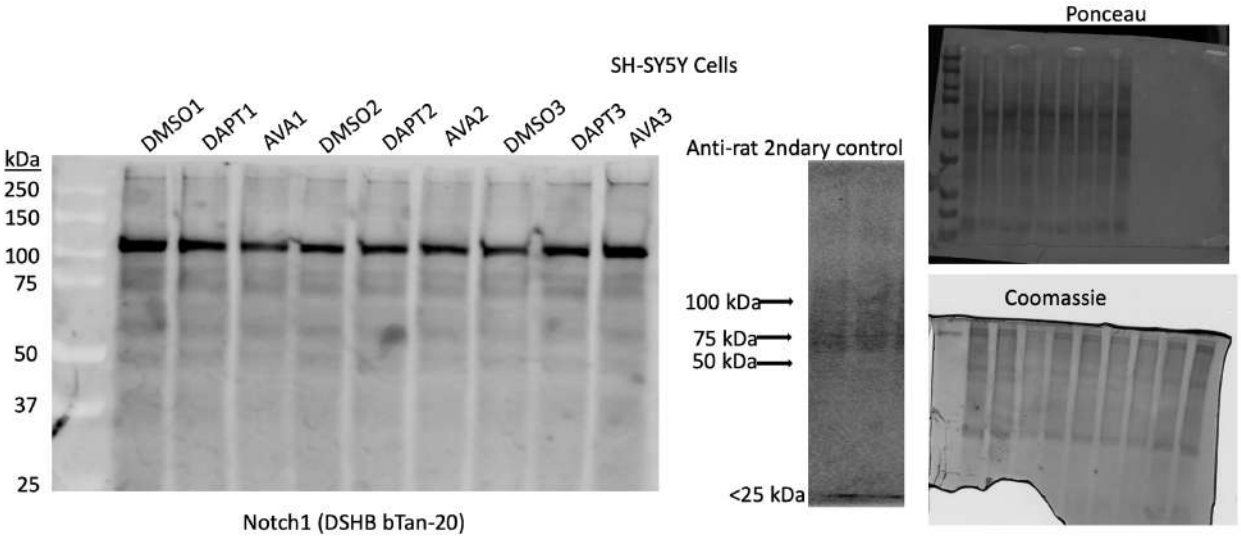

Figure 3.83: Western blot for Notch1 in SH-SY5Y cells treated with DMSO, 10 uM DAPT, 2 uM Avagacestat, or 10 uM at-RA for 120 hours, with the last drug-treated media replacement occurring 24 hours prior to cell harvesting. Transfer conditions were slightly

modified to favour the transfer of larger proteins: Methanol in transfer buffer was reduced from 20% to 15%, and transfer time was extended by 10% (66 minutes instead of 60 minutes).

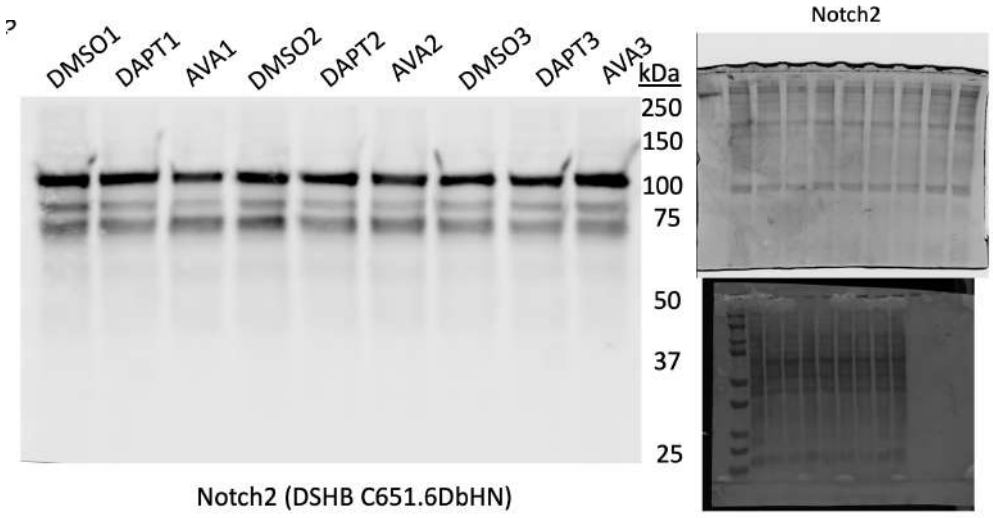

Figure 3.84: Western blot for Notch2 in SH-SY5Y cells treated with DMSO, 10 uM DAPT, 2 uM Avagacestat, or 10 uM at-RA for 120 hours, with the last drug-treated media replacement occurring 24 hours prior to cell harvesting. Transfer conditions were slightly modified to favour the transfer of larger proteins: Methanol in transfer buffer was reduced from 20% to 15%, and transfer time was extended by 10% (66 minutes instead of 60 minutes).

The Notch1 and Notch2 Western blots were repeated for SH-SY5Y cells in biological triplicate, and the transfer conditions were altered to assess the impact of variable transfer conditions on the appearance of lower molecular weight bands (<75 kDa; *Figure 3.83; Figure 3.84*). In this blot transfer, the methanol concentration was decreased by 25% (15% methanol instead of 20%), and the electric current was run as before, but for 10% longer (66 minutes instead of 60 minutes). We found that these conditions strongly diminished the intensity of the bands 75 kDa and below for both Notch1 and Notch2.

3.7.4 Both Full-length Notch ~100 kDa and smaller bands appearing on Western blot increase in the nucleus as cell confluency increases

The use of DAPT as a potent Notch inhibitor is widespread across the literature, despite about a 180-fold variability in inhibitor potency across studies. The lack of change between the 100 kDa band in the presence of absence of GSIs brought into question the validity of our detection methods. The difference between the S2- and S3-cleaved Notch is about 3 kDa on western blot. Therefore, it may be that the inhibitors DAPT and Avagacestat are blocking Notch effectively, but the ratiometric differences between the S2 and S3 products that fall into a single band are not detectable due to insufficient resolution on SDS-PAGE. To sufficiently differentiate the S2- from the S3- Notch cleavage product, we employed nuclear/cytoplasmic fractionation with the use of an antibody that only recognizes the S3-cleaved Notch molecule.

Activated Notch will travel to the nucleus and activate the transcription of a number of target genes. Therefore, if a potential truncated Notch1 ICD band were to be biologically relevant as a transcriptional regulator, it should appear in the nucleus, along with the full-length NICD around 100 kDa in mass. There is also a subcellular distinction in the S2 and S3 proteolytic products of Notch, where the S2 product is tethered to the membrane, while the S3 product localizes to the nucleus. After initially detecting these bands on Western blots for Notch1/2, we were interested to see if we could discriminate between S2-cleaved γ-secretase substrate and S3-cleaved γ-secretase product. We were also interested to see if the smaller bands detected on the Notch blots were found in the nucleus. We used a subcellular fractionation protocol to isolate the nuclear fraction from the cytoplasmic fraction. Using this approach, we expected that only the γ-secretase cleaved activated NICD and not the membrane-tethered Notch should appear in the nuclear fraction. We also hypothesized that the suspected truncated NICDs

should also be enriched in the nuclear fraction, and lower in abundance in the cytoplasmic fraction.

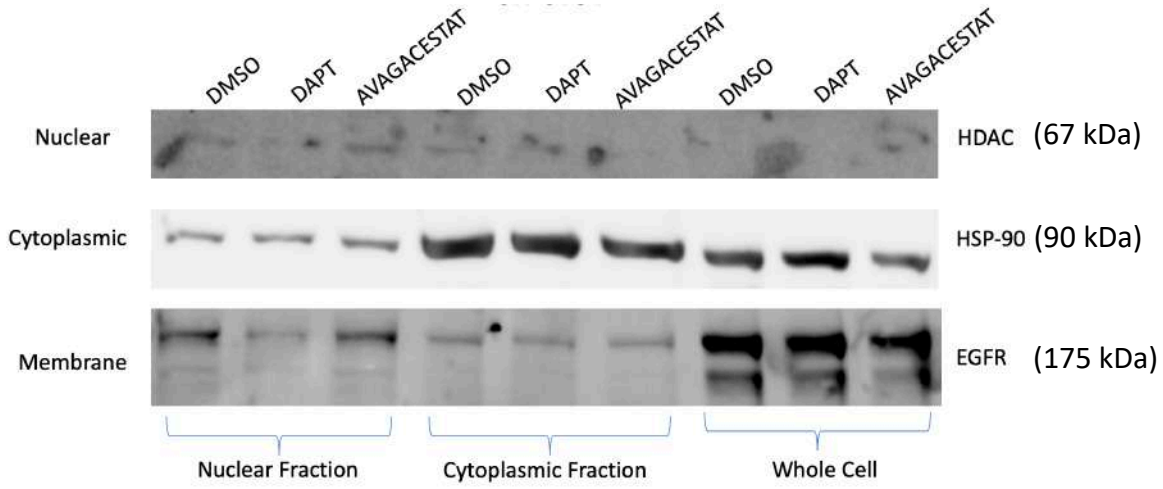

Figure 3.85: Verification of subcellular fractionation using standard protein markers. The effectiveness of the subcellular fractionation protocol was assessed by measuring relative amounts of known proteins (histone deacetylase (HDAC; 67 kDa), Heat-shock Protein-90 (HSP-90; 90 kDa), or Epidermal-like growth factor receptor (EGFR; 175 kDa) with selective localizations (membrane, nuclear, or cytosol) in the nuclear, cytoplasmic, and whole-cell fractions. One biological replicate was blotted per fraction per treatment group.

To validate the effectiveness of the initial cellular fractionation, standard protein markers were used to assess contents of the nuclear, cytoplasmic, and whole cell SH-SY5Y lysates (*Figure 3.85*). Although very faint, Histone Deacetylase was detected (67 kDa) in the nuclear fraction, with minor signal showing in the cytoplasmic fraction but not in the whole-cell lysate. Next, Heat shock protein-90 was used as a cytoplasmic marker (90 kDa). Although fainter bands were found in the nuclear and whole-cell fractions, most of the signal was found in the cytoplasmic fractions. Lastly, majority of the signal from membrane marker Epidermal Like Growth Factor Receptor (EGFR) appear in the whole-cell fractions (175 kDa).

Because the S2 and S3 Notch cleavage products are both found at ~100 kDa and are calculated to be only ~3 kDa apart in mass, we found an antibody with an epitope that only becomes exposed after γ-secretase cleavage of Notch1. Therefore, combined with the subcellular

fractionation, we wanted to use this antibody to differentially blot for the activated NICD and not the membrane-tethered S2-cleaved Notch.

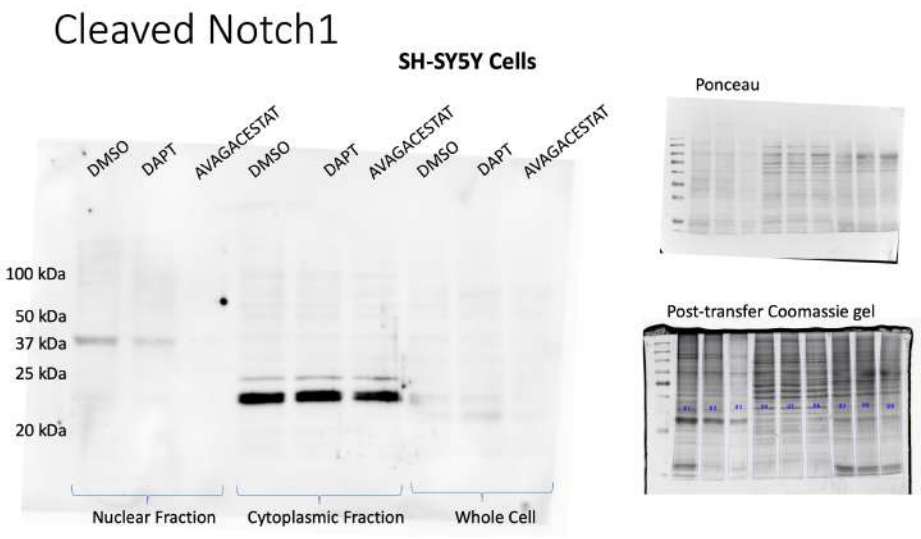

Figure 3.86: Western blot for activated Notch1 in SH-SY5Y cells treated with DMSO, DAPT, or Avagacestat and separated into subcellular fractions. One biological replicate was blotted per treatment group.

Surprisingly, we noticed that this antibody (that recognizes the N-terminus of the NICD) predominantly detected a ~40 kDa band in the nuclear fraction, which roughly correlates to the complimentary ~45 kDa band detected when using an antibody with an epitope near the C-terminal end of the NICD (*Figure 3.86*). It is suspected that the relatively low abundance of the ~100 kDa NICD in the nucleus is the reason for its poor detection. We also detected a strong band in the cytoplasmic fraction appear to be ~23 kDa that did not decrease in response to GSIs.

3.7.4 Both Full-length NICD ~100 kDa and smaller suspected truncated NICD bands appearing on Western blot increase in the nucleus as cell confluency increases

After detecting the dominant truncated Notch1 ICD band in the nuclear fraction of SH-SY5Y cells and observing its depletion in response to γ-secretase inhibition, we wanted to see how cellular confluency affected the relative intensity of Notch activation for full-length NICD, and the suspected truncated NICD fragments that we observed ~40-50 kDa. We hypothesized that, because canonical Notch activation is cell-cell contact-dependent, we would observe the increase in nuclear full-length 100-kDa NICD with an increase in cellular confluency (*Figure 3.87*). We also hypothesized that the suspected cryptic cleavage of the Notch ICD to form the truncated NICD would be independent of cell-cell contacts and γ-secretase cleavage and would therefore not increase with an increase in cellular density on the plate.

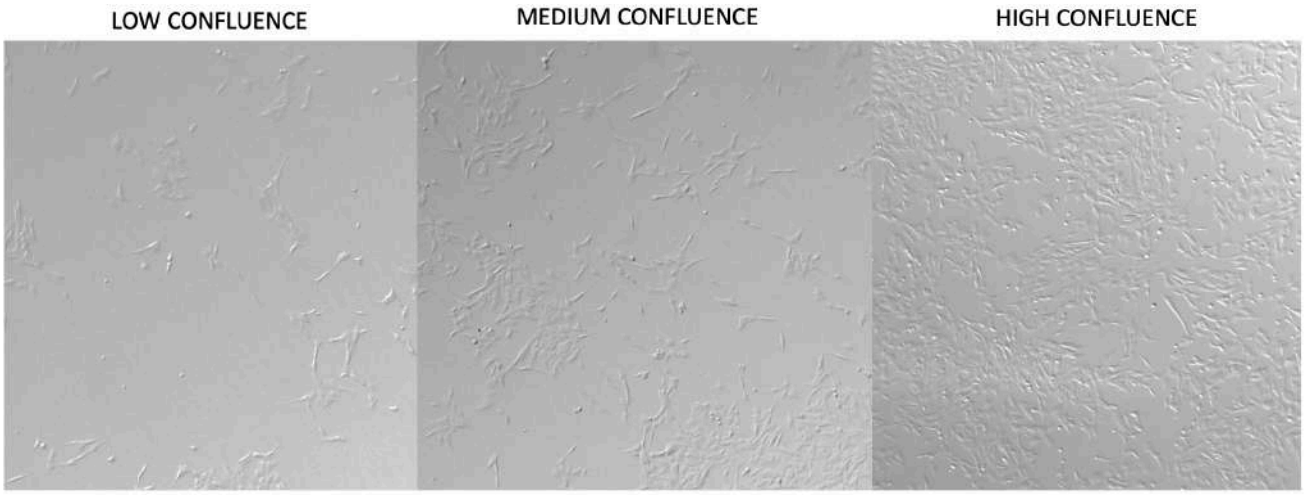

Figure 3.87: Representative images of SH-SY5Y cells before harvesting at low, medium, and high-confluency.

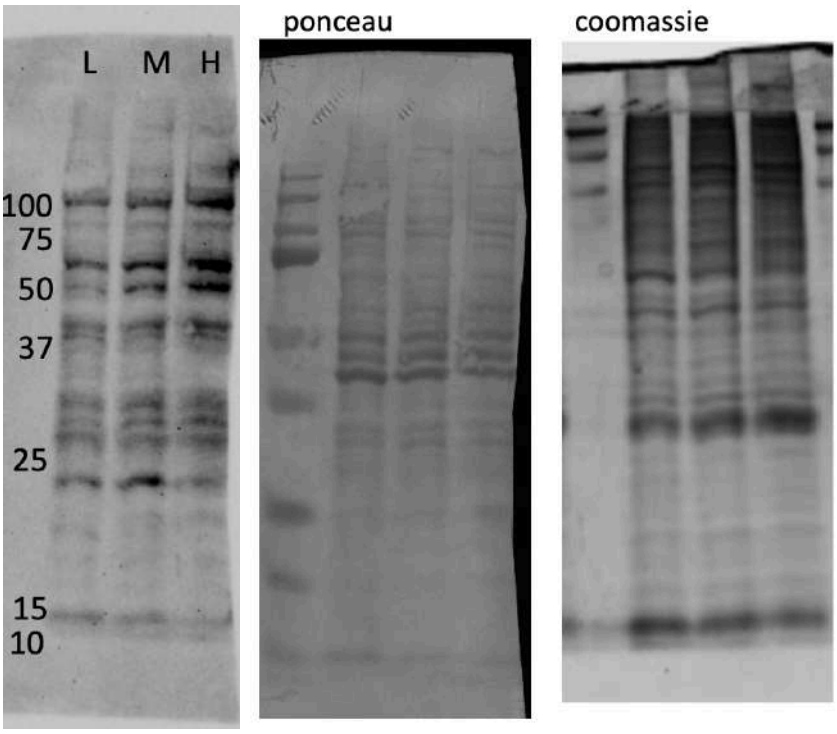

Figure 3.88: Western blot of activated-Notch1 ICD in the nuclear fraction of low, medium, and high-confluency SH-SY5Y cells. This antibody has an epitope on the N-terminus of the NICD that is only exposed after γ-secretase cleavage.

An antibody that recognizes an epitope that becomes exposed only after γ-secretase has cleaved Notch1 from the membrane was used to blot for Notch1 in the nuclear fraction of SH-SY5Y cells grown in low, medium, or high confluency (*Figure 3.88*). As confluency increases, the levels of Notch activity also increase. In addition to the ~100 kDa band that increases with increasing confluency, ~60 kDa, ~50 kDa, and ~40 kDa bands were also seen to increase with increasing confluency. In order to observe the 100 kDa band absent in *Figure 3.86*, 40 ug of total protein was loaded to each well instead of the 20 ug/well used in *Figure 3.86*.

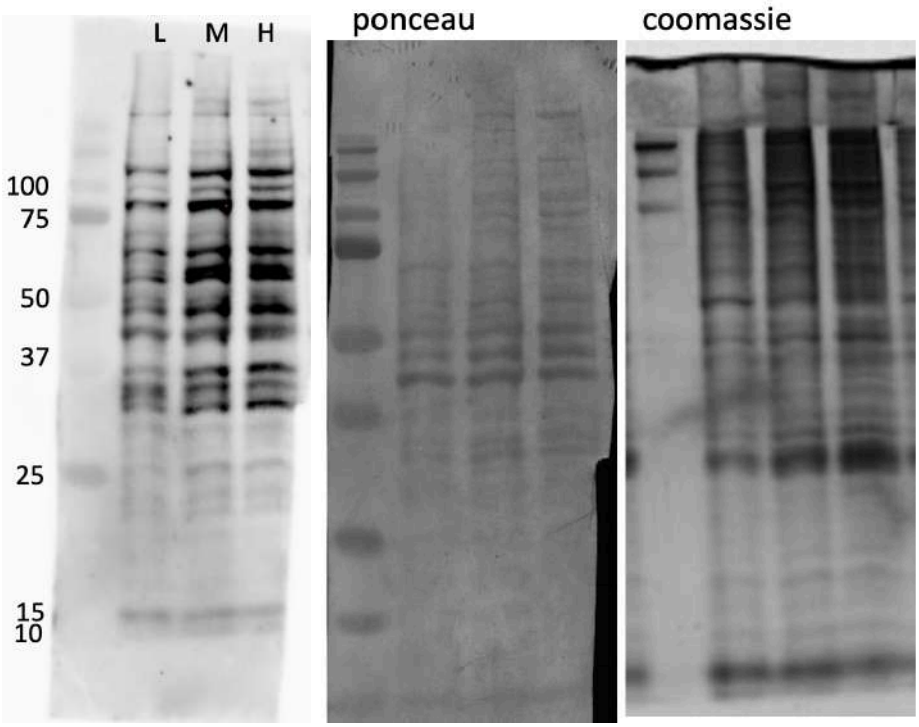

Figure 3.89: Western blot of Notch1 ICD in the nuclear fraction of low, medium, and high-confluency SH-SY5Y cells. This antibody has an epitope near the C-terminus of the NICD.

To see whether this correlation of cellular density and notch activity was repeatable, we used an orthogonal method in which we used a monoclonal antibody from the Developmental Studies Hybridoma Bank (DSHB) that recognizes an epitope within the C-terminal domain of Notch1 (*Figure 3.89*). We also found that increasing cellular confluency increased the levels of Notch1 found in the nucleus of SH-SY5Y cells using this antibody.

3.7.5 As cell confluency increases, Western blotting for Notch2 ~100 kDa in the nucleus decreases and the cryptic Notch2 band ~50 kDa increases in the nucleus

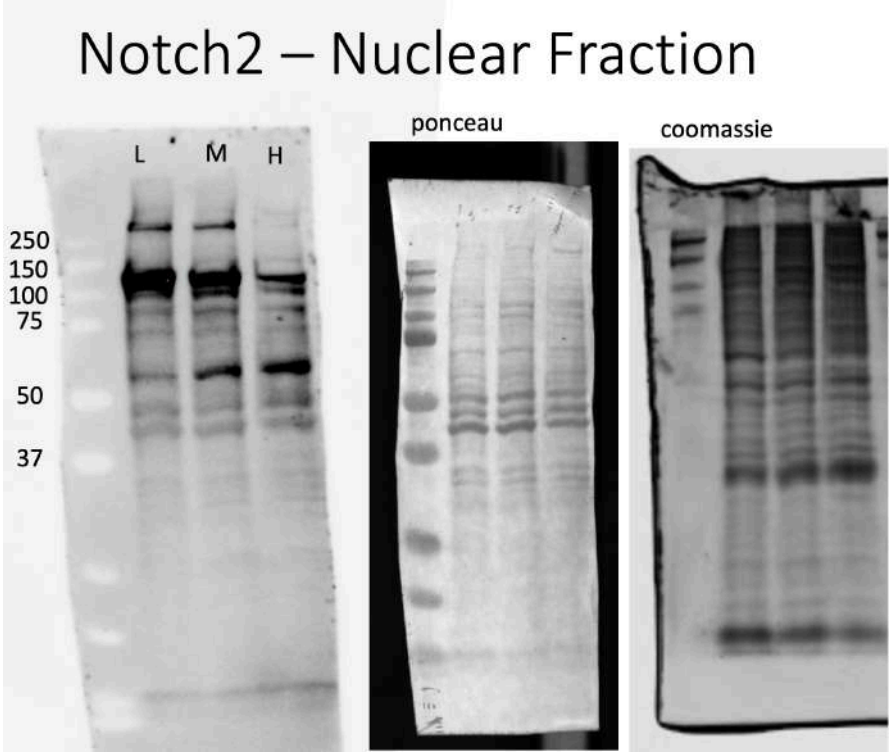

Figure 3.91: Western blot of Notch2 ICD in the nuclear fraction of low, medium, and high-confluency SH-SY5Y cells. This antibody has an epitope near the C-terminus of the NICD of Notch2.

After observing the change in nuclear Notch1 levels with increasing confluency, we were interested to see how levels of Notch2 were affected by changes in cellular confluency. To do this, we performed a western blot using the same low confluency, medium confluency, or high-confluency SH-SY5Y lysates, this time using a monoclonal antibody that has an epitope on the C-terminus of Notch2 (*Figure 3.91*). Contrary to Notch1, we found that as cellular confluency increased, the level of the 100 kDa Notch2 fragment in the nucleus decreased. A ~55 kDa Notch2 fragment was detected that seemed to reciprocally increase with increasing confluency as the ~100 kDa band intensity decreased.

3.7.6 Multiple antibodies with independent epitopes on Notch1 detect several cryptic cleavage fragments

After observing that nearly all detected bands on the Notch blots using three independent antibodies with unique epitopes increased in abundance in nuclear isolates in response to increases in cellular confluency, with the exception of Notch2, we were interested in also using these antibodies to assess Notch cleavage responses in the presence or absence of the GSI DAPT. If all of the three antibodies detected the suspected cryptic Notch ICD cleavage fragments, this would provide an independent means of verifying the identity of these bands. Additionally, it would assess the dependency of this suspected cryptic cleavage on γ-secretase, by modulating its activity via DAPT.

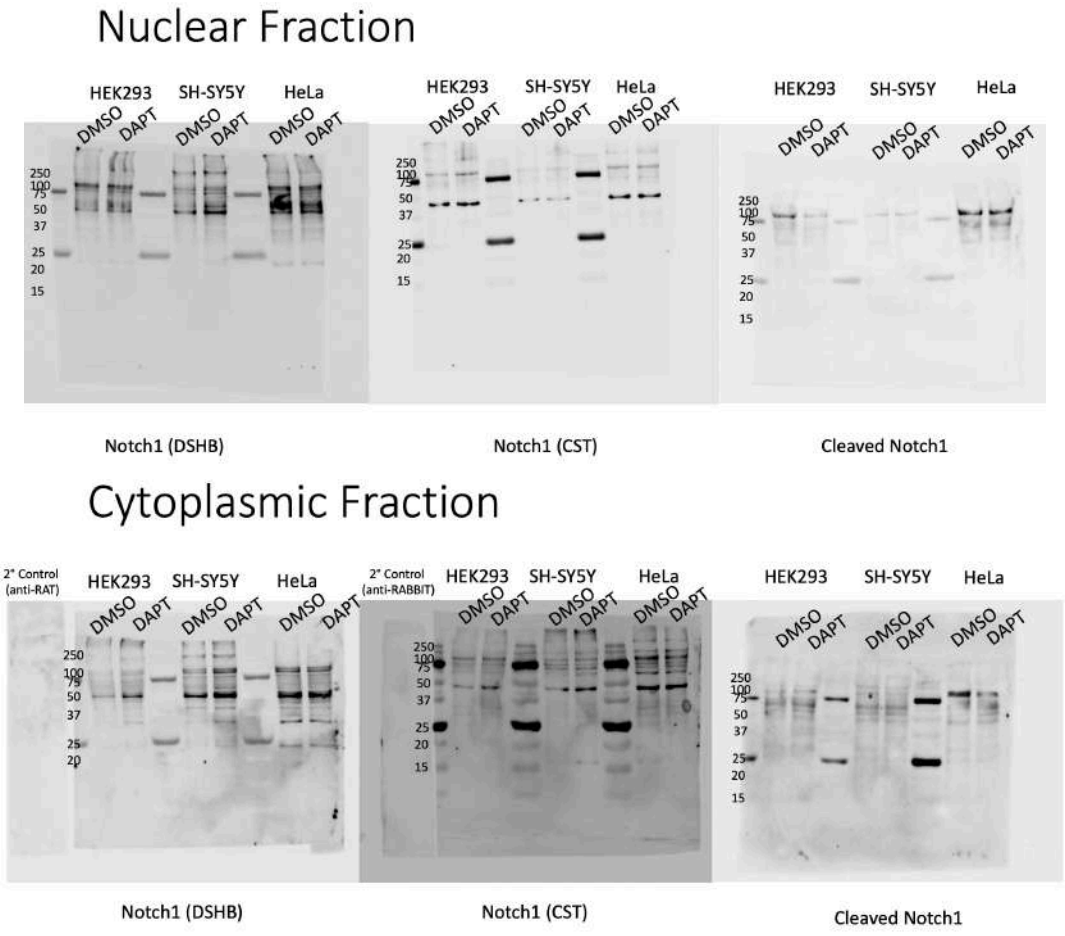

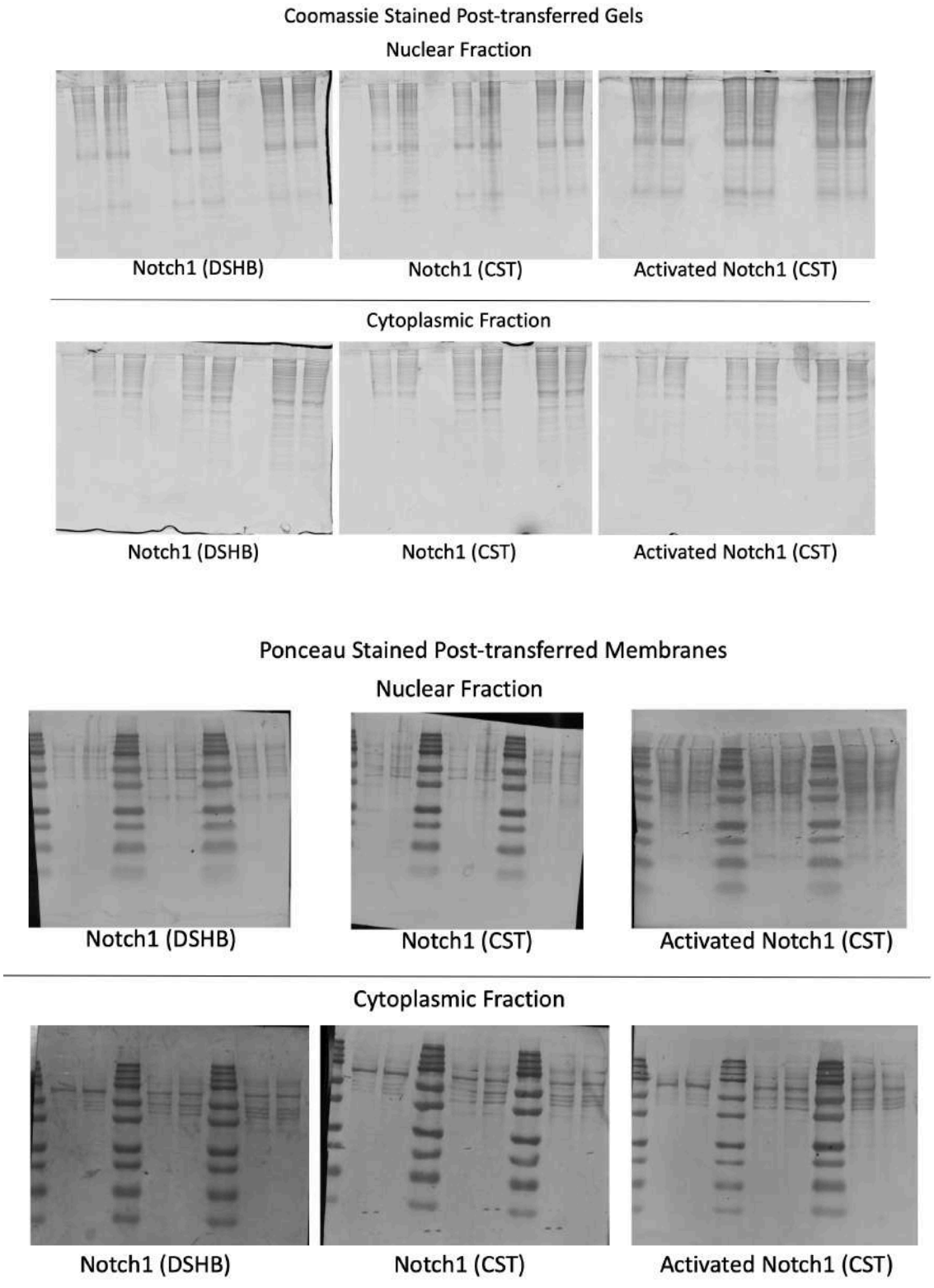

Figure 3.92: Western blots using 3 orthogonal antibodies for Notch1 in nuclear isolates of HEK 293, HeLa, and SH-SY5Y cells treated with DMSO, 10 uM DAPT, or 2 uM Avagacestat for 120 hours, last replacing the drug-containing media 24 hours before cell harvesting.

We detected complimentary bands using the three Notch1 antibodies, and also found that in many cases, DAPT did not sufficiently inhibit γ-secretase-mediated cleavage of Notch1 or the cryptic formation of truncated NICDs, particularly when the drug-containing media is last replaced 24 hours prior to cell harvesting (*Figure 3.92*).

3.7.7 The cryptic proteolytic Notch1 fragments and their compliment fragments correspond to predicted proteolytic cleavage sites on the Notch intracellular domain

When western blotting for Notch1 using two antibodies with different epitopes (one near the C-terminus and the other on the exposed region of the γ-secretase cleaved Notch1 ICD N-terminus), we expected to see a 4 total bands representing full-length Notch1 (~270 kDa), and the products of S1, S2, and S3 cleavage events (~100 – 110 kDa). However, we noticed unique banding profiles for each antibody, with multiple prominent bands appearing well below the predicted cleavage products.

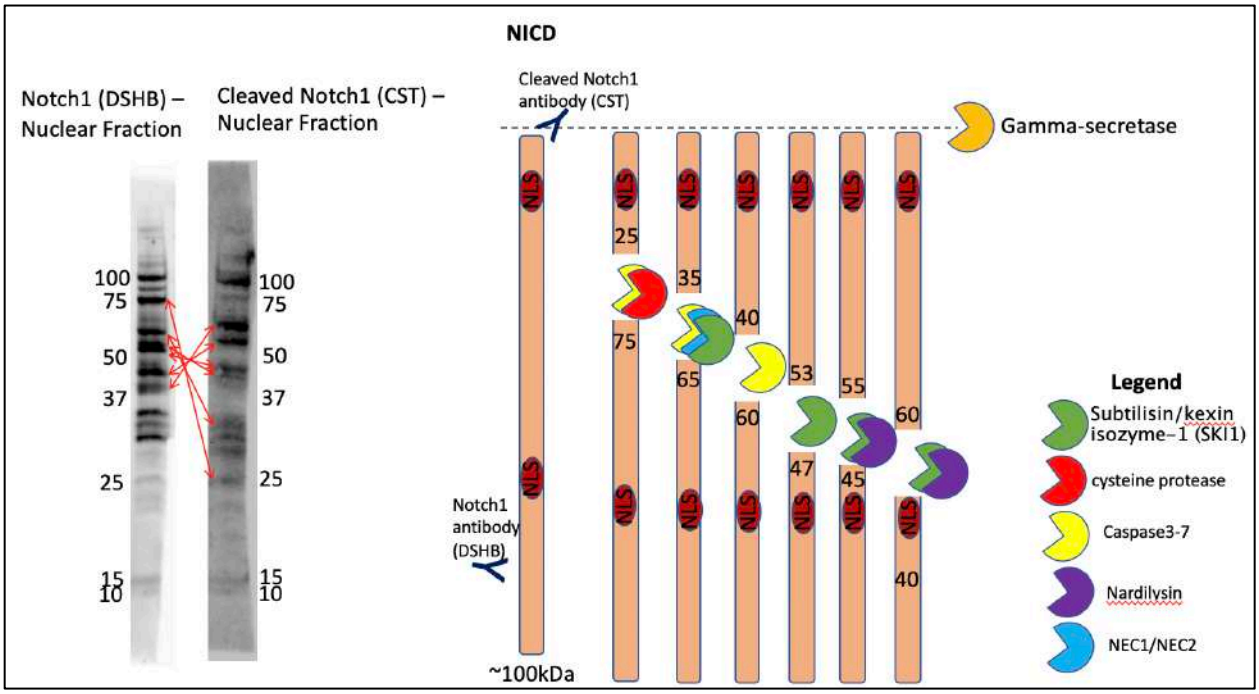

Figure 3.93: Side by side comparison of Western blot of a nuclear isolate of SH-SY5Y cells using two antibodies that recognize opposite termini of the Notch1 ICD (left). A eukaryotic linear motif analysis found potential proteolytic cleavage sites that correspond to the complimentary Notch fragments (right).

We compared the two blots side by side to see if the bands correlated as complementary fragments (*Figure 3.93*). We identified 6 complementary sets of potentially novel cleavage products that are outside current knowledge of canonical Notch proteolytic processing. Furthermore, a eukaryotic linear motif analysis (www.elm.eu.org) revealed probable proteolytic cleavage sites that correlate with potential cleavage locations that would account for each of the found complementary fragment pairs found on Western blot. Each of these potential cleavage sites was also tightly associated spatially with predicted modification sites and regulatory protein binding sites. Three lower molecular weight bands detected by the Notch1 DSHB antibody did not match to complimentary fragments, and may represent unmapped degradation products of the NICD.

4.0 Discussion

Assessing γ-secretase activity in cells can be problematic, especially when endogenous expression levels of APP or Notch are too low to detect appreciably. There are several assays published in the literature to quantify γ-secretase activity, specifically in regard to substrates APP and Notch (Mayer *et al*., 2008; Kreft *et al*., 2008; Yang *et al*., 2008; Gillman *et al*., 2010). All of these assays make use of the exogenous overexpression of substrates APP and Notch. Recent evidence has shown that this may be problematic as the γ-secretase response to GSIs is dependent on relative levels of substrates and the enzyme itself (Burton *et al*., 2008; McKee *et al*., 2013). This finding explains a profound level of variation in the literature. For example, DAPT has shown a 180-fold difference in selective potency across the literature, depending on which γ-secretase activity assay is used. Overall, our goal was to develop and validate a cell-based assay that together can reliably quantify γ-secretase activity levels in an endogenous cellular context. We were able to validate our assay by showing similar results from three statistically-independent methods in tandem. Our assay revealed novel biological findings including a GSI time-dependent γ-secretase Notch/APP biphasic selectivity switch and novel proteins resembling truncated Notch ICD fragments that may have biological relevance as an extension of the current Notch signalling model.

4.1 Validation of the high-throughput cell-based assay to quantify the cleavage of endogenous levels of Notch and APP by γ-secretase

We found that when the γ-secretase inhibitor-containing media was replaced 72 hours prior to harvesting/fixation (supposed lower GSI concentration), γ-secretase-mediated Notch activation was inhibited, and APP cleavage was slightly stimulated. However, when the drug-containing media was last replaced 24 hours prior to fixation/harvesting (supposed higher GSI

concentration), APP cleavage by γ-secretase was inhibited Notch activation was slightly stimulated. The reason for this phenomenon remains unclear, and further research could investigate feedback mechanisms upstream or downstream of this event.

In summary, we were able to show, through a complimentary combination of Western blotting, Immunocytochemistry, and a BrdU proliferation assay the biphasic γ-secretase response that would explain an Aβ stimulation at low GSI concentration, and the successful inhibition of the accumulation of Aβ at higher GSI concentrations.

Future experiments to validate our findings would include Western blots for APP-CTF in HEK 293 and HeLa cells that were last replaced with treated media 72 hours prior to harvesting. In addition, a dose-response study would be necessary to understand if a difference in GSI concentration that underlies this phenomenon or an alternate confounding factor. Because the observation of a substrate selectivity switch in response to potential differences in GSI concentration is novel, additional GSIs with characterized selectivity's, such as LY411575, which is thought to be an extremely potent GSI, should be assessed using our quantitative assay.

To improve the assay to better understand the APP/Notch substrate switch phenomenon, disentangling α-secretase activity from β-secretase activity is required and could be accomplished through Western blotting and immunocytochemistry using antibodies against sAPP-α and sAPP-β. In addition, monitoring AB42 and AB40 production via ELISA, or even a BACE1 activity assay would be useful to more directly address the Aβ-stimulation phenomenon. Lastly, because it has been shown that γ-secretase's response to GSI's at different concentrations may depend on the proportional levels of substrates and enzyme, Western blotting for ADAM10, BACE1, and PSEN1/2 would allow for the detection of potential changes in enzymes as a cellular reflex response to pharmacological inhibition.

4.2 The APP/Notch1 substrate selectivity of γ-secretase depends on GSI concentration

Interestingly, no significant change in Notch1 or Notch2 was observed by Western blot when the inhibitors were last replenished 24 hours prior to harvesting. However, when the inhibitors were replenished 72 hours prior to harvesting, Western blotting and immunocytochemistry both detected significant decreases in activated Notch1 protein levels with DAPT treatment. This is statistically independent evidence to support the idea of a selectivity switch of γ-secretase in response to inhibitors DAPT and Avagacestat.

We suspect that the major result of last changing the drug-containing media 72 hours prior to experiment termination versus 24 hours is a substantial decrease in available GSI. The stability of DAPT and Avagacestat in mammalian cell culture conditions remains unclear, however, we suspect that the levels of available GSI in culture media begins to decrease substantially after applied. A previous study has shown that treatment of HEK 293 cells with 10 nM DAPT results in decreases instead of increases in APP-C83 paired with higher levels of Aβ (Dovey *et al*., 2001). Although we are initially supplying the cells with 10 uM DAPT, we suspect that the level of DAPT remaining in the media at 72 hours may be below this potency threshold (*Figure 4.1*). Our study used GSI concentrations similar to those used in cell culture experiments across the literature. However, a validation study needs to be done to test a range of concentrations of DAPT and Avagacestat, and harvesting cells at the same time points. This would confirm that our results are because of differences in GSI concentration and not an alternate confounding parameter. Additionally, the experiments can be repeated with cells being harvested either 24 hours or 72 hours after the last treatment replenishment and samples of the media can be analysed via nuclear magnetic resonance (NMR) to assess relative levels of DAPT and Avagacestat remaining in the culture media.

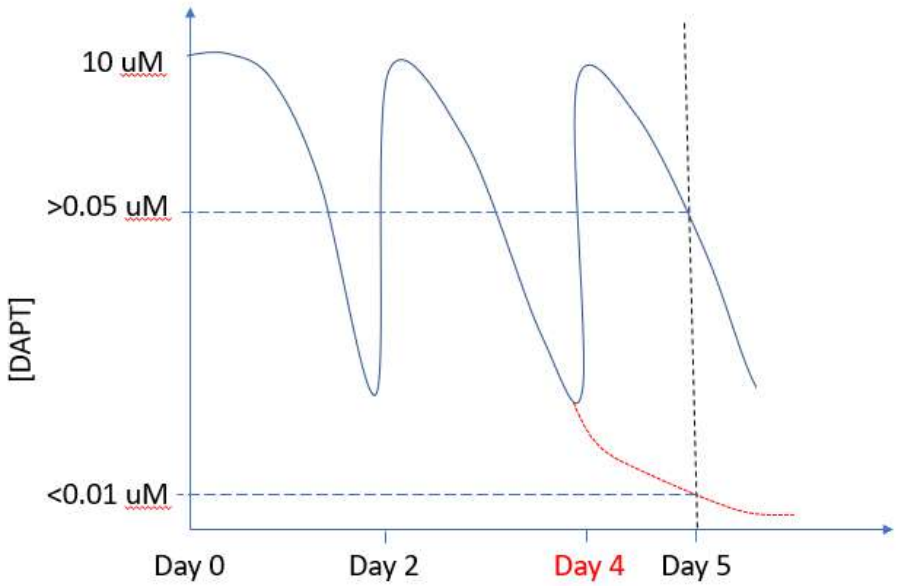

Figure 4.1: Hypothetical model to predict concentrations of available GSI when the drug-containing media was last replaced on Day 4 (blue line), or Day 2 (red line).

With the expectation that changing the media either 24 hours or 72 hours prior to experiment termination sufficiently alters the concentration of GSIs, our results showing this APP/Notch selectivity switch are complimentary to the results of numerous other studies. The Aβ rise phenomenon has been thoroughly shown in the literature in *in vivo* mouse models and *in vitro* cell culture and cell-free studies where Aβ has been seen to spike above baseline when DAPT and other GSIs are used at low concentrations (Dovey *et al*., 2001; Siemers *et al*., 2005; Lanz *et al*., 2006; Burton *et al*., 2008; Matsuoka *et al*., 2009; Barthet *et al*., 2011; Li *et al*., 2012; Ortega *et al*., 2013; Barnwell *et al*., 2014). However, to our knowledge, other substrates such as the Notch receptor have not been studied in relation to this phenomenon.

4.3 An extension of the model to explain the Aβ rise phenomenon

There are currently three independent models to explain the Aβ rise phenomenon in response to low level GSI, which will be further discussed in relation to our findings in this

chapter. First, the Barnwell Model proposes that the rise in Aβ is not because of a change in γ-secretase activity, but primarily due to an accumulation of C99 in endocytic vesicles instead of Aβ, which allows a bypass of the Endothelin-like Converting Enzyme (ECE)-mediated degradation of Aβ (Barnwell *et al*., 2014). Next, the Ortega Model (Ortega *et al*., 2013) proposes that the rise in Aβ is accounted for by α-secretase saturation, which prevents the breakdown of APP-C99 to APP-C83. Lastly, the model proposed by Svedruzic *et al*., (2013) focuses on the γ-secretase kinetic activity changes through complex interaction with other substrates and proteolytic enzymes in the amyloidogenic pathway. They also propose that levels of Notch modulate γ-secretase's ability to process APP. Our current findings both compliment and extend the findings of these three studies, leading to a revised model to explain the Aβ rise phenomenon, as well as extending the model to account for selectivity changes of Notch.

4.3.1 Intracellular sAPPα, but not extracellular sAPPα corresponds to the γ-secretase biphasic response to GSIs

sAPP-α is the APP-C83 complimentary N-terminal product that results from α-secretase cleavage. It has been found that cleavage by α-secretase is strongly regulated by γ-secretase activity, and that protein levels of the proteolytic fragment, sAPP-α increase in response to γ-secretase inhibition (Siegenthaler *et al*., 2016). As a statistically-independent means to quantify the apparent APP potency shift that occurs with the γ-secretase inhibitors treated either 24-hours or 72-hours before cell harvesting, sAPP-α and APP-CTF protein levels were assessed as a proxy for γ-secretase activity when DAPT or Avagacestat were supplemented in media for SH-SY5Y cells either 24 hours, 72 hours, or 120 hours prior to cell harvesting (*Figure 3.41*). We observed a biphasic sAPP-α intracellular accumulation via Western blot that complements our

results showing the biphasic APP/Notch γ-secretase activity response to lower/higher GSI concentrations.

Furthermore, Barnwell *et al*., (2014) proposed a model to at least partly explain the Aβ rise phenomenon. They proposed that for the case of low-concentration γ-secretase inhibitor treatment, the γ-cleavage of APP-C99 (BACE1 product) accumulates through the endocytic pathway, and Aβ bypasses the endothelin-converting enzyme (ECE)-mediated degradation in recycling endosomes, before returning to the plasma membrane and being cleaved by uninhibited γ-secretase enzymes. They developed this model after noticing the abolishment of the Aβ rise phenomenon with ECE-inhibitor treatment.

Our data reveals that the level of sAPP-α changed dramatically depending on the time since last treatment. The harvesting of cells 24-hours after GSI treatment resulted in about a 4-fold increase in sAPP-α protein levels, indicative of γ-secretase inhibition. This sAPP-α rise disappears when cells are harvested 72 hours post-treatment, paralleling the results from the immunostaining non-membranous APP-CTF showing the loss of GSI potency when cells are harvested 72 hours post-treatment versus 24-hours post treatment. When cells were harvested 120 hours post-treatment, a 3-fold decrease in sAPP-α compared to the DMSO-control resulted, suggesting a complete potency shift from γ-secretase inhibition to γ-secretase activation (*Figure 3.41*).

In a similar experiment, Barnwell *et al*. (2014) looked at the effect of varying concentrations of DAPT on Aβ levels treated for 2 hours, 4 hours, and 8 hours in SH-SY5Y cells ectopically expressing APP. They found robust increases in Aβ levels in cells treated with concentrations below 100 nM, with larger rises occurring when cells were treated for longer time periods. They also found that APP-C83 and sAPP-α in the media were both linearly dose-

responsive and not involved in this paradoxical Aβ rise that was occurring at low DAPT concentrations. Our current results compliment the findings of Barnwell *et al*. (2014) with one exception: we detect significant decreases in levels of intracellular sAPP-α levels as GSI treatment time increases. This could be an indication of an internal vesicle-specific mechanism. PSEN1/2 knockout cells show an accumulation of endosomes and endo-lysosomal dysfunction due to lack of PSEN-mediated lysosomal calcium homeostasis (Coen *et al*., 2012).

Our data recapitulates the results of the previous studies noting the Aβ rise. However, an expansion of the current understanding around the Aβ-stimulating effect of low-level GSIs is required in light of our new findings. First of all, we noticed that the intracellular levels of sAPP-α (likely produced within intracellular vesicles) fell 2-3-fold below DMSO-controls when cells were not replenished with fresh GSI for 120 hours. Barnwell *et al*. (2014) observed dose-responsive linear increases in extra-cellular sAPP-α in response to the GSIs and did not observe a biphasic response, a finding that at least in part lead them to suspect that γ-secretase activity is not directly involved in the phenomenon. In addition to observing dose-responsive increases in APP-CTFs, they concluded that the Aβ rise phenomenon must be independent of γ-secretase activity. With our novel findings indicating that intracellular sAPP-α levels have a strong biphasic response to GSIs and previous evidence indicating the contrary in secreted sAPP-α, an endosomal/lysosomal-specific mechanism can be proposed. This type of mechanism agrees with the ECE-bypass explanation proposed previously, with the exception being that γ-secretase-dependent α-secretase activity is actually strongly implicated in the phenomenon.

To see if this result was consistent with the protein levels of APP-83, the complement proteolytic fragment of sAPP-α, we Western blotted for APP-C83 in the same samples. Overall, treatment with GSIs resulted in an overall increase in APP-C83 across the time points, likely due

to the relatively slow turnover of this membrane-tethered γ-secretase substrate on cellular membranes. The accumulation of relatively-stable membrane-tethered APP-C83 in response to α-secretase stimulation is presumably too great to be overcome by γ-secretase-mediated breakdown and inhibited α-secretase activity; whereas soluble APP-α levels are more transient and more accurately reflect the intracellular α-secretase activity levels in space and time.

4.3.2 The scale of the biphasic GSI response is cell-type specific and may depend on relative substrate expression levels

The quantitative assay was used to assess γ-secretase activity in response to GSIs not only in SH-SY5Y cells, but also in HEK 293 and HeLa cells. We were interested to see if the biphasic response is cell-type specific, or if it is found consistently across cell types. We found that, although much less pronounced, HEK 293 and HeLa cells followed the same overall trend as SH-SY5Y cells. The difference in response magnitude represents a cell-specific response to γ-secretase inhibition.

Although there are multiple cell-based assays that show 10 uM of DAPT is sufficient to detect robust reductions in the levels of NICD detected on WB (Yang *et al*., 2008; Ye *et al*., 2014), the concentration after 72 hours is likely considerably lower than this. In addition, these assays make use of different cell lines that are ectopically overexpressing γ-secretase substrates APP or Notch, which recent evidence suggests may cause a false potency measure that is up to 180-fold higher for DAPT compared to potency measurements taken with endogenous substrate levels (McKee *et al*., 2012). Therefore, the level of expression of APP, and likely also Notch, influence the potency of γ-secretase inhibitors such as Avagacestat and DAPT (Burton *et al*., 2008; McKee *et al*., 2012). One study revealed that the protein expression levels of γ-secretase substrate APP effect the GSI response potency (Burton *et al*., 2008). Furthermore, Svedruzic *et*

al. (2008) found that when titrating various concentrations of Notch1 substrate into microsomes containing γ-secretase half-saturated with APP, low levels of Notch1 stimulated the activity of γ-secretase, whereas higher levels of Notch1 above a certain threshold started inhibiting APP cleavage by γ-secretase. Therefore, as APP:Notch1 ratios are relatively high, APP cleavage should be stimulated. Alternatively, as APP:Notch1 ratios decrease between cell types or treatment conditions, so should APP cleavage by γ-secretase.

Because we are using non-transfected cell lines, it could be that we are observing more biologically-relevant selective potencies for GSI's DAPT and Avagacestat on substrates Notch and APP. Our data compared to the data of previous studies suggests that the potency of γ-secretase inhibitors is cell-type specific and relies heavily on the substrate expression levels of both APP and Notch.

To test whether this accounted for the differences in GSI potency between HEK 293, HeLa, and SH-SY5Y, the average total APP and Notch intensity was calculated and presented as a ratio, APP:Notch1. SH-SY5Y cells had a APP:Notch1 ratio of 682:1, whereas HEK 293 and HeLa cells had a ratio of 518:1 and 464:1, respectively. The Human Protein Atlas predicted APP:Notch1 ratios of 412:1, 239:1, and 197:1 for SH-SY5Y, HEK 293, and HeLa cells respectively (*Figure A1.5.2*).

Although there is a trend that correlates the APP:Notch1 ratio for each cell type with its amplitude of inhibition/stimulation, it is difficult to assess what APP level is required to reach saturation for each cell type. This is because functional γ-secretase comes in 6 different functional assemblies, and it is difficult to predict the level of expression, assembly, and activation of γ-secretase at any given time.

We were also interested in seeing if potential changes in APP:Notch1 ratio may be playing a role in the differences in GSI response between cells last treated 24 hours or 72 hours prior to fixation. We found that SH-SY5Y cells treated 72 hours prior to fixation showed an overall increase in APP:Notch1 ratio in response to GSIs, although not statistically significant (*Figure A1.5.1*). Alternatively, SH-SY5Y cells last replaced with drug-containing media 24 hours prior to fixation showed an overall decrease in APP:Notch1 ratio in response to GSIs. When the proportion of Notch1 in the cell is relatively low (high APP:Notch1 ratio), APP cleavage should be stimulated. This is actually what was observed for cells last treated with γ-secretase inhibitors 72 hours prior to fixation. The inverse result is also observed: as the Notch1 proportion rises (SH-SY5Y cells last treated with GSIs 24 hours prior to fixation), so does the Notch1 cleavage selectivity, while the selectivity to cleave APP sufficiently drops as to not overcome inhibition with low-level inhibitor.

4.3.3 γ-secretase-mediated endo-lysosomal dysfunction and intracellular vesicle accumulation may account for the dose-dependent biphasic response to GSIs

To test whether our results indicate that APP-CTF may be accumulating on internal membranes, we immunostained APP-CTF in the presence and absence of DAPT and Avagacestat to visualize the resulting cellular localization of APP-CTF. We found APP-CTF signal accumulating on intracellular vesicles in response to treatment with DAPT and Avagacestat. This could be the accumulation of endocytic vesicles containing membrane-bound APP-CTFs, which accrue due to a decrease in proteolysis by γ-secretase, and a resulting increase in production by α-secretase.

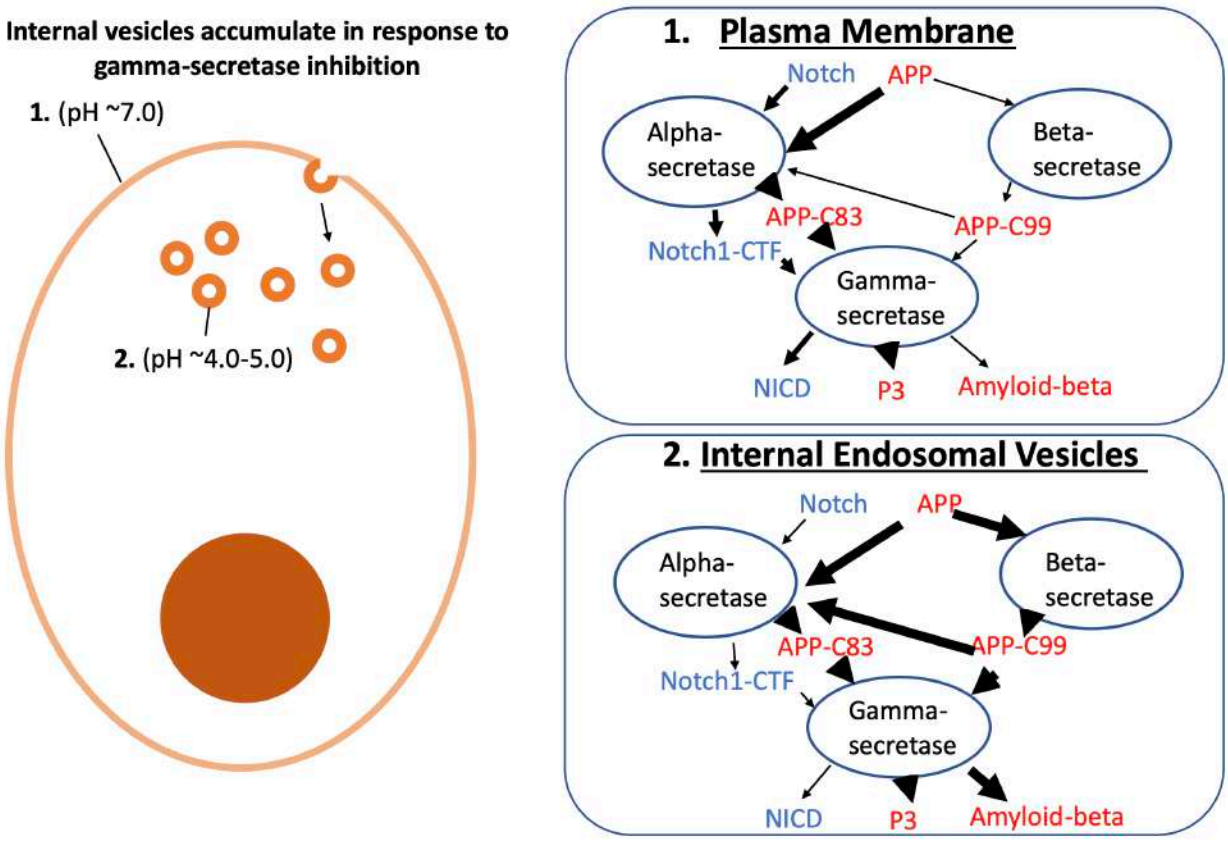

Figure 4.2: An extended model to explain the Aβ rise phenomenon and APP/Notch selectivity switch: membrane internalization.

The inconsistency seen between the clear GSI potency shift observed through the levels of sAPP-α and the lack of GSI potency shift observed between 24-hour and 72-hour treatments in the APP-CTF blot may be explained by the accumulation of APP-CTF on internal membranes. This is because PSEN2-containing γ-secretase localizes primarily to internal vesicles such as late-endosomes and lysosomes versus PSEN1-containing γ-secretase that is more broadly distributed across membranes, including the plasma membrane (Wolfe & Yankner, 2016; Sannerud *et al*., 2016). Because the cells were collected and used for western blot and not the extracellular media, the pool of sAPP-α strongly indicating a GSI potency shift is restricted to α-secretase activity on internal membranes, which would be in physical association with a higher

proportion of PSEN2-containing γ-secretase complexes and less of the PSEN1-containing γ-secretase complexes, which may have differential responses to the γ-secretase inhibitors. Therefore, in our experiments, sAPP-α protein levels serve as a proxy for γ-secretase activity exclusively on internal membranes, whereas APP-C83 protein levels serves as a marker for γ-secretase activity on both internal membranes and the plasma membrane. This could account for some of the variation in the changes in APP-C83 in response to GSIs treated at 24 hours, 72 hours, or 120 hours prior to cell harvesting.

Future cell culture experiments could investigate the locational-specific γ-secretase activity to establish if the observed GSI potency shift is different between the pool of γ-secretase on the plasma membrane (PSEN1) and the pool of γ-secretase on internal membranes (PSEN2). To do this, the above experiment can be repeated, however the media and cells can both be collected, and levels of sAPP-α can be compared between the cells and media. Additionally, changes in membrane-tethered APP can be assessed in response to GSIs treated at different concentrations and time points by immunostaining APP-CTF and staining the plasma membrane exclusively and comparing this data with data from experiments where all membranes, internal and external are stained equally.

α-secretase cleavage of APP normally occurs in the secretory pathway and does not rely on the endocytic pathway like β-secretase does (Zhang & Song, 2013). It is believed that α-secretase activity is optimal at the plasma membrane and trans-golgi network, whereas β-secretase activity mainly occurs after the initial endocytosis of APP. This could be due to differential pH optimums. BACE1 activity has a low pH optimum around 4.5, making its activity dependent on acidic endosomes between 4.0-5.0 (Cole & Vassar, 2007). ADAM10 activity has

an optimal pH closer to physiological pH of 7.0 and its activity is not dependent on acidic subcellular micro-environments (*Figure 4.2*).

Not only did we observe the involvement of intracellular sAPP-α in this response-shift, but we also noticed a biphasic change in total non-membrane-associated APP-CTF in response to the time since last inhibitor replenishment. This suggests that the direct kinetics of γ-secretase may actually play a role in this phenomenon. Additional evidence to support this idea comes from our observation that as the concentration of GSI decreased, the selectivity of γ-secretase switched as to favour the cleavage of APP and not the Notch receptor. This comes with the assumption that as time before last drug replenishment increases the concentration of available GSI decreases. To verify these findings, the experiments could be repeated with varying concentrations of DAPT and Avagacestat all treated for the same time period before harvesting or fixing for immunostaining.

As an extension to these findings, work was recently done using a familial AD (FAD) mutation of APP (APP_{Swe}), a K670M/N671L mutation where lysine and methionine are replaced by asparagine and leucine directly adjacent to the β-cleavage site of APP (Citron *et al*., 1992). This mutation leads to an increase in β-cleavage that causes the excessive accumulation of Aβ leading to early-onset AD. It was recently shown that *in vitro* and *in vivo* models expressing the APP_{Swe} variant do not experience the Aβ rise that usually accompanies low-concentrations of GSIs (Burton *et al*., 2008). In these models, Aβ decreases in a dose-dependent manner. This discovery extends the Barnwell model to suggest that the ECE-bypass is only partly responsible for the Aβ stimulation with low-concentration GSIs and that a more complex interaction between α-secretase, β-secretase, and γ-secretase may be involved.

A computational kinetic model developed by Ortega *et al*., (2013) that recapitulates the Aβ stimulation *in vitro* in cell-based assays with HEK 293 cells and *in vivo* clinical trials with Semagacestat, shows that a rise in β-secretase activity alone is not sufficient to overcome the low-concentration γ-secretase inhibition, and that saturation of α-secretase by way of competition between increased C99 levels and C83 would be necessary to account for Aβ stimulation. Although this explains how low-level γ-secretase inhibition could lead to higher levels of Aβ, it doesn't explain our current findings as to how at supposed lower concentrations of γ-secretase inhibitor, Notch γ-cleavage is inhibited while APP γ-cleavage is stimulated; and at higher GSI concentrations, APP γ-cleavage is inhibited and Notch1 γ-cleavage is enhanced.

Svedruzic *et al*., (2013) proposed that γ-secretase activity is directly involved in the Aβ rise phenomenon. They showed that by titrating varying concentrations of the Notch receptor lacking the ECD (the direct γ-secretase substrate) into cells, APP-cleavage by γ-secretase could be both stimulated (when Notch was provided at low levels) or inhibited (when Notch was provided at higher levels). They proposed that idea that perhaps a single γ-secretase molecule can bind to multiple substrate molecules at a time, and lower concentrations of Notch bound to γ-secretase would improve the binding kinetics of APP substrates, whereas at high concentrations, Notch would saturate γ-secretase binding sites.

4.3.4 GSI concentration modulates γ-secretase substrate selectivity independent of BACE1

Previous work has revealed that cells with FAD mutations that overproduce Aβ are resistant to the Aβ rise phenomenon that occurs at low GSI concentrations (Burton *et al*., 2008). To address whether an increase in BACE1 activity is responsible for the Aβ rise that occurs at low GSI concentrations, we combined DAPT with a potent BACE1 inhibitor LY2886721. According to Western blotting of sAPP-α (*data not shown*) and immunocytochemistry (*Figure*

3.24), we found that BACE1 inhibition did not eliminate the biphasic trend, but instead slightly enhanced it. The overproduction of C99 as a result of BACE1 that competes for cleavage by α-secretase to the point of saturation, which would then lead to more C99 cleavage by γ-secretase despite low level competitive inhibition is not a sufficient theory to account for the phenomenon.

Incorporating our findings with the current literature regarding the Aβ rise phenomenon requires an extension of the current model. Our data combined with the experimental results of Barnwell *et al*. (2014) suggests differential α-secretase responses to GSI inhibition. They show that changes in α-secretase activity don't compliment the biphasic Aβ response evidenced by a linear dose-dependent increase in sAPP-α secreted in the media. On the contrary, our data suggests that α-secretase activity does change at lower GSI concentrations to reflect APP γ-cleavage stimulation instead of inhibition.

Additionally, several studies have shown endo-lysosomal calcium dysfunction and the resulting accumulation of endosomes in FAD mutations on PSEN1, as well as PSEN K/O studies (Zhang *et al,* 2006; Coen *et al*., 2012). The key factor to the Aβ rise may be endocytic internalization, that reflects an optimal pH for BACE1 activity ~4.0-5.0, and less-so for α-secretase activity that optimally operates at pH ~7.0. It may be that at low-GSI concentration, the GSIs are still able to cause PSEN-mediated endosome accumulation, increasing the β : α-secretase activity ratio, but the GSI concentration is not high enough to sufficiently block APP or Notch1 processing by γ-secretase. The shift in localization of APP and Notch processing from the plasma membrane (where Notch and APP are both relatively abundant) to endocytic vesicles (where APP-CTFs are abundant but less Notch) may also explain the NICD-rise phenomenon that occurs at higher GSI concentrations, as shown by Svedruzic *et al*. (2012) that showed when the Notch1:APP ratio was high, APP γ-cleavage was inhibited, while when the Notch1:APP ratio

decreased, Notch1 promoted APP cleavage by γ-secretase. If internalized, the Notch receptor is protected from trans-association with its ligands, rendering it resistant to proteolytic processing. At the same time, APP does not rely on interaction with a ligand for subsequent proteolysis, and as such may be less resistant to processing by the secretases once internalized.

The above model is based on the assumption that expression levels of substrates and enzymes remain constant. Because the Aβ phenomenon seems to be dependent on APP : Notch1 ratios (Svedruzic *et al*., 2012), it may by the case that expressional differences between cells with low-level GSI versus cells with high-level GSI account for at least part of the APP/Notch1 cleavage output differences by γ-secretase. To answer this question, cells could be treated with variable concentrations of GSI and Western blotting can be used to assess protein levels of full-length Notch and APP substrates, α-secretase, β-secretase, and PSEN1/2.

Our data showing a drastic difference in APP-containing internal vesicles in cells treated either 24 hours or 72 hours prior to fixation (*Figure 3.72*), paired with the literature showing DAPT-mediated endosome accumulation (Zhang *et al,* 2006) supports our model of membrane internalization to account for the increase in Aβ. Also, Coen *et al*. found that knocking out PSEN1/2 caused the rapid accumulation of endo-lysosomal vesicles as a function of calcium homeostasis defects (Coen *et al*., 2012).

4.4 Detection of Novel Western blot bands that may be Biologically-Relevant Truncated Notch Molecules

Western blotting was performed on HEK 293, HeLa, and SH-SY5Y cells treated with or without DAPT or Avagacestat. The drug-containing media was last replenished 24-hours before harvesting cells. No significant differences in Notch1 band intensities were observed between control and treatment groups, consistent across cell types. However, a number of prominent bands were detected between 25-79 kDa. The bands found between ~65-79 kDa were found

consistently across cell types, however, the band profile between ~25-60 kDa were unique for each cell type tested. HEK 293 cells showed two bands in this region (~40 kDa and ~50 kDa). HeLa cells showed a single strong band in this region at ~45 kDa. SH-SY5Y cells showed a unique pair of bands in this region (~50 kDa and ~60 kDa).

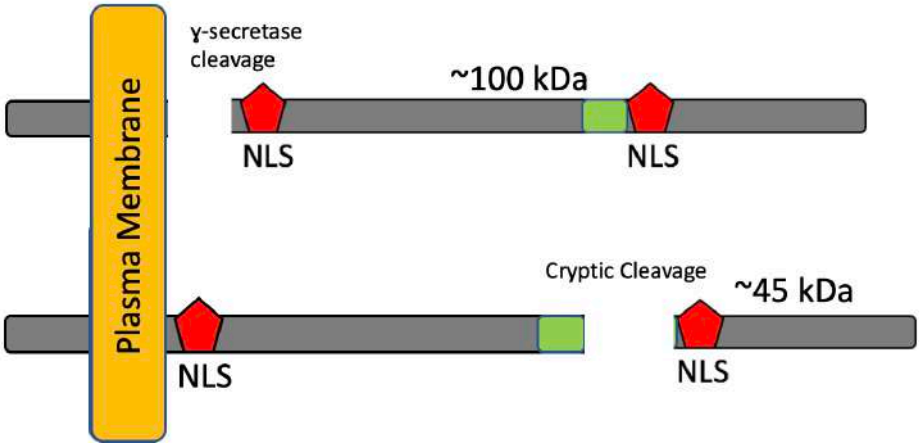

Figure 4.3: Illustration of the prominent truncated Notch1 ICD fragment with NLS adjacent to *in silico* predicted cleavage site.

We observed the appearance of prominent cell-type specific Notch1 bands on Western blot that resemble truncated NICD fragments, with the most prominent bands appearing to be ~45-60 kDa (*Figure 4.3*). It may be the case that these bands do not actually represent Notch1 and are instead off-target epitopes of the antibody. However, using three different antibodies, two with epitopes near the C-terminal end of the NICD, and one on the post-γ-cleaved exposed region of the NICD, we detected these bands using all three antibodies. To verify that these bands are actually truncated NICD fragments, a Notch1 knockdown experiment could be done to see if these truncated bands remain after Notch protein expression has been blocked in the cells.

Additionally, the bands can be extracted from the gel and the trypsin-digested protein contents can be analyzed via Mass Spectrometry to confirm the peptide identity.

4.5 In Silico Predicted Cleavage sites correspond to Complimentary NICD bands found on Western blot

Fassa *et al*. (2007) discovered that a cysteine protease inhibitor abolished the prominent Notch-ICD band that appeared on their HEK293 cell western blots at approximately 79 kDa. Our results also detect this fragment of the Notch-ICD in SH-SY5Y, HEK293, and HeLa nuclear extracts. A eukaryotic linear motif analysis (www.elm.eu.org) of the ICD of human Notch1 revealed a Caspase3-7 cleavage motif that would yield a C-terminal fragment of approximately 79 kDa, and an N-terminal fragment of approximately 21 kDa of mass until the membrane-spanning domain. This cleavage site lies in the loop region between the second and third ankyrin helices. There is also a NEC1/NEC2 cleavage site and a subtilisin/kexin cleavage site both about 2 residues downstream of the Caspase3-7 cleavage site. However, none of these proprotein convertases are cysteine proteases, so they would not account for the enzyme characterized by Fassa *et al* (2007). Alternatively, the caspases are cysteinyl aspartyl proteases, which may account for the protease that was successfully inhibited by Fassa *et al*. (2007) when using a selective cysteine protease pharmacological inhibitor. In addition to the caspase cleavage site, there was also a PKA phosphorylation site, a 14-3-3 protein binding site, and a cyclin binding domain that all overlapped or directly flanked the cleavage site. The phosphorylation of this site by PKA may act as a regulatory switch to allow or prevent Caspase-mediated cleavage. 14-3-3 proteins are a class of highly-conserved regulatory proteins. The cyclin binding domain may work in conjunction with the 14-3-3 binding domain to regulate the probability of cleavage occurring at the site. Caspase3 is localized to the nucleoplasm and not the cytosol, so it could be

the case that this cleavage event may be occurring only after intramembranous cleavage by γ-secretase and Notch localizes to the nucleus. Our results showing an enrichment of this 79 kDa Notch ICD fragment in nuclear fractions despite it lacking the N-terminal NLS would support this idea. We also detected the correlative complimentary band at approximately 21 kDa in our western blot using an antibody that recognizes γ-cleaved Notch-1 at the N-terminus of the intracellular fragment.

Next, in our nuclear extracts of SH-SY5Y cells, we detected reciprocal fragments of a suspected cleavage, producing bands at approximately 35 kDa (N-terminal) and 65 kDa (C-terminal). Using the eukaryotic linear motif analysis, we identified a proprotein convertase cleavage site (subtilisin/kexin) that would theoretically yield fragments of these proportions. The subtilisin/kexin class of proprotein convertases are a class of promiscuous serine proteases that are notably responsible for activating a number of prohormones. A NEK2 phosphorylation site was also found to overlap with the cleavage domain, as well as an actin binding motif, and a glycosaminoglycan site. The phosphorylation site is likely involved in acting as a regulatory switch to promote or prevent cleavage at this site. The actin-binding domain may function to assist the trafficking of the protein fragment throughout the cell. However, the glycosaminoglycan binding site remains puzzling because normally these proteoglycan additions are reserved for extracellular proteins.

Complimentary Notch1 bands were also detected that predict a cleavage to occur that produces fragments of 40 kDa and 60 kDa respectively. The eukaryotic linear motif analysis revealed a Caspase3-7 cleavage site that overlapped with a di-arginine ER-retention signal, a 14-3-3 protein binding site, a a Forkhead-associated (FHA) domain, and a PKA phosphorylation site. The presence of the ER retention motif is interesting. It likely plays a role in regulation of

appropriate conformation in the ER, where the ER-retention signal can be inactivated by phosphorylation or 14-3-3 protein association once the appropriate protein conformation is attained, and the transition to the Golgi can occur. The phosphorylation of this site by PKA may also act as a regulatory switch to allow or prevent Caspase-mediated cleavage. 14-3-3 proteins are a class of highly-conserved regulatory proteins. The FHA domain is a phosphopeptide recognition domain that may work in conjunction with the 14-3-3 proteins to regulate the functionality of the ER-retention signal and act as a regulatory switch for Caspase-mediated cleavage at this site.

A subtilisin/kexin-1 cleavage site was found on the eukaryotic linear motif analysis that may be responsible for producing the two reciprocal bands of 50 kDa and 50 kDa detected on western blot in the nuclear fraction of the Sh-SY5Y cells. This site is overlapped by a cyclin binding domain, FHA domain, and a casein kinase-1 phosphorylation site, all of which may play a role in regulating this cleavage event.

Furthermore, complimentary Notch1 fragments were detected via Western blot that were 55 kDa and 45 kDa respectively. At this region, there are two cleavage sites in close proximity. A nardilysin cleavage site overlaps with a C-terminal USP-7 deubiquitination site, an SH3 protein-protein binding domain, a C-terminal amidation site, a nuclear localization signal (NLS), and a ubiquitination site. A Subtilisin/Kexin cleavage site overlaps with an N-terminal USP7 domain, a sumoylation site, and an NLS.

Lastly, on western blot we detected reciprocal Notch1 bands that were 60 kDa and 40 kDa respectively. This site overlaps with a C-terminal USP7 site, a PKA phosphorylation site, a PIKK phosphorylation site, and an NLS.

The presence of a second NLS just C-terminal of the ankyrin repeats that would appear on the exposed end of a Notch ICD fragment cleaved at one of these three peptidase cleavage sites may be a novel, biologically relevant mechanism of Notch signalling. The presence of phosphorylation sites overlapping with nearly all of these peptidase sites suggests that these cleavage sites are biologically relevant and require covalent modifications as part of a regulatory switch mechanism.

The possibility that Notch may be cleaved at different domains throughout its intracellular architecture would allow for the possibility that it can be released in its full form, containing the TAD domain, ankyrin repeats, RAM domain, and PEST domain, or it can act in the nucleus in a truncated form that has modified activity and association with transcriptional regulators and cofactors in an active or repressive manner. This would expand the current framework around Notch signalling from a binary ON/OFF switch to a broader spectrum of signal outputs that may be independent of γ-secretase cleavage of Notch.

In initial Western blots for Notch2 in SH-SY5Y cells, we also noticed the appearance of a prominent band around 55 kDa in size. To test whether the production of a truncated Notch ICD is cell-contact dependent, or dependent on subsequent cleavage by γ-secretase, we performed a Western blot using the Notch2 antibody on low, medium, or high-confluency SH-SY5Y cells. Interestingly, we noticed that the 55 kDa band intensity increased as cells became more confluent, and the full-length ICD ~100kDa decreased with confluency, all within the nuclear fraction. This suggests that the proteolytic processing of the Notch2 ICD shifts in a contact-dependent manner. It may be that when cell-cell contacts are less abundant, normal γ-secretase-mediated Notch2 signalling predominates; whereas when intercellular contacts increase, γ-secretase-mediated Notch2 signalling is replaced by a downstream protease that releases a ~55

kDa fragment to the nucleus that may act in an active or repressive manner in the transcription of Notch target genes.

A comparative eukaryotic linear motif analysis between the Notch1 and Notch2 protein sequences revealed a DMQDN Caspase-3 cleavage domain only on Notch2 and not Notch1 that would account for the formation of this ~55 kDa Notch2 ICD band. Interestingly, this is the exact same sequence found on PKC-delta upon the initiation of apoptosis in response to cellular stress. CPP32 (a specific Caspase-3) recognizes and cleaves the DMQDN domain on PKC-delta to activate it. To test whether CPP32 is the protease responsible for prominent truncated bands in Notch1/2, selective pharmacological inhibition can be used.

Final Remarks

In the present study, we combined immunofluorescence staining, western blotting, and the bromo-deoxyuridine (BrdU) cell proliferation assay as three orthogonal methods to sensitively quantify the γ-secretase cleavage of Notch and APP in SH-SY5Y human neuroblastoma cells, which rely on active Notch signalling to maintain proliferation. With the exception of the BrdU assay, the tripartite assay was also validated using HEK 293 and HeLa cells. Using our assay, we found that the selectivity for γ-secretase to cleave APP versus Notch was dependent on the time the GSI was replenished before harvesting, which may directly reflect a GSI concentration-dependent selective potency. In addition, a number of novel Notch1 bands (25-75 kDa) were discovered on western blot that may be novel biologically relevant γ-secretase-independent proteolytic products that could play a role in differentially activating or competitively inhibiting the expression of Notch target genes. The Notch proteolytic profile detected on Western blot was cell-type specific and unique between HEK 293 human stem cells, and human cancer lines HeLa and SH-SY5Y cells. In summary, using our high-throughput cell-

based assay, cleavage of APP and Notch activation by γ-secretase was sensitively quantified; while a novel profile of cell-type specific proteolytic fragments of the Notch ICD have been identified that may have biological implications in normal development and the pathological proliferation and metastasis of some cancers.

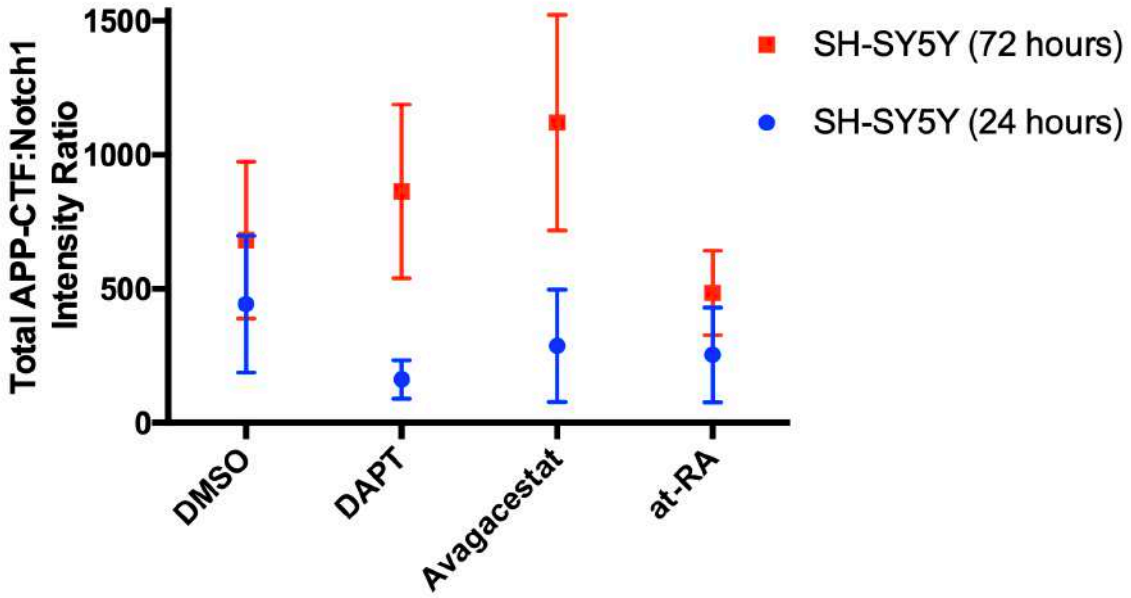

Figure A1.5.1: Total APP:Notch1 immunocytochemistry signal intensity for SH-SY5Y cells last treated with DAPT, Avagacestat, or at-RA either 24 hours or 72 hours prior to cell fixation

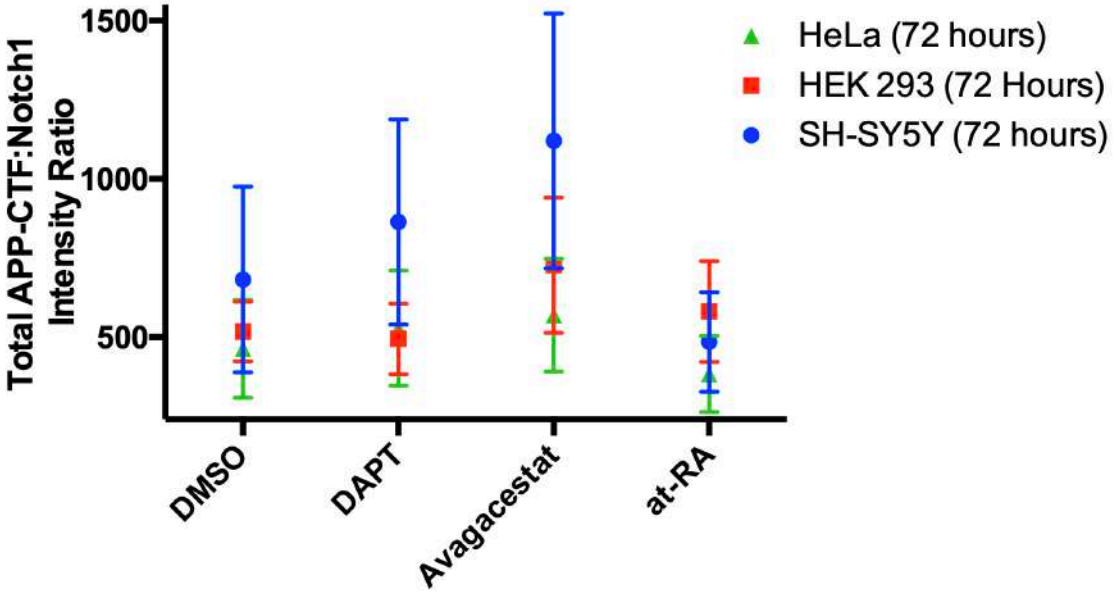

Figure A1.5.2: Total APP:Notch1 immunocytochemistry signal intensity for HEK 293, HeLa, and SH-SY5Y cells last treated with DAPT, Avagacestat, or at-RA 72 hours prior to cell fixation

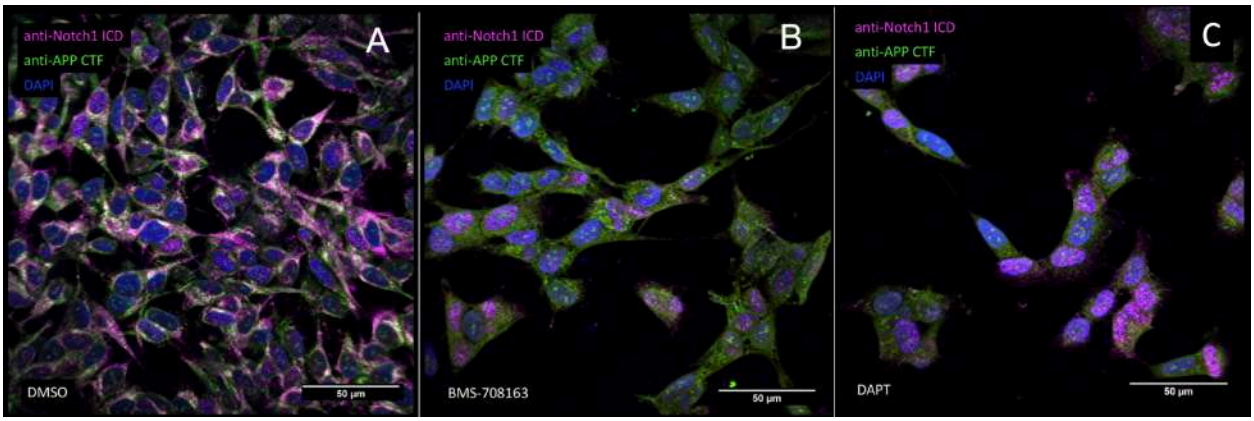

Figure A1.5.3: Representative images of Notch1 (magenta) and APP-CTF (green) immunostainings.

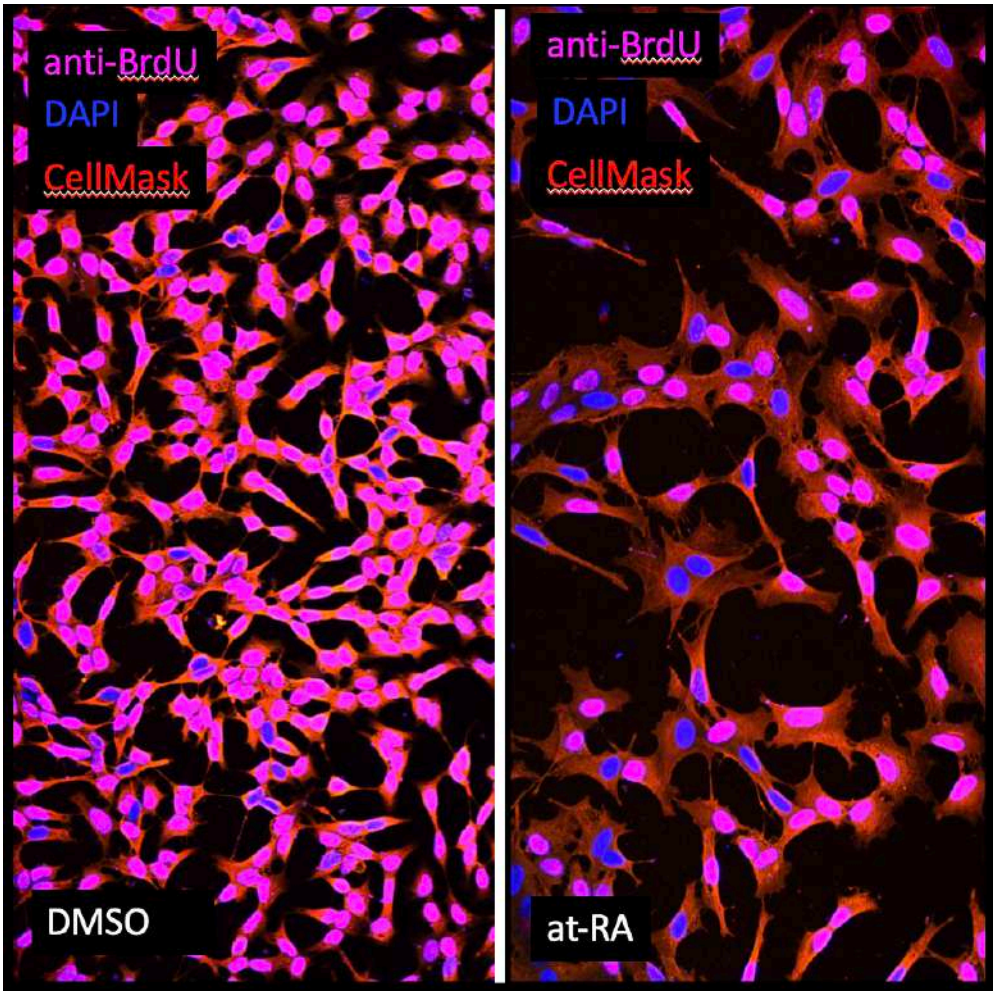

Figure A1.5.4: Representative images of BrdU cell proliferation assay. DMSO versus at-RA treated SH-SY5Y cells treated with 10 uM BrdU for 24 hours and stained using the G3G4 monoclonal anti-BrdU antibody.

Appendix II – Methodology

BCA vs. Solid-phase; BSA vs. Tubulin

When comparing the BCA assay and solid-phase Coomassie based assay, the BCA assay consistently yielded lower consistency of protein loaded between different samples on a gel.

When comparing BSA vs. Tubulin as protein standards in the solid-phase Coomassie-based total protein assay, BSA (5.7% CV) outperformed Tubulin (11% CV) to yield the lowest variability of protein loaded between samples.

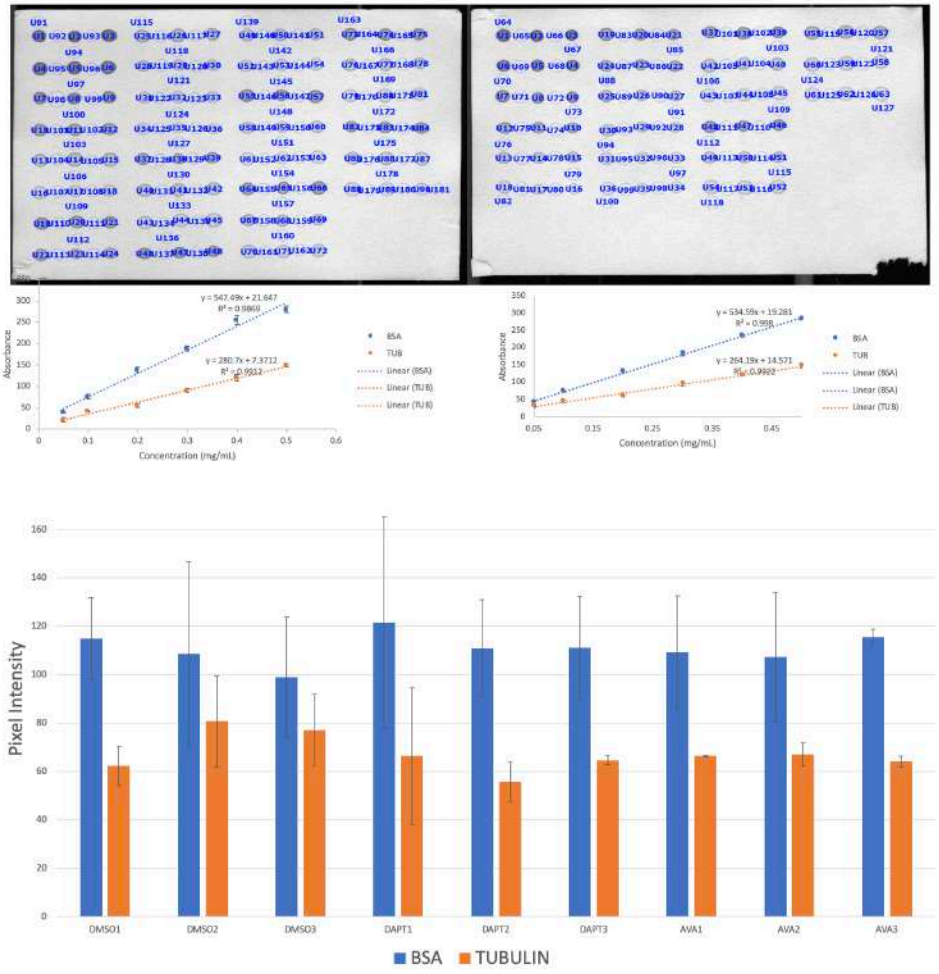

Figure AII.6.1: Total protein intensities of 9 samples of Coomassie-stained gels using BSA vs. Tubulin as a protein standard for total protein quantification using solid-phase Coomassie-based protein assay. BSA as a protein standard minimized inter-sample protein loading variation with a coefficient of variance of 0.057, when compared with the tubulin inter-sample variation of 0.11.

Nuclear Notch Analysis ImageJ Macro

```
img_name=getTitle();
run("Split Channels");
close();
close();
run("8-bit");
selectWindow("C1-"+img_name);
setOption("BlackBackground", false);
run("Make Binary", "method=Default background=Default calculate");
run("Fill Holes", "stack");
imageCalculator("Subtract create stack", "C2-"+img_name,"C1-"+img_name);
selectWindow("Result of C2-"+img_name);
setAutoThreshold("Default dark");
//run("Threshold...");
setThreshold(5, 255);
setBatchMode(true);
dir = File.directory;
name = File.nameWithoutExtension;
run("ROI Manager...");
makeRectangle(0, 3, 1893, 1896);
roiManager("Add");
roiManager("Select", 0);
roiManager("Multi Measure");
saveAs("results", dir + name + ".csv");
setBatchMode(false);
selectWindow("Result of C2-"+img_name);
close();
selectWindow("C1-"+img_name);
run("Invert", "stack");
imageCalculator("Subtract create stack", "C2-"+img_name,"C1-"+img_name);
selectWindow("Result of C2-"+img_name);
setAutoThreshold("Default dark");
//run("Threshold...");
setThreshold(5, 255);
setBatchMode(true);
dir = File.directory;
name = File.nameWithoutExtension;
run("ROI Manager...");
makeRectangle(0, 3, 1893, 1896);
roiManager("Add");
roiManager("Select", 0);
roiManager("Multi Measure");
saveAs("results", dir + name + "nuc" + ".csv");
setBatchMode(false);
close();
close();
close();
```

APP Analysis ImageJ Macro

```
img_name=getTitle();
dir = File.directory;
name = File.nameWithoutExtension;
run("Split Channels");
selectWindow("C1-"+img_name);
close();
selectWindow("C2-"+img_name);
close();
selectWindow("C3-"+img_name);
run("ROI Manager...");
makeRectangle(0, 3, 2045, 2045);
roiManager("Add");
roiManager("Select", 0);
roiManager("Multi Measure");

setBatchMode(true)
saveAs("results", dir + name + "APP" + ".csv");
setBatchMode(false);

imageCalculator("Subtract create stack", "C3-"+img_name,"C4-"+img_name);

setBatchMode(true)
dir = File.directory;
name = File.nameWithoutExtension;
run("ROI Manager...");
makeRectangle(0, 3, 2045, 2045);
roiManager("Add");
roiManager("Select", 0);
roiManager("Multi Measure");
selectWindow("Result of C3-"+img_name);
saveAs("results", dir + name + "cleaved" + ".csv");
setBatchMode(false);

close();
close();
close();
```

BrdU Analysis ImageJ Macro

```
img_name=getTitle();
run("Split Channels");
close();
run("8-bit");
selectWindow("C1-"+img_name);
setOption("BlackBackground", false);
run("Make Binary", "method=Default background=Default calculate");
run("Analyze Particles...", "size=15.00-Infinity circularity=0.30-1.00 show=Outlines display
clear summarize stack");
close();
setBatchMode(true);
dir = File.directory;
name = File.nameWithoutExtension;
selectWindow("Summary of C1-"+img_name);
saveAs("results", dir + name + ".csv");
setBatchMode(false);

selectWindow("C1-"+img_name);
run("Invert", "stack");
imageCalculator("Subtract create stack", "C2-"+img_name,"C1-"+img_name);
selectWindow("Result of C2-"+img_name);
run("Make Binary", "method=Default background=Default calculate");
run("Analyze Particles...", "size=15.00-Infinity circularity=0.30-1.00 show=Outlines display
clear summarize stack");

setBatchMode(true);
dir = File.directory;
name = File.nameWithoutExtension;
selectWindow("Summary of Result of C2-"+img_name);
saveAs("results", dir + name + "brdu" + ".csv");
setBatchMode(false);

close();
close();
close();
close();
```

APP-containing vesicles Quantification ImageJ Macro

```
img_name=getTitle();;
run("8-bit");
run("Split Channels");
selectWindow("C2-"+img_name);
close();
selectWindow("C1-"+img_name);
close();
imageCalculator("Subtract create", "C3-"+img_name,"C4-"+img_name);
selectWindow("Result of C3-"+img_name);
setThreshold(5, 255);
run("Analyze Particles...", "  show=Outlines display summarize add");
setBatchMode(true);
dir = File.directory;
name = File.nameWithoutExtension;
selectWindow("Summary");
saveAs("results", dir + name + "vesicles" + ".csv");
setBatchMode(false);
close();
close();
close();
close();
```

References

Albright, C. F., Dockens, R. C., Meredith, J. E., Olson, R. E., Slemmon, R., Lentz, K. A., … Tong, G. (2012). Pharmacodynamics of Selective Inhibition of gamma-Secretase by Avagacestat. Journal of Pharmacology and Experimental Therapeutics, 344(3), 686–695. doi:10.1124/jpet.112.199356

Anderson, D. D., Eom, J. Y., & Stover, P. J. (2012). Competition between sumoylation and ubiquitination of serine hydroxymethyltransferase 1 determines its nuclear localization and its accumulation in the nucleus. Journal of Biological Chemistry, 287(7), 4790-4799.

Bai, X. C., Yan, C., Yang, G., Lu, P., Ma, D., Sun, L., ... & Shi, Y. (2015). An atomic structure of human γ-secretase. Nature, 525(7568), 212.

Barnwell, E., Padmaraju, V., Baranello, R., Pacheco-Quinto, J., & Crosson, C. (2014). Evidence of a Novel Mechanism for Partial c-Secretase Inhibition.

Baron, M., Aslam, H., Flasza, M., Fostier, M., Higgs, J. E., Mazaleyrat, S. L., & Wilkin, M. B. (2002). Multiple levels of Notch signal regulation. Molecular membrane biology, 19(1), 27-38.

Barthet, G., Shioi, J., Shao, Z., Ren, Y., Georgakopoulos, A., & Robakis, N. K. (2011). Inhibitors of γ-secretase stabilize the complex and differentially affect processing of amyloid precursor protein and other substrates. The FASEB Journal, 25(9), 2937-2946.

Benilova, I., Karran, E., & De Strooper, B. (2012). The toxic Aβ oligomer and Alzheimer's disease: an emperor in need of clothes. Nature neuroscience, 15(3), 349.

Bland, C. E., Kimberly, P., & Rand, M. D. (2003). Notch-induced proteolysis and nuclear localization of the Delta ligand. Journal of Biological Chemistry, 278(16), 13607-13610.

Blaumueller, C. M., Qi, H., Zagouras, P., & Artavanis-Tsakonas, S. (1997). Intracellular cleavage of Notch leads to a heterodimeric receptor on the plasma membrane. *Cell*, *90*(2), 281-291.

Bolduc, D. M., Montagna, D. R., Gu, Y., Selkoe, D. J., & Wolfe, M. S. (2016). Nicastrin functions to sterically hinder γ-secretase–substrate interactions driven by substrate transmembrane domain. Proceedings of the National Academy of Sciences, 113(5), E509-E518.

Burton, C. R., Meredith, J. E., Barten, D. M., Goldstein, M. E., Krause, C. M., Kieras, C. J., ... & Lin, X. A. (2008). The amyloid-β rise and γ-secretase inhibitor potency depend on the level of substrate expression. Journal of Biological Chemistry, 283(34), 22992-23003.

Cao, H., Hu, Y., Wang, P., Zhou, J., Deng, Z., & Wen, J. (2012). Down-regulation of Notch receptor signaling pathway induces caspase-dependent and caspase-independent apoptosis in lung squamous cell carcinoma cells. Apmis, 120(6), 441-450.

Chang, H. H., Lee, H., Hu, M. K., Tsao, P. N., Juan, H. F., Huang, M. C., ... & Huang, S. F. (2010). Notch1 expression predicts an unfavorable prognosis and serves as a therapeutic target of patients with neuroblastoma. Clinical Cancer Research, 16(17), 4411-4420.

Chang, Y., Tesco, G., Jeong, W. J., Lindsley, L., Eckman, E. A., Eckman, C. B., ... & Guénette, S. Y. (2003). Generation of the β-amyloid peptide and the amyloid precursor protein C-terminal fragment γ are potentiated by FE65L1. Journal of Biological Chemistry, 278(51), 51100-51107.

Citron, M., Oltersdorf, T., Haass, C., McConlogue, L., Hung, A. Y., Seubert, P., ... & Selkoe, D. J. (1992). Mutation of the β-amyloid precursor protein in familial Alzheimer's disease increases β-protein production. Nature, 360(6405), 672.

Coen, K., Flannagan, R. S., Baron, S., Carraro-Lacroix, L. R., Wang, D., Vermeire, W., ... & Wuytack, F. (2012). Lysosomal calcium homeostasis defects, not proton pump defects, cause endo-lysosomal dysfunction in PSEN-deficient cells. J Cell Biol, 198(1), 23-35.

Cole, S. L., & Vassar, R. (2007). The Alzheimer's disease β-secretase enzyme, BACE1. Molecular neurodegeneration, 2(1), 22.

Coric, V., Salloway, S., van Dyck, C. H., Dubois, B., Andreasen, N., Brody, M., ... & Pilcher, G. (2015). Targeting prodromal Alzheimer disease with avagacestat: a randomized clinical trial. JAMA neurology, 72(11), 1324-1333.

Coric, V., van Dyck, C. H., Salloway, S., Andreasen, N., Brody, M., Richter, R. W., ... & Colby, S. (2012). Safety and tolerability of the γ-secretase inhibitor avagacestat in a phase 2 study of mild to moderate Alzheimer disease. Archives of neurology, 69(11), 1430-1440.

Coyle, J. T., Price, D. L., & Delong, M. R. (1983). Alzheimer's disease: a disorder of cortical cholinergic innervation. Science, 219(4589), 1184-1190.

Crump, C. J., Castro, S. V., Wang, F., Pozdnyakov, N., Ballard, T. E., Sisodia, S. S., ... & Li, Y. M. (2012). BMS-708,163 targets presenilin and lacks notch-sparing activity. Biochemistry, 51(37), 7209-7211.

de Celis, J. F., Barrio, R., del Arco, A., & Garcia-Bellido, A. (1993). Genetic and molecular characterization of a Notch mutation in its Delta-and Serrate-binding domain in Drosophila. Proceedings of the National Academy of Sciences, 90(9), 4037-4041.

de Celis, J. F., & Garcia-Bellido, A. (1994). Modifications of the notch function by Abruptex mutations in Drosophila melanogaster. Genetics, 136(1), 183-194.

Demarest, R. M., Ratti, F., & Capobianco, A. J. (2008). It's T-ALL about Notch. Oncogene, 27(38), 5082.

Deregowski, V., Gazzerro, E., Priest, L., Rydziel, S., & Canalis, E. (2006). Role of the RAM domain and ankyrin repeats on notch signaling and activity in cells of osteoblastic lineage. Journal of Bone and Mineral Research, 21(8), 1317-1326.

De Strooper, B. (2003). Aph-1, Pen-2, and nicastrin with presenilin generate an active γ-secretase complex. Neuron, 38(1), 9-12.

Doerfler, P., Shearman, M. S., & Perlmutter, R. M. (2001). Presenilin-dependent γ-secretase activity modulates thymocyte development. Proceedings of the National Academy of Sciences, 98(16), 9312-9317.

Dovey, H. F., John, V., Anderson, J. P., Chen, L. Z., de Saint Andrieu, P., Fang, L. Y., ... & Hu, K. L. (2001). Functional gamma-secretase inhibitors reduce beta-amyloid peptide levels in brain. Journal of neurochemistry, 76(1), 173-181.

Dyczynska, E., Sun, D., Yi, H., Sehara-Fujisawa, A., Blobel, C. P., & Zolkiewska, A. (2007). Proteolytic processing of delta-like 1 by ADAM proteases. Journal of Biological Chemistry, 282(1), 436-444.

Encinas, M., Iglesias, M., Liu, Y., Wang, H., Muhaisen, A., Cena, V., ... & Comella, J. X. (2000). Sequential treatment of SH-SY5Y cells with retinoic acid and brain-derived neurotrophic factor gives rise to fully differentiated, neurotrophic factor-dependent, human neuron-like cells. Journal of neurochemistry, 75(3), 991-1003.

Fassa, A., Parisiadou, L., Robakis, N. K., & Efthimiopoulos, S. (2007). Novel processing of Notch 1 within its intracellular domain by a cysteine protease. Neurodegenerative Diseases, 4(2-3), 148-155.

Fehon, R. G., Kooh, P. J., Rebay, I., Regan, C. L., Xu, T., Muskavitch, M. A., & Artavanis-Tsakonas, S. (1990). Molecular interactions between the protein products of the neurogenic loci Notch and Delta, two EGF-homologous genes in Drosophila. Cell, 61(3), 523-534.

Ferrari-Toninelli, G., Bonini, S. A., Uberti, D., Buizza, L., Bettinsoli, P., Poliani, P. L., ... & Memo, M. (2010). Targeting Notch pathway induces growth inhibition and differentiation of neuroblastoma cells. Neuro-oncology, 12(12), 1231-1243.

Fre, S., Huyghe, M., Mourikis, P., Robine, S., Louvard, D., & Artavanis-Tsakonas, S. (2005). Notch signals control the fate of immature progenitor cells in the intestine. Nature, 435(7044), 964.

Garg, V., Muth, A. N., Ransom, J. F., Schluterman, M. K., Barnes, R., King, I. N., ... & Srivastava, D. (2005). Mutations in NOTCH1 cause aortic valve disease. Nature, 437(7056), 270.

Gazave, E., Lapébie, P., Richards, G. S., Brunet, F., Ereskovsky, A. V., Degnan, B. M., ... &

Renard, E. (2009). Origin and evolution of the Notch signalling pathway: an overview from eukaryotic genomes. BMC evolutionary biology, 9(1), 249.

Gillman, K. W., Starrett Jr, J. E., Parker, M. F., Xie, K., Bronson, J. J., Marcin, L. R., ... & Meredith Jr, J. E. (2010). Discovery and evaluation of BMS-708163, a potent, selective and orally bioavailable γ-secretase inhibitor. ACS Medicinal Chemistry Letters, 1(3), 120-124.

Godyń, J., Jończyk, J., Panek, D., & Malawska, B. (2016). Therapeutic strategies for Alzheimer's disease in clinical trials. Pharmacological Reports, 68(1), 127-138.

Goriely, A., Dumont, N., Dambly-Chaudiere, C., & Ghysen, A. (1991). The determination of sense organs in Drosophila: effect of the neurogenic mutations in the embryo. Development, 113(4), 1395-1404.

Gupta-Rossi, N., Le Bail, O., Gonen, H., Brou, C., Logeat, F., Six, E., ... & Israël, A. (2001). Functional interaction between SEL-10, an F-box protein, and the nuclear form of activated Notch1 receptor. Journal of Biological Chemistry, 276(37), 34371-34378.

Haapasalo, A., & Kovacs, D. M. (2011). The many substrates of presenilin/γ-secretase. Journal of Alzheimer's disease, 25(1), 3-28.

Hardy, J. A., & Higgins, G. A. (1992). Alzheimer's disease: the amyloid cascade hypothesis. Science, 256(5054), 184-186.

Heitzler, P., & Simpson, P. (1991). The choice of cell fate in the epidermis of Drosophila. Cell, 64(6), 1083-1092.

Hemming, M. L., Elias, J. E., Gygi, S. P., & Selkoe, D. J. (2008). Proteomic profiling of γ-secretase substrates and mapping of substrate requirements. PLoS biology, 6(10), e257.

Hooper, C., Chapple, J. P., Lovestone, S., & Killick, R. (2007). The Notch-1 intracellular domain is found in sub-nuclear bodies in SH-SY5Y neuroblastomas and in primary cortical neurons. Neuroscience letters, 415(2), 135-139.

Jacobsen, T. L., Brennan, K., Arias, A. M., & Muskavitch, M. A. (1998). Cis-interactions between Delta and Notch modulate neurogenic signalling in Drosophila. Development, 125(22), 4531-4540.

Joutel, A., Corpechot, C., Ducros, A., Vahedi, K., Chabriat, H., Mouton, P., ... & Maciazek, J. (1996). Notch3 mutations in CADASIL, a hereditary adult-onset condition causing stroke and dementia. Nature, 383(6602), 707.

Kao, H. Y., Ordentlich, P., Koyano-Nakagawa, N., Tang, Z., Downes, M., Kintner, C. R., ... & Kadesch, T. (1998). A histone deacetylase corepressor complex regulates the Notch signal transduction pathway. Genes & development, 12(15), 2269-2277.

Karch, C. M., Cruchaga, C., & Goate, A. M. (2014). Alzheimer's disease genetics: from the bench to the clinic. Neuron, 83(1), 11-26.

Kelley, M. R., Kidd, S., Deutsch, W. A., & Young, M. W. (1987). Mutations altering the structure of epidermal growth factor-like coding sequences at the Drosophila Notch locus. Cell, 51(4), 539-548.

Klueg, K. M., Parody, T. R., & Muskavitch, M. A. (1998). Complex proteolytic processing acts on Delta, a transmembrane ligand for Notch, during Drosophila development. Molecular biology of the cell, 9(7), 1709-1723.

Kolev, V., Kacer, D., Trifonova, R., Small, D., Duarte, M., Soldi, R., ... & Prudovsky, I. (2005). The intracellular domain of Notch ligand Delta1 induces cell growth arrest. FEBS letters, 579(25), 5798-5802.

Kopan, R., & Ilagan, M. X. G. (2009). The canonical Notch signaling pathway: unfolding the activation mechanism. Cell, 137(2), 216-233.

Kovacs, D. M., Fausett, H. J., Page, K. J., Kim, T. W., Moir, R. D., Merriam, D. E., ... & Hyman, B. T. (1996). Alzheimer–associated presenilins 1 and 2: neuronal expression in brain and localization to intracellular membranes in mammalian cells. Nature medicine, 2(2), 224.

Kreft, A., Harrison, B., Aschmies, S., Atchison, K., Casebier, D., Cole, D. C., ... & Huryn, D. (2008). Discovery of a novel series of Notch-sparing γ-secretase inhibitors. Bioorganic & medicinal chemistry letters, 18(14), 4232-4236.

Kurooka, H., & Honjo, T. (2000). Functional interaction between the mouse notch1 intracellular region and histone acetyltransferases PCAF and GCN5. Journal of Biological Chemistry, 275(22), 17211-17220.

Lanz, T. A., Karmilowicz, M. J., Wood, K. M., Pozdnyakov, N., Du, P., Piotrowski, M. A., ... & Fei, Q. (2006). Concentration-dependent modulation of amyloid-β in vivo and in vitro using the γ-secretase inhibitor, LY-450139. Journal of Pharmacology and Experimental Therapeutics, 319(2), 924-933.

LaVoie, M. J., Fraering, P. C., Ostaszewski, B. L., Ye, W., Kimberly, W. T., Wolfe, M. S., & Selkoe, D. J. (2003). Assembly of the γ-secretase complex involves early formation of an intermediate subcomplex of Aph-1 and nicastrin. Journal of Biological Chemistry, 278(39), 37213-37222.

LaVoie, M. J., & Selkoe, D. J. (2003). The Notch ligands, Jagged and Delta, are sequentially processed by α-secretase and presenilin/γ-secretase and release signaling fragments. Journal of Biological Chemistry, 278(36), 34427-34437.

Lawrence, N., Klein, T., Brennan, K., & Arias, A. M. (2000). Structural requirements for notch

signalling with delta and serrate during the development and patterning of the wing disc of Drosophila. Development, 127(14), 3185-3195

Lee, M. K., Slunt, H. H., Martin, L. J., Thinakaran, G., Kim, G., Gandy, S. E., ... & Sisodia, S. S. (1996). Expression of presenilin 1 and 2 (PS1 and PS2) in human and murine tissues. Journal of Neuroscience, 16(23), 7513-7525.

Li, T., Huang, Y., Jin, S., Ye, L., Rong, N., Yang, X., ... & Harrison, D. C. (2012). γ-Secretase modulators do not induce Aβ-rebound and accumulation of β-C-terminal fragment. Journal of neurochemistry, 121(2), 277-286.

Matsumoto, A., Onoyama, I., Sunabori, T., Kageyama, R., Okano, H., & Nakayama, K. I. (2011). Fbxw7-dependent degradation of Notch is required for control of "stemness" and neuronal-glial differentiation in neural stem cells. Journal of Biological Chemistry, 286(15), 13754-13764.

Matsuoka, Y., Li, T., Huang, Y., Jin, S., Ye, L., Rong, N., ... & Lau, L. F. (2009). γ-secretase inhibitor, but not modulator, causes Aβ overshoot and accumulation of β-CTF. Alzheimer's & Dementia: The Journal of the Alzheimer's Association, 5(4), P422.

Mayer, S. C., Kreft, A. F., Harrison, B., Abou-Gharbia, M., Antane, M., Aschmies, S., ... & Diamantidis, G. (2008). Discovery of begacestat, a Notch-1-sparing γ-secretase inhibitor for the treatment of Alzheimer's disease. Journal of medicinal chemistry, 51(23), 7348-7351.

McKee, T. D., Loureiro, R. M., Dumin, J. A., Zarayskiy, V., & Tate, B. (2013). An improved cell-based method for determining the γ-secretase enzyme activity against both Notch and APP substrates. Journal of neuroscience methods, 213(1), 14-21.

Mikulca, J. A., Nguyen, V., Gajdosik, D. A., Teklu, S. G., Giunta, E. A., Lessa, E. A., ... & Raffa, R. B. (2014). Potential novel targets for A lzheimer pharmacotherapy: II. Update on secretase inhibitors and related approaches. Journal of clinical pharmacy and therapeutics, 39(1), 25-37.

Mishra-Gorur, K., Rand, M. D., Perez-Villamil, B., & Artavanis-Tsakonas, S. (2002). Down-regulation of Delta by proteolytic processing. The Journal of cell biology, 159(2), 313-324.

Morohashi, Y., Kan, T., Tominari, Y., Fuwa, H., Okamura, Y., Watanabe, N., ... & Tomita, T. (2006). C-terminal fragment of presenilin is the molecular target of a dipeptidic γ-secretase-specific inhibitor DAPT (N-[N-(3, 5-difluorophenacetyl)-L-alanyl]-S-phenylglycine t-butyl ester). Journal of Biological Chemistry, 281(21), 14670-14676.

Mueller, M. C., Baranowski, B. J., & Hayward, G. C. (2018). New Insights on the Role of Residue 673 of APP in Alzheimer's Disease. Journal of Neuroscience, 38(3), 515-517.

Niimura, M., Isoo, N., Takasugi, N., Tsuruoka, M., Ui-Tei, K., Saigo, K., ... & Iwatsubo, T. (2005). Aph-1 contributes to the stabilization and trafficking of the γ-secretase complex through mechanisms involving intermolecular and intramolecular interactions. Journal of Biological Chemistry, 280(13), 12967-12975.

Noaman, N., & Coorssen, J. R. (2018). Coomassie does it (better): A Robin Hood approach to total protein quantification. Analytical biochemistry, 556, 53-56.

Öberg, C., Li, J., Pauley, A., Wolf, E., Gurney, M., & Lendahl, U. (2001). The Notch intracellular domain is ubiquitinated and negatively regulated by the mammalian Sel-10 homolog. Journal of Biological Chemistry, 276(38), 35847-35853.

Okochi, M., Steiner, H., Fukumori, A., Tanii, H., Tomita, T., Tanaka, T., ... & Haass, C. (2002). Presenilins mediate a dual intramembranous γ-secretase cleavage of Notch-1. The EMBO journal, 21(20), 5408-5416.

O'Neil, J., Grim, J., Strack, P., Rao, S., Tibbitts, D., Winter, C., ... & Draetta, G. (2007). FBW7 mutations in leukemic cells mediate NOTCH pathway activation and resistance to γ-secretase inhibitors. Journal of Experimental Medicine, 204(8), 1813-1824.

Ortega, F., Stott, J., Visser, S. A., & Bendtsen, C. (2013). Interplay between α-, β-, and γ-secretases determines biphasic amyloid-β protein level in the presence of a γ-secretase inhibitor. Journal of Biological Chemistry, 288(2), 785-792.

Påhlman, S., Ruusala, A. I., Abrahamsson, L., Mattsson, M. E., & Esscher, T. (1984). Retinoic acid-induced differentiation of cultured human neuroblastoma cells: a comparison with phorbolester-induced differentiation. Cell differentiation, 14(2), 135-144.

Park, M. J., Taki, T., Oda, M., Watanabe, T., Yumura-Yagi, K., Kobayashi, R., ... & Hayashi, Y. (2009). FBXW7 and NOTCH1 mutations in childhood T cell acute lymphoblastic leukaemia and T cell non-Hodgkin lymphoma. British journal of haematology, 145(2), 198-206.

Prince, M. J., Wu, F., Guo, Y., Robledo, L. M. G., O'Donnell, M., Sullivan, R., & Yusuf, S. (2015). The burden of disease in older people and implications for health policy and practice. The Lancet, 385(9967), 549-562.

Qi, H., Rand, M. D., Wu, X., Sestan, N., Wang, W., Rakic, P., ... & Artavanis-Tsakonas, S. (1999). Processing of the notch ligand delta by the metalloprotease Kuzbanian. Science, 283(5398), 91-94.

Sannerud, R., Esselens, C., Ejsmont, P., Mattera, R., Rochin, L., Tharkeshwar, A. K., ... & Vermeire, W. (2016). Restricted location of PSEN2/γ-secretase determines substrate specificity and generates an intracellular Aβ pool. Cell, 166(1), 193-208.

Selkoe, D. J. (1998). The cell biology of β-amyloid precursor protein and presenilin in

Alzheimer's disease. Trends in cell biology, 8(11), 447-453.

Selkoe, D. J., Abraham, C. R., Podlisny, M. B., & Duffy, L. K. (1986). Isolation of low-molecular-weight proteins from amyloid plaque fibers in Alzheimer's disease. Journal of neurochemistry, 46(6), 1820-1834

Selkoe, D. J., & Hardy, J. (2016). The amyloid hypothesis of Alzheimer's disease at 25 years. EMBO molecular medicine, 8(6), 595-608.

Sherrington, R., Rogaev, E. I., Liang, Y. A., Rogaeva, E. A., Levesque, G., Ikeda, M., ... & Tsuda, T. (1995). Cloning of a gene bearing missense mutations in early-onset familial Alzheimer's disease. Nature, 375(6534), 754.

Shimizu, H., Tosaki, A., Kaneko, K., Hisano, T., Sakurai, T., & Nukina, N. (2008). Crystal structure of an active form of BACE1, an enzyme responsible for amyloid β protein production. Molecular and cellular biology, 28(11), 3663-3671.

Siegenthaler, B. M., Bali, J., & Rajendran, L. (2016). γ-Secretase regulates the α-secretase cleavage of the Alzheimer's disease, amyloid precursor protein. Matters, 2(2), e201601000003.

Simpson, P. (1990). Lateral inhibition and the development of the sensory bristles of the adult peripheral nervous system of Drosophila. Development, 109(3), 509-519.

Small, D., Kovalenko, D., Kacer, D., Liaw, L., Landriscina, M., Di Serio, C., ... & Maciag, T. (2001). Soluble Jagged 1 represses the function of its transmembrane form to induce the formation of the Src-dependent chord-like phenotype. Journal of Biological Chemistry, 276(34), 32022-32030.

Smith, P. K., Krohn, R. I., Hermanson, G. T., Mallia, A. K., Gartner, F. H., Provenzano, M., ... & Klenk, D. C. (1985). Measurement of protein using bicinchoninic acid. Analytical biochemistry, 150(1), 76-85.

Spasic, D., Raemaekers, T., Dillen, K., Declerck, I., Baert, V., Serneels, L., ... & Annaert, W. (2007). Rer1p competes with APH-1 for binding to nicastrin and regulates γ-secretase complex assembly in the early secretory pathway. The Journal of cell biology, 176(5), 629-640.

Sprinzak, D., Lakhanpal, A., LeBon, L., Santat, L. A., Fontes, M. E., Anderson, G. A., ... & Elowitz, M. B. (2010). Cis-interactions between Notch and Delta generate mutually exclusive signalling states. Nature, 465(7294), 86.

Struhl, G., & Adachi, A. (2000). Requirements for presenilin-dependent cleavage of notch and other transmembrane proteins. Molecular cell, 6(3), 625-636.

Sun, X., & Artavanis-Tsakonas, S. (1997). Secreted forms of DELTA and SERRATE define

antagonists of Notch signaling in Drosophila. Development, 124(17), 3439-3448.

Svedružić, Ž. M., Popović, K., Smoljan, I., & Šendula-Jengić, V. (2012). Modulation of γ-secretase activity by multiple enzyme-substrate interactions: implications in pathogenesis of Alzheimer's disease. PloS one, 7(3), e32293.

Tani, S., Kurooka, H., Aoki, T., Hashimoto, N., & Honjo, T. (2001). The N-and C-terminal regions of RBP-J interact with the ankyrin repeats of Notch1 RAMIC to activate transcription. Nucleic acids research, 29(6), 1373-1380.

Terui, Y., Saad, N., Jia, S., McKeon, F., & Yuan, J. (2004). Dual role of sumoylation in the nuclear localization and transcriptional activation of NFAT1. Journal of Biological Chemistry, 279(27), 28257-28265.

Thinakaran, G., Borchelt, D. R., Lee, M. K., Slunt, H. H., Spitzer, L., Kim, G., ... & Hardy, J. (1996). Endoproteolysis of presenilin 1 and accumulation of processed derivatives in vivo. Neuron, 17(1), 181-190.

Tong, G., Wang, J. S., Sverdlov, O., Huang, S. P., Slemmon, R., Croop, R., ... & Berman, R. M. (2012). Multicenter, randomized, double-blind, placebo-controlled, single-ascending dose study of the oral γ-secretase inhibitor BMS-708163 (Avagacestat): tolerability profile, pharmacokinetic parameters, and pharmacodynamic markers. Clinical therapeutics, 34(3), 654-667.

Tournoy, J., Bossuyt, X., Snellinx, A., Regent, M., Garmyn, M., Serneels, L., ... & Hartmann, D. (2004). Partial loss of presenilins causes seborrheic keratosis and autoimmune disease in mice. Human molecular genetics, 13(13), 1321-1331.

van Es, J. H., van Gijn, M. E., Riccio, O., van den Born, M., Vooijs, M., Begthel, H., ... & Clevers, H. (2005). Notch/γ-secretase inhibition turns proliferative cells in intestinal crypts and adenomas into goblet cells. Nature, 435(7044), 959.

Varnum-Finney, B., Wu, L., Yu, M., Brashem-Stein, C., Staats, S., Flowers, D., ... & Bernstein, I. D. (2000). Immobilization of Notch ligand, Delta-1, is required for induction of notch signaling. Journal of cell science, 113(23), 4313-4318.

Weng, A. P., Ferrando, A. A., Lee, W., Morris, J. P., Silverman, L. B., Sanchez-Irizarry, C., ... & Aster, J. C. (2004). Activating mutations of NOTCH1 in human T cell acute lymphoblastic leukemia. Science, 306(5694), 269-271.

Wesley, C. S., & Saez, L. (2000). Analysis of Notch lacking the carboxyl terminus identified in Drosophila embryos. The Journal of cell biology, 149(3), 683-696.

Wolfe, M. S., Xia, W., Ostaszewski, B. L., Diehl, T. S., Kimberly, W. T., & Selkoe, D. J. (1999). Two transmembrane aspartates in presenilin-1 required for presenilin endoproteolysis and γ-secretase activity. Nature, 398(6727), 513.

Wolfe, M. S., & Yankner, B. A. (2016). Sorting out presenilins in Alzheimer's disease. Cell, 166(1), 13-15.

Wu, G., Hubbard, E. J. A., Kitajewski, J. K., & Greenwald, I. (1998). Evidence for functional and physical association between Caenorhabditis elegans SEL-10, a Cdc4p-related protein, and SEL-12 presenilin. Proceedings of the National Academy of Sciences, 95(26), 15787-15791.

Wu, G., Lyapina, S., Das, I., Li, J., Gurney, M., Pauley, A., ... & Kitajewski, J. (2001). SEL-10 is an inhibitor of notch signaling that targets notch for ubiquitin-mediated protein degradation. Molecular and cellular biology, 21(21), 7403-7415.

Xia, X., Qian, S., Soriano, S., Wu, Y., Fletcher, A. M., Wang, X. J., ... & Zheng, H. (2001). Loss of presenilin 1 is associated with enhanced β-catenin signaling and skin tumorigenesis. Proceedings of the National Academy of Sciences, 98(19), 10863-10868.

Yamamoto, N., Yamamoto, S. I., Inagaki, F., Kawaichi, M., Fukamizu, A., Kishi, N., ... & Nakafuku, M. (2001). Role of Deltex-1 as a transcriptional regulator downstream of the Notch receptor. Journal of Biological Chemistry, 276(48), 45031-45040.

Yang, T., Arslanova, D., Gu, Y., Augelli-Szafran, C., & Xia, W. (2008). Quantification of gamma-secretase modulation differentiates inhibitor compound selectivity between two substrates Notch and amyloid precursor protein. Molecular brain, 1(1), 15.

Ye, Y., & Fortini, M. E. (1998). Characterization of Drosophila Presenilin and its colocalization with Notch during development. Mechanisms of development, 79(1-2), 199-211.

Ye, X., Tai, W., Bao, X., Chen, X., & Zhang, D. (2014). FLZ inhibited γ-secretase selectively and decreased Aβ mitochondrial production in APP-SH-SY5Y cells. Naunyn-Schmiedeberg's archives of pharmacology, 387(1), 75-85.

Zhang, M., Haapasalo, A., Kim, D. Y., Ingano, L. A. M., Pettingell, W. H., Kovacs, D. M., ... & Pettingell, W. H. (2006). Presenilin/γ-secretase activity regulates protein clearance from the endocytic recycling compartment. The FASEB journal, 20(8), 1176-1178.

Zhang, S., Wang, Z., Cai, F., Zhang, M., Wu, Y., Zhang, J., & Song, W. (2017). BACE1 cleavage site selection critical for amyloidogenesis and Alzheimer's pathogenesis. Journal of Neuroscience, 37(29), 6915-6925.

Zhang, X., & Song, W. (2013). The role of APP and BACE1 trafficking in APP processing and amyloid-β generation. Alzheimer's research & therapy, 5(5), 46.